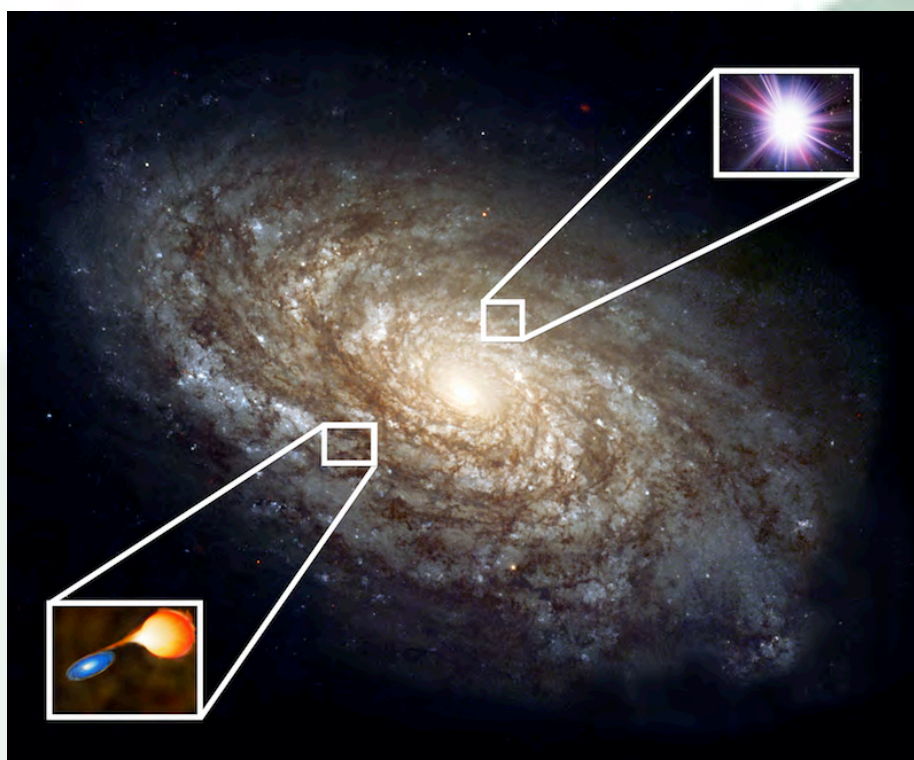




# NURSERIES OF SUPERNOVAE

A STUDY OF YOUNG HIGH REDSHIFT  
TYPE IA SUPERNOVA HOST GALAXIES

TEDDY FJELDGAARD FREDERIKSEN



PHILOSOPHIÆ DOCTOR

Dark Cosmology Centre

This thesis has been submitted to  
the PhD School of The Faculty of Science  
University of Copenhagen

### Cover art:

In every galaxy there are stellar systems that form the progenitors of type Ia supernovae. This picture depicts the galaxy NGC 4414, where SN 1974G was discovered (not depicted here). Upper inset: An artistic depiction of a supernova (symbolizing a core-collapse supernova). Lower inset: An artistic depiction of a Type Ia progenitor system.

### Credits:

Main picture: Hubble Heritage Team (AURA/STScI/NASA)

Upper inset: (Backyard Observatory Supernova Search (BOSS),  
<http://www.bosssupernova.com/whatisasupernova.htm>)

Lower inset: NASA/CXC/M. Weiss

Submission: *December, 2013*

Defense: *—, 2014*

Supervisor: *Jens Hjorth*

Opponents: *Maximilian Stritzinger*  
*Filippo Mannucci*



# CONTENTS

---

<b>Contents</b>	<b>v</b>
<b>Acronyms</b>	<b>ix</b>
<b>List of Figures</b>	<b>xi</b>
<b>List of Tables</b>	<b>xvii</b>
<b>Acknowledgements</b>	<b>xix</b>
<b>Abstract</b>	<b>xxi</b>
<b>Dansk Resumé</b>	<b>xxii</b>
<b>1 Introduction</b>	<b>1</b>
1.1 The 2011 Nobel Prize in Physics . . . . .	1
1.2 SN cosmology . . . . .	4
1.2.1 Supernova explosions . . . . .	5
1.2.2 The History of SNe . . . . .	5
1.2.3 Core Collapse SNe . . . . .	6
1.2.4 Type Ia SNe . . . . .	7
1.2.5 Delay Time Distribution . . . . .	9
1.2.6 Host correlations . . . . .	10
1.3 Galaxy Evolution . . . . .	13
1.3.1 Star Formation Rate . . . . .	14
1.3.2 Main Sequence of Galaxies . . . . .	14
1.3.3 Metallicity . . . . .	14
1.3.4 Spectral Energy fitting . . . . .	15
1.3.5 Fundamental Metallicity Relation . . . . .	15
1.4 Frontier science with X-shooter . . . . .	16
1.5 Thesis Outline and Description . . . . .	16
<b>2 The First Supernova</b>	<b>19</b>
2.1 Introduction . . . . .	19
2.2 Data . . . . .	20
2.2.1 Spectroscopic Data . . . . .	20
2.2.2 Flux Calibration Quality . . . . .	22
2.2.3 Photometric Data . . . . .	22

2.3	Analysis . . . . .	22
2.3.1	Broad-Band SED Fitting . . . . .	22
2.3.2	Resampling of the X-shooter Spectrum . . . . .	24
2.3.3	Host Extinction . . . . .	24
2.3.4	Metallicity . . . . .	25
2.3.5	Star formation . . . . .	26
2.3.6	Lyman- $\alpha$ . . . . .	26
2.4	Discussion & Conclusions . . . . .	28
<b>3</b>	<b>The Twin in the Subaru Deep Field</b>	<b>35</b>
3.1	Introduction . . . . .	35
3.2	Data . . . . .	36
3.3	Analysis . . . . .	37
3.4	DISCUSSION . . . . .	39
3.5	Conclusions . . . . .	40
<b>4</b>	<b>High redshift SN host sample</b>	<b>43</b>
4.1	Introduction . . . . .	43
4.2	Data & Sample Selection . . . . .	44
4.2.1	Spectroscopic Data . . . . .	45
4.2.2	Photometric Data . . . . .	45
4.3	Analysis . . . . .	45
4.3.1	SED Fitting . . . . .	45
4.3.2	Emission line redshifts . . . . .	46
4.3.3	Photometric redshift test . . . . .	48
4.3.4	Special Cases . . . . .	49
4.3.5	A reference sample . . . . .	51
4.4	Discussions . . . . .	51
4.4.1	DTD Evolution . . . . .	54
4.4.2	A New A+B Model . . . . .	58
4.4.3	Fraction of Prompt Supernovae . . . . .	59
4.5	Conclusions & Outlook . . . . .	62
	<b>Coauthorstatements</b>	<b>79</b>
	<b>Bibliography</b>	<b>91</b>





## ACRONYMS

---

AGN	Active Galactic Nuclei
BAO	Baryonic Acoustic Oscillations
CANDELS	Cosmic Assembly Near-IR Deep Extragalactic Legacy Survey
CC SN	Core-collapse supernova
CMB	Cosmic Microwave Background
C/O WD	Carbon-Oxygen White Dwarf
DTD	Delay Time Distribution
EW	Equivalent Width
FOV	Field of View
HST	Hubble Space Telescope
IDL	Interactive Data Language (programming language)
IMF	Initial mass function
IR	Infra-red
NIR	Near infra-red
Phot-z	Photometric redshift
SDF	Subaru Deep Field
SED	Spectral Energy Distribution
SFH	Star-formation history
SFR	Star-formation rate
sSFR	Specific star-formation rate
SN	Supernova
SN Ia	Type Ia (one-A) supernova
SNe	Supernovae (plural)
Spec-z	Spectroscopic redshift
SSP	Single stellar population
ToO	Target-of-Opportunity
UV	Ultra-violet
VLT	Very Large Telescope (Cerro Paranal, Chile)
WD	White Dwarf



## LIST OF FIGURES

---

1.1	Constraints (68%, 95%, and 99.7% contours) on the energy density of the Matter and Dark Energy components of the Universe. Constraints from SNe (Union 2.1 Compilation) are shown in blue. Additional cosmological constants from the Cosmic Microwave Background (CMB, in orange) and Baryonic Acoustic Oscillations (BAO, in green) are also shown. Figure from Suzuki et al. (2012).	3
1.2	The first rendition of a Hubble diagram using SNe by Kowal (1968).	5
1.3	The onion-like structure of an evolved massive star (not to scale). (Credits: User:Rursus (R. J. Hall), via Wikimedia Commons)	6
1.4	An artist's impression of a single degenerate system. (Credits: NASA/CXC/M. Weiss)	7
1.5	A schematic of the phases in the evolution of SD progenitors (adapted from Wang & Han, 2012). The star to the left is labeled A and the star to the right is labeled B. The A star will explode as a type Ia SN.	8
1.6	Delay time distribution of different double degenerate (left) and single degenerate (right) models (figure from Wang & Han, 2012). The three circles with error bars at the top are measurements of the observed delay times (Maoz et al., 2011).	9
1.7	SN Ia light curves before and after correction. The broader light curves (slow decline rates) are brighter than the narrow light curves (fast decline rates). After correcting for brightness and stretch all light curves overlap. (Credit: <a href="http://www-supernova.lbl.gov/">http://www-supernova.lbl.gov/</a> )	10
1.8	Top: Mean spectrum of high- and low-stretch SN host galaxy. Bottom: The difference between the two mean spectra, overplotted with a B-type stellar template. Figure taken from Brandt et al. (2010).	11
1.9	Hubble residual as a function of the stellar mass of the host galaxy. Figure from Childress et al. (2013b).	12
1.10	Picture of a star forming nebula. New stars are emerging from the molecular cloud as small dots at the end of small antennae along the circumference of the cloud. (Credit: NASA/ESA/STScI J. Hester and P. Scowen)	13
2.1	Pre-explosion <i>HST</i> F775W (i-band, rest frame u-band) image with the X-shooter slit configuration overlaid (red). The peak luminosity of the host galaxy is marked by ticks (blue). The size of the tick marks is $1''$ , corresponding to 8.6 kpc at the redshift of SN Primo. The faint part to the south is also part of the galaxy (see Rodney et al., 2012). The location of the SN is marked by a plus (blue).	21
2.2	The SED of the SN Primo host derived from broad-band photometry. In red (gray) are the photometric points after (before) the subtraction of the emission-line flux. Overplotted is the best-fitting model SED from FAST.	23

2.3	The detected emission lines in the X-shooter spectrum of the host of SN Primo. The spectrum is flux-calibrated and corrected for Galactic extinction. The solid (red) line shows the best fitting gaussian line profiles. The [O II] $\lambda\lambda 3726, 3729$ line is fitted with a double gaussian line profile. The gray bands mark regions excluded due to sky lines. In the $H\beta$ fit the line center was fixed to $\lambda_{H\beta}(1+z)$ , where $\lambda_{H\beta} = 486.1325$ nm and $z$ is the redshift. $Ly\alpha$ is detected, but located close to the Earth's atmospheric UV cutoff. . . . .	25
2.4	The $O_{32}$ and $R_{23}$ line ratios of the host of SN Primo together with the photoionization models of Kewley & Dopita (2002). The dashed lines and gray bands show the line ratios and $1\sigma$ error bars derived from the spectrum. Left: $O_{32}$ (Equation 2.5) versus the ionization parameter $q$ . From top down the metallicities are $Z = 0.05, 0.1, 0.2, 0.5, 1.0, 1.5,$ and $2.0 Z_{\odot}$ . Right: $R_{23}$ (Equation 2.3) versus the metallicity. From the top down $q = 30, 15, 8, 4, 2, 1, 0.5 \times 10^7$ cm s <sup>-1</sup> . . . . .	26
2.5	BPT diagnostic diagram (Baldwin, Phillips, & Terlevich, 1981). The x-axis denotes the ratio $\log([N II] \lambda 6586/H\alpha)$ and the y-axis the ratio $\log([O III] \lambda 5007/H\beta)$ . The data point marks the host galaxy of SN Primo, with the arrow denoting the upper-limit of the ratio derived from the non-detection of [N II] $\lambda 6586$ . The vertical bar denotes the $1\sigma$ error bar of the ratio. For illustrative purposes we overplot the 15 emission-line hosts from the Lampeitl et al. (2010) sample of SN Ia host galaxies with SDSS spectra. . . . .	27
2.6	The Lyman- $\alpha$ line in the SN Primo host spectrum. The systemic velocity is determined from $H\alpha$ , [O III] $\lambda\lambda 4959, 5007$ , and [O II] $\lambda 3729$ . . . . .	28
2.7	The SFR-mass relation for SN Ia host galaxies. The (red) asterisk denotes the host of SN Primo with error bars. Filled (blue) circles mark star-forming hosts in each sample. The (magenta) crosses marks the passive hosts in each sample. The solid and dotted (green) lines show the correlation between SFR and stellar mass for $z \sim 0$ (bottom), $z = 1$ (middle), and $z = 2$ (top) from Daddi et al. (2007, $z = 2$ ) and Elbaz et al. (2007, $z \sim 0$ and $z = 1$ ). The solid section of each line marks the range of validity of the relations. (a) The low redshift sample ( $z < 0.21$ ) from SDSS (Lampeitl et al., 2010). The dashed line marks the cut, $\log(sSFR) = -10.6$ , between star forming and passive galaxies. The contours mark the region enclosing 68% and 95% of the star-forming sample. (b) The high redshift samples from HST (Thomson & Chary, 2011, $0.95 < z < 1.8$ , open (orange) circles) and SNLS (Sullivan et al., 2010, $0.2 < z < 1.0$ , filled (blue) circles / (magenta) crosses). The apparent upper diagonal ridge-line for the Sullivan et al. (2010) data is due to shortcomings in their SED fitting. . . . .	29
2.8	Metallicity–luminosity relation for SN Ia host galaxies. The (red) asterisk denotes the host of SN Primo with error bars. The (blue) filled circles denotes the sample of Prieto et al. (2008, $z < 0.04$ , median error bar plotter to the lower left). . . . .	30

3.1	<p>ZEBRA fit and resultant <math>z</math>-PDF of hSDF0705.25. The left panel shows the actual photometry (filled circles), the best-fitting galaxy template (solid line), and its synthetic photometry (empty circles). The vertical error bars denote the photometric uncertainty, and the horizontal error bars show the width of the filter. The <math>1\sigma</math> upper limit on the photometry in the <i>GALEX FUV</i> band is shown as the downturned arrow. The header gives the designation of the SN host galaxy, most probable photo-<math>z</math> (<math>z_p</math>), the <math>\chi^2</math> per degree of freedom of the fit, and the absolute <math>B</math>-band magnitude the galaxy would have at <math>z_p</math>. The right panel shows the resultant <math>z</math>-PDF peaking at <math>z_p = 1.552 \pm 0.018</math>. The red line marks the spectroscopic redshift obtained in this work. . . . .</p>	37
3.2	<p>X-shooter 1D and 2D spectrum of hSDF0705.25. The spectrum has been corrected for Galactic extinction. The solid (red) line shows the fit to the emission lines assuming a Gaussian line profile. The dashed line shows a scaled version of the <math>H\alpha</math> line assuming the same FWHM (in velocity units) and extinction in the host of <math>E(B - V) = 0</math> mag (upper) and <math>E(B - V) = 0.5</math> mag (lower). Color version available online. . . . .</p>	38
3.3	<p>The Fundamental Metallicity Relation (FMR). The parameter <math>\mu_{0.32} = \log(M_*) - 0.32 \log(SFR)</math> is the projection in the stellar mass, SFR plane. The two circles (red) are the two high-redshift SN Ia host galaxies with measured gas-phase metallicity, hSDF0705.25 and SN Primo (Frederiksen et al., 2012). The crosses are the binned data from the Sloan Digital Sky Survey (York et al., 2000, SDSS) used in Mannucci et al. (2010). The diamonds (blue) are GRB host galaxies used to calibrate the low metallicity slope in Mannucci et al. (2011, <math>z &lt; 1</math>). The squares are lensed galaxies from Christensen et al. (2012, yellow, <math>z &gt; 1</math>) and Richard et al. (2011, green, <math>z &gt; 1.5</math>). The dark (blue) line is the parameterization of Mannucci et al. (2011) (solid in the range of validity, extrapolation in dashed blue, high metallicity as constant, low metallicity as straight line). The two SN Ia host galaxies (<math>z = 1.5</math>) are fully consistent with the FMR of star-forming field galaxies. . . . .</p>	41
4.1	<p>The emission line spectrum of the host of SN Quayle at <math>z = 2.370</math>. The solid lines show the best-fitting Gaussian line profiles. When fitting the <math>H\alpha</math> and [N II] 6583 line the width is fixed to the width of the [O III] 5007 line (in velocity units). The dashed line shows the predicted line profile of [O III] 4959 assuming a line ratio of the [O III] 4959,5007 doublet of 1 : 3. . . . .</p>	47
4.2	<p>The emission line spectrum of the host of SN Cleveland at <math>z = 1.406</math>. The solid lines show the best-fitting Gaussian line profiles. The dashed line shows the expected line shape of <math>H\beta</math> calculated from the <math>H\alpha</math> line, assuming Case-B recombination and no host extinction. The over prediction <math>H\beta</math> flux, is most probably due to extinction in the host of SN Cleveland. . . . .</p>	48

4.3	The emission line spectrum of the host of SN Wilson. Top: Identifying the strong emission line as [O III] 5007 ( $z = 1.91$ ). The other expected emission lines have very low signal-to-noise. When fitting [O II] 3726,3729 and $H\beta$ we fix the line width to the width of [O III] 5007 (in velocity units). The [O II] 3726,3729 doublet is fitted with a double gaussian profile, with fixed 1 : 1 line ratio and a fixed ratio between the wavelength of the red and the blue peak. Bottom: Identifying the strong emission line as $H\alpha$ ( $z = 1.22$ ). The dashed lines are the predicted $H\beta$ and [O III] 4959,5007 line shapes. For the $H\beta$ line we assume Case-B recombination and no extinction in the host galaxy. For the [O III] 4959,5007 we assume a line ratio of 1 : 3 and that the [O III] 5007 and $H\alpha$ lines have comparable (equal) line fluxes (as seen in the hosts of SN Primo, Cleveland and Quayle). The [O III] 4959,5007 doublet seems inconsistent with the low-redshift solution. . . .	49
4.4	Cumulative distribution of the residual between the phot- $z$ and spec- $z$ . The thin lines (SN Ia: red, CCSN: blue, Unknown: green) show the distribution of each individual host galaxy, where all but two are within 10%. Thick solid line shows the combined distribution of all hosts (the bias is 1.8%) and the dashed line shows the distribution after excluding the two outliers. The two outliers are Polk (left-most curve) and Obama (right-most curve). . . . .	50
4.5	Transformation function between stellar ages derived using FAST and GalMC. The solid line is the empirical transformation derived from the SN sample. The dotted line is the one-to-one line. The dashed line is a forth-order polynomial fit to the empirical transform. . . . .	52
4.6	SFR vs stellar mass. The solid lines mark the 68% and 95% contours. Red contours show the distribution of SN Ia, blue contours show CC SN and green contours show unknown classifications. Left: Assuming the best fitting SFH (see Table 4.4). Right: Assuming an exponential SFH. . . . .	52
4.7	Spectral Energy Distribution of all the SN host galaxies. The black points mark the photometry and the solid curve marks the best fitting SED. Red curves mark fits to SN Ia hosts, the blue curves mark CC SN hosts, and the green curves mark hosts of SN with unknown classification. . . . .	53
4.8	Cumulative distribution of stellar masses. The red curve marks the distribution of SN Ia hosts, the blue curve marks CC SN hosts, and the green curve marks hosts of SN with unknown classification. The solid black line shows a comparative sample of field galaxies (NMBS). To show the effect of changing SFH we plot the cumulative distribution under the assumption of both individual best SFH (left) and tau-model SFH (right) for all hosts. . . . .	54
4.9	Cumulative distribution of stellar masses. Colors as in Figure 4.8. Individual best SFH (left) and tau-model SFH (right) . . . . .	54
4.10	Cumulative distribution of star-formation rate. Colors as in Figure 4.8. Individual best SFH (left) and tau-model SFH (right) . . . . .	55
4.11	Distribution of stellar main sequence mass. Colors as in Figure 4.8. Individual best SFH (left) and tau-model SFH (right). The dotted line marks the distribution when the three youngest SN Ia hosts are forced to have no extinction (i.e. age-extinction degeneracy). . . . .	55

4.12	Left: The evolution of the A/B ratio as a function of redshift. The data points in increasing order of redshift are Mannucci et al. (2005); Dilday et al. (2008); Smith et al. (2012); Sullivan et al. (2006); and this work (two red bins). The three low redshift points are derived from SDSS SNe samples, and the medium redshift point is from SNLS SNe. Right: The evolution of the specific SFR within SN samples of Lampeitl et al. (2010, SDSS, low- $z$ ), Sullivan et al. (2010, SNLS, medium- $z$ ), Thomson & Chary (2011, high- $z$ ), and our sample (high- $z$ ). The gray band shows the evolution of the cosmic sSFR predicted by Elbaz et al. (2011) and the gray diamonds show the MS of field galaxies from Elbaz et al. (2007, $z \sim 0$ and $z = 1$ ) and Daddi et al. (2007, $z = 2$ ). All SN samples are consistent with the MS within the uncertainties, but show a general tendency to be more star forming on average than the MS. . . . .	56
4.13	$A/B$ -ratio vs. sSFR range of literature samples. The lower square data-points are SDSS samples where the $A/B$ -ratios are taken from Mannucci et al. (2005); Dilday et al. (2008); Smith et al. (2012) respectively and the range $sSFR$ of SDSS SNe is estimated from Lampeitl et al. (2010). The middle data-point is the SNLS SN samples with the $A/B$ -ratio from Sullivan et al. (2006) and the $sSFR$ -range from Sullivan et al. (2010). The upper circles data-point is from this study. The solid lines and hashed regions mark the relation in Equation 4.21 using $k$ from Equation 4.25 (horizontally hashed, green). . . . .	59
4.14	Left: The delay-to-prompt ratio, $k$ , and its dependence on the value of $t_{\text{split}}$ . For each value of $t_{\text{split}}$ we calculate the maximum and minimum value of $k$ by assuming that all ambiguous SN hosts belong either to the prompt or delayed bin of the DTD. Ambiguous hosts are hosts with two stellar populations, one in each bin, or hosts with a constant SFH that have a stellar age larger than $t_{\text{split}}$ . The value of $k$ is insensitive to small changes in $t_{\text{split}}$ . Right: Prompt fraction calculated from the delay-to-prompt ratio (see Equation 4.27). . . . .	60
4.15	The SN rate as a function of sSFR. The measurements of Mannucci et al. (2005); Sullivan et al. (2006); Smith et al. (2012); Gao & Pritchett (2013) (yellow stars, red triangles, green diamonds, and blue circles, respectively). The black line show Equation 4.24 fitted to the data (except Mannucci et al., 2005). The gray dashed-dotted line show the A+B model of Gao & Pritchett (2013). . . . .	61
4.16	Schematic of the DTD model of Rodney et al. (2013, red; dotted line: powerlaw only) and the one used in our analysis (blue). (Left: log-log scale, Right: log-linear scale.) The 2-bin DTD (A+B model) used in our analysis is not fixed to any absolute scale, we therefore choose to set the scale such that the area under the curve (i.e. the time-integrated SN rate) is equal to the Rodney et al. (2013) curve. The upper and lower bounds marked by blue dashed lines correspond to the stellar age of the youngest and oldest host. . . . .	61
4.17	Triangular plot of the GalMC MCMC chain for Primo. . . . .	68
4.18	Triangular plot of the GalMC MCMC chain for Agnew. . . . .	69
4.19	Triangular plot of the GalMC MCMC chain for Macrinus. . . . .	70
4.20	Triangular plot of the GalMC MCMC chain for Wilson. . . . .	71
4.21	Triangular plot of the GalMC MCMC chain for Geta. . . . .	72
4.22	Triangular plot of the GalMC MCMC chain for Washington. . . . .	73
4.23	Triangular plot of the GalMC MCMC chain for Cleveland. . . . .	74
4.24	Triangular plot of the GalMC MCMC chain for Tiberius. . . . .	75

4.25	Triangular plot of the GalMC MCMC chain for Caligula. . . . .	76
4.26	Triangular plot of the GalMC MCMC chain for Quayle. . . . .	77

## LIST OF TABLES

---

2.1	Photometry of the host of SN Primo . . . . .	31
2.2	Summary of SED fitting using FAST. . . . .	32
2.3	Emission lines detected in the spectrum of the host of SN Primo. . . . .	32
2.4	Spectroscopic summary. . . . .	33
3.1	Spectroscopic summary . . . . .	39
3.2	Derived properties of the SN host galaxy hSDF0705.25 . . . . .	39
4.1	All triggered sources under our program. . . . .	47
4.2	Full list of all SN-like transients in the CANDELS and CLASH surveys . . . . .	63
4.3	Full list of the high-z sample. . . . .	65
4.4	Bayesian Information Criterion (BIC) . . . . .	66
4.5	Stellar parameters from GalMC. . . . .	67



## ACKNOWLEDGEMENTS

---

First and for most I would like to thank my supervisor Jens Hjorth for his tremendous efforts through out the past three year. I have at times been taking more then my share of his time and patience. He has helped me grow my potential and not just as a scientist. A great thanks for mentoring also goes to my DARK committee: Steen, Anja, Justyn (who is no longer at DARK), and Thomas (who took over for Justyn).

My supervisor managed to set up a six-month stay for me with the team of Nobel Laureate Adam Riess at Space Telescope Science Institute in Baltimore where I had the opportunity to work with at many talented and inspiring people. Among the Baltimore people some deserved a special mentioning: Steve, Dave, Dan, and Adam, thank you for making me feel welcome (and thank you for throwing me a fare-well party).

A great thanks also goes to all the people how have given me practical help by reading through my thesis drafts. Especially Mitch deserves a huge thank you for the countless session where he has helped me getting rid of badly formed sentences. A special thanks also goes to Mille for providing valuable feedback.

I would also like to thank the whole DARK community for making it a joy to go to work each day for the last five years. During the last few month of my thesis I greatly appreciated the moral support from my officemates, Ece and Johannes, my fellow PhD students and DARK'ers in general.

But my greatest thank you goes to my loving husband! It is his love, support and occasional kick that brought me where I am today. Thank you, my love!



# ABSTRACT

---

Type Ia supernovae (SNe) have long been the gold standard for precision cosmology and after several decades of intense research the supernova (SN) community was in 2011 honored by giving the Nobel Prize in physics for the discovery of Dark Energy to the leaders of the two big SN collaborations: Saul Perlmutter (Supernova Cosmology Project), Adam Riess, and Brian Schmidt (High-Z team).

After decades of study we still do not know the detailed mechanism that governed SNe explosions, but we are today in the situation where the SN sample size has become large enough for the statistical errors to be smaller than the systematic errors. The down side to this is that we can not improve the SNe further as cosmological probes before we know the source of the systematic dispersions. On the other hand the systematic offsets might actually be the measurements that will lead to new information on the detailed mechanisms that governs the SN explosions.

In the first of three papers I investigate the host galaxy of the first SN Ia found in the Cosmic Assembly Near-IR Deep Extragalactic Legacy Survey (CANDELS) SN search. From long slit spectroscopy using the Xshooter spectrograph and broadband photometry I determine the gas-phase metallicity, stellar mass and stellar age for this  $z = 1.55$  host galaxy. I am also able to rule out the presence of any AGN through emission-line ratios. The host is classified as a highly star forming, low mass, low metallicity galaxy. It is a clear outlier in star formation and stellar mass compared to most low redshift ( $z < 0.2$ ) SNe, but consistent with intermediate ( $0.2 < z < 1.0$ ) and high ( $z > 1$ ) redshift SNe. This is mainly due to the change in specific star-formation rate as a function of redshift. This can potentially impact the use of high redshift SN Ia as standard candles.

In the second paper I investigate one of the high redshift SN Ia hosts found in the Subaru Deep Field (SDF) SN search. The SDF SN search relies heavily on photometric redshifts and transients previously identified as active galactic nuclei (AGN) to reproduce the cosmic SN rate. Due to the small number statistic, especially at high redshift, catastrophic redshift outliers and miss-identified transients can bias the inferred SN rate. I confirm the photometric redshift of  $z = 1.55$  and from emission-line ratios I can also rule out AGN activity. I found a young host galaxy with high star-formation rate and sub-solar metallicity.

In the last paper I analyze the full high redshift ( $z > 1$ ) SN host sample from the CANDELS and CLASH SN search. I determine the stellar properties of each host by fitting the broad-band photometry using the GalMC SED-fitting code. I measure the fraction of SNe with very short delay times by assuming a simple two-bin form of the delay time distribution (DTD), known as the A+B model. This simple model predicts that the shape of the DTD does not change if the ratio of the two parameters  $A/B \propto sSFR$ . I find that the  $A/B$ -ratio is consistent with this relation out to redshift  $z \sim 2$ . From the assumption that the DTD slope is constant I propose a new form of the A+B model.

## DANSK RESUMÉ

---

Type Ia supernovaer (SN'er) har længe været indbegrebet af præcisionskosmologi, og efter flere årtiers intensiv forskning blev supernova fælleskabet i 2011 hædret med Nobelprisen i fysik for opdagelsen af mørk energi til lederne af de to største SN-grupper: Saul Perlmutter (Supernova Cosmology Project), Adam Riess og Brian Schmidt (High-Z team).

Efter årtiers forskning kender vi stadig ikke de detaljerede mekanismer som styrer SN-eksplosionerne, men vi er i dag i en situation hvor mængden af observerede SN'er er blevet så stor at de statistiske usikkerheder er blevet mindre end de systematiske usikkerheder. Ulempen ved det er at vi ikke kan forbedre SN'erne yderligere som kosmologiske værktøjer før vi kender kilden til de systematiske usikkerheder. På den anden side kan de systematiske usikkerheder være de målinger der vil føre til ny information om de detaljerede mekanismer der styrer SN-eksplosioner.

I den første af tre artikler undersøger jeg værtsgalakserne for den første SN Ia fundet i CANDELS (Cosmic Assembly Near-IR Deep Extragalactic Legacy Survey) SN search. Ved hjælp af spektroskopi med X-shooter-spektrografen og bredbånds-fotometri bestemmer jeg metalliciteten i gasfasen, stjernemassen og stjernealderen for denne  $z = 1.55$  værtsgalakse. Jeg formår også at udelukke tilstedeværelsen af en aktiv galaksekerne gennem emissionslinjeforhold. Værtsgalakserne er klassificeret som en meget stjernedannende, lavmasse-, lavmetallicitets-galakse. Den skiller sig tydeligt ud i stjernemasse og stjernedannelse sammenlignet med lavrødforskydnings-SN'er ( $z < 0.2$ ), men er konsistent med mellem- ( $0.2 < z < 1.0$ ) og højrødforskydnings-SN'er ( $z > 1$ ). Dette skyldes mest ændringerne i den specifikke stjernedannelsesrate som funktion af rødforskydningen. Dette kan potentielt påvirke brugen af højrødforskydnings-SN'er som standardlysilder.

I anden artikel undersøger jeg en af SN Ia-værtsgalakserne fundet i Subaru Deep Field (SDF) SN search. SDF SN search er afhængig af fotometriske rødforskydninger og transienter der tidligere er identificeret som aktive galaksekerne for at kunne reproducere den kosmiske SN rate. Grundet det lave antal SN'er, især ved høj rødforskydning, kan markante rødforskydningsafvigere og fejlidentificerede transienter påvirke den afledte SN-rate. SDF-transientens værtsgalakse blev observeret med X-shooter-spektrografen. Jeg bekræfter den fotometriske rødforskydning på  $z = 1.55$  og via emissionslinjeforhold kan jeg også udelukke aktivitet fra en aktiv galaksekerne. Jeg finder en ung værtsgalakse med høj stjernedannelses rate og en metallicitet mindre end solens.

I den sidste artikel analyserer jeg det fulde højrødforskydningsdatasæt ( $z > 1$ ) over SN-værtsgalakser fra CANDELS og CLASH SN search. Jeg bestemmer stjerneegenskaberne for hver værtsgalakse ved at fitte bredbånds-fotometrien med SED-fitte-programmet GalMC. Jeg bestemmer andelen af SNe med meget kort Delay Time ved at antage en simpel to-punktsform af Delay Time Distribution (DTD), kaldet A+B-modellen. Denne simple model forudsiger, at formen på DTD'en er uforandret hvis forholdet mellem de to parameter  $A/B \propto s\text{SFR}$ . Jeg finder at  $A/B$ -forholdet er konsistent med denne relation op til rødforskydning  $z \sim 2$ . Ud fra antagelsen at formen på DTD'en er konstant udleder jeg en ny analytisk form af A+B-modellen.

# 1

## INTRODUCTION

*Somewhere, something incredible is waiting to be known.*

Carl Sagan

The word cosmology originates from Greek and means the study of the cosmos. Today, cosmologists study how the Universe behaves at the grandest of scales: How does the Universe expand? How is the matter in the Universe distributed? The first question has been the interest of cosmologists since Edwin Hubble first measured the expansion of the Universe by analyzing measurements of Cepheid variables in other galaxies.

To measure the expansion history of the Universe (denoted  $H(t)$ ), we need to know the size<sup>1</sup> of the Universe at different times. Fortunately, information about the size of the Universe is imprinted in the light that reaches us as cosmological redshift. While the redshift is relatively straightforward to determine, it is more difficult to infer the time when the light is emitted. But because light travels at a finite speed, and we don't move compared to cosmological scales, time and distance are connected. Independently measuring redshifts and distances to objects makes it possible to derive the expansion history. Such objects whose distance can be inferred will in this thesis be called cosmological probes.

Today, we have more cosmological probes available than simply variable stars like Cepheids: Supernova explosions (SN), the Cosmic Microwave Background (CMB), Baryonic Acoustic Oscillations (BAO), Parallax, Surface-Brightness Fluctuations (SBF), Light Echoes, Expanding Photosphere Method (EPM), just to mention a few. Not all distance methods are applicable at distances relevant for cosmology, but they can be used as rungs on a ladder, each used to calibrate and refine the next method. Figure 1.1 shows how combining multiple probes can yield tight constraints on cosmological parameters.

### 1.1 THE 2011 NOBEL PRIZE IN PHYSICS

In 2011 the Nobel Prize in Physics was awarded to Saul Perlmutter, Adam Riess, and Brian Schmidt for the discovery of the accelerated expansion of the Universe. Perlmutter and Schmidt led the two competing teams Supernova Cosmology Project and High-Z team respectively (The High-Z was later led by Riess). Both teams showed independently that the expansion of the Universe was speeding up at an ever increasing rate. The source of this accelerated expansion was dubbed Dark Energy.

The supernovae (SNe) were used as standard candles to infer the distance to the explosion. From the observations of the SN light curve, it is possible to infer the intrinsic brightness of the

---

<sup>1</sup>Parameterized by the scale factor  $a$ .

SN. The intrinsic and observed brightness of a source is related as

$$F = \frac{L}{4\pi D_{\text{lum}}^2}, \quad (1.1)$$

where  $F$  is the observed flux,  $L$  the intrinsic luminosity, and  $D_{\text{lum}}$  the so-called luminosity distance to the source. Assuming a smooth, homogeneous and isotropic universe, it is possible to derive the so-called Friedmann equation from General Relativity:

$$\frac{H(z)^2}{H_0^2} = E(z)^2 = \sum_i \Omega_i (1+z)^{q_i}, \quad (1.2)$$

where  $E(z)$  is a convenient dimensionless representation of the Hubble parameter,  $H(z)$ , and  $H_0$  is the Hubble constant. The  $\Omega_i$  and  $q_i$  parameters are density and scaling parameters, respectively, of each energy component of the Universe. Radiation, matter, curvature, and the cosmological constant scales as  $q_i = 4, 3, 2$ , and  $0$ , respectively. For a specially flat Universe, the luminosity distance is calculated as

$$D_{\text{lum}}(z) = (1+z) \frac{c}{H_0} \int_0^z \frac{1}{E(z)} dz. \quad (1.3)$$

From this equation, it is clear that if the distance and redshift to a set of objects is known it is possible to infer the energy components of the Universe. It was from the SN explosions that we learned that there must exist a new energy component: Dark Energy (see Figure 1.1), which dominates the expansion today. This has been possible because the intrinsic luminosity of the SNe can be inferred to better than 0.1 magnitude<sup>2</sup> (Conley et al., 2011), which is why SNe are the cornerstone in precision cosmology.

---

<sup>2</sup>A 0.1 magnitude variation corresponds to a variation in the intrinsic luminosity of 9.2% (error propagation).

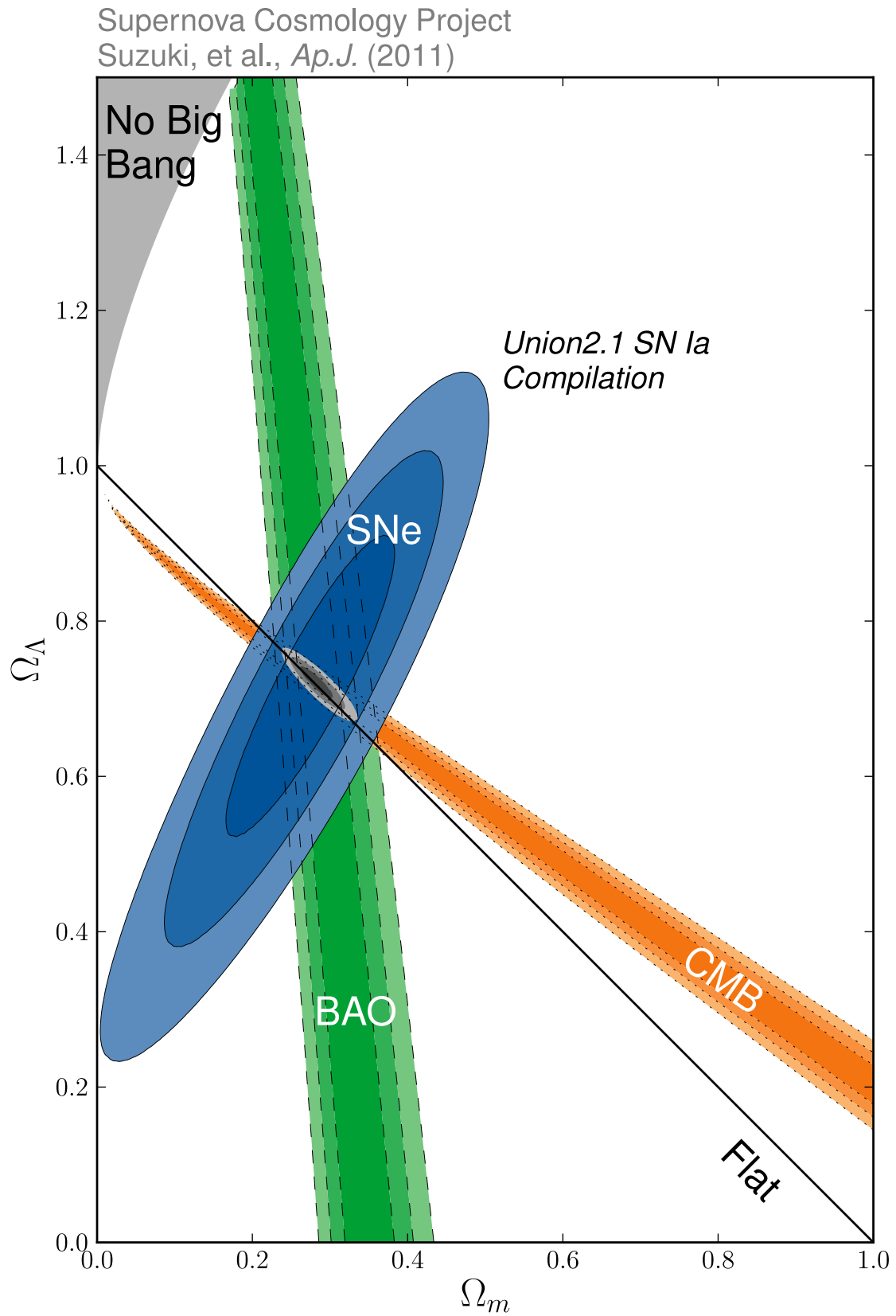


Figure 1.1 Constraints (68%, 95%, and 99.7% contours) on the energy density of the Matter and Dark Energy components of the Universe. Constraints from SNe (Union 2.1 Compilation) are shown in blue. Additional cosmological constants from the Cosmic Microwave Background (CMB, in orange) and Baryonic Acoustic Oscillations (BAO, in green) are also shown. Figure from Suzuki et al. (2012).

## 1.2 SN COSMOLOGY

The most important and most well-studied cosmological probes are the supernovae (SNe). Today, we know that there are two classes of SNe: thermonuclear (SN Ia) and core collapse (CC SN). The class mostly used as cosmological probes are the type Ia SNe since these are on average brighter and make a more coherent class of objects. All SN Ia explode at approximately the same luminosity, so the difference in brightness of a SN compared to another is due to a larger distance to the fainter one. The intrinsic scatter of the peak brightness of SN Ia in cosmological applications are on the order of 0.1 magnitude or less after correcting for light-curve shape and color at peak brightness (Conley et al., 2011, their Table 4). The intense study of SNe throughout the last few decades means that we have now reached the point where we are dominated by systematic uncertainties, not sample size. To further improve SNe as cosmological probes requires a knowledge of what is driving the scatter in the SN peak magnitude.

Since the quality of the spectral templates that are used to classify SNe also influence the scatter, a better calibration, especially in the rest-frame UV is one way of reducing the scatter. At higher redshift, the optical window will probe the rest-frame UV and the well-studied part of the spectrum is redshifted into the infrared (IR).

Another approach to understanding the source of the scatter is the notion that it is not our observations, but rather the SN population itself that is increasing the scatter due to mechanisms in the SN progenitors or explosions that are not yet understood. Further knowledge would then be gained by looking at correlations within the SN population.

Two important correlations — discovered in the 1990s — relate the peak brightness<sup>3</sup> to the shape of the light curve (Phillips, 1993) and the color near maximum (Riess et al., 1996), which push the intrinsic dispersion down to the order of 0.1 magnitudes or less. The correlation with respect to light-curve shape states that SNe with broader light curves are brighter than SNe with narrow light curves. It is believed that an intrinsically bright SN can sustain a longer light curve due to a larger amount of radioactive <sup>56</sup>Ni being synthesized in the explosion, which can then power the light curve for longer. Through modeling of the light curve, it is possible to infer a total <sup>56</sup>Ni-mass,  $m_{\text{Ni}}$ . The second correlation with the color near maximum is directly related to the dimming due to extinction along the line-of-sight, mainly in the host galaxy of the SN.

More recently, residual correlations with host properties have emerged. It was noticed that after a cosmological fit, the residuals between the magnitudes predicted by the cosmological expansion and the observed magnitude correlated with the stellar mass of the host galaxy (Hamuy et al., 2000; Kelly et al., 2010; Lampeitl et al., 2010; Sullivan et al., 2010; Childress et al., 2013b). Other host galaxy properties have also been proposed as the driver of this residual correlation. Hayden et al. (2013) used a linear combination of star formation and stellar mass,  $\mu_\alpha$ , that traces stellar mass, metallicity or age. They find that the residual correlations are strongest when  $\alpha$  is in the range that traces metallicity. This means that the underlying driver of the SN correlations is somehow connected to the metallicity of the environment of the SN.

Almost all of our current knowledge of how SNe and their hosts are connected is based on low- and intermediate-redshift samples like the Sloan Digital Sky Survey's (SDSS) SN sample found in Stripe 82 or the SN Legacy Survey (SNLS). In this thesis work, I will further investigate how SNe and their host galaxies are related by focusing on high redshift SNe ( $z > 1$ ) where the cosmic star-formation density was higher and the average metallicity was lower.

---

<sup>3</sup>Used to find the luminosity distance to the SN.

### 1.2.1 SUPERNOVA EXPLOSIONS

SNe are very energetic explosions that are bright enough to be seen across cosmic distances. The nomenclature we use today is based on observational characteristics that were observed long before we knew what the underlying physical mechanisms involved in the explosions were. This is why the thermonuclear explosions are called type Ia SN and core collapse SN are denoted among others as: type Ib, type Ic, type II, etc.

### 1.2.2 THE HISTORY OF SNE

Kirshner (2010) presents a general overview of the historical events that led to the nomenclature that is used today. The following is a short summary.

In the 1920s when — due to the work of Hubble — it became clear that the spiral nebulae were in fact distant galaxies, it also became clear that the novae seen in these extragalactic nebulae must be very different than the novae seen in the Milky Way.

Baade and Zwicky systematically studied this new class of extragalactic novae in the 1930s. By pure chance, none of the SNe that had spectra exhibited the presence of hydrogen. In the early 1940s, Minkowski began to see spectra of SNe that indeed show the presence of hydrogen. Baade's original group of SNe was therefore called type I and Minkowski's new group was called type II. The utility of type I SNe was noticed early by Baade as the SNe showed a dispersion of approximately one magnitude, making them suitable as distance indicators.

Later work during the 1970s and 1980s improved the knowledge of the spectral shape of type I SNe, and resulted in the current classification scheme used today, where type I SNe are subdivided into type Ia (Si features), type Ib (He features) and type Ic (no H, He or Si). The application of SNe in cosmology was first done by Kowal (1968) who produced a Hubble

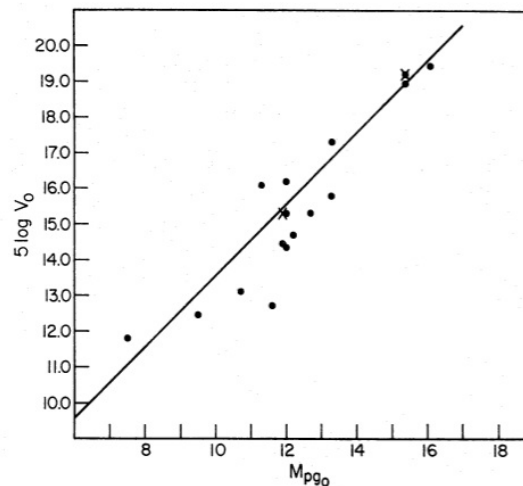


FIG. 1. The redshift-magnitude relation for supernovae of type I. The dots refer to individual supernovae, and the crosses represent averages for the Virgo and Coma clusters, as explained in the text.

Figure 1.2 The first rendition of a Hubble diagram using SNe by Kowal (1968).

diagram using 19 type I SNe (See Figure 1.2).

### 1.2.3 CORE COLLAPSE SNE

In this thesis, I will focus primarily on thermonuclear SNe and their applications in cosmology, but for completeness I will give a short review of core collapse SNe.

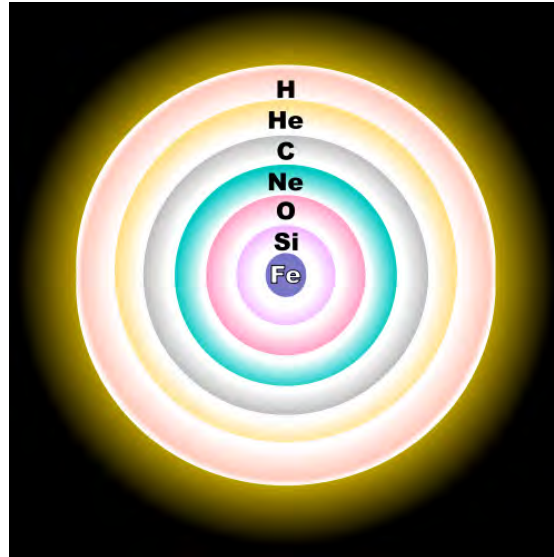


Figure 1.3 The onion-like structure of an evolved massive star (not to scale). (Credits: User:Rursus (R. J. Hall), via Wikimedia Commons)

Core collapse SNe are explosions of massive stars. Stars with masses above  $\sim 8M_{\odot}$  end their life when the star has burned the fuel in the core from hydrogen all the way up to iron, which results in an onion-like structure (Figure 1.3) of the star prior to the explosion. The SN explosion is then initiated by the decrease in radiation pressure when nucleosynthesis of iron stops. Then, the pressure due to the gravity of the outer layers exceeds the electron degeneracy pressure which starts a chain reaction of electron capture — literally pushing the electron into the protons to form neutrons — that rapidly shrinks the core to approximately the size of the earth. The outer layers start to free fall and bounce onto the newly formed neutron star which starts a shockwave traveling outwards through the outer layers of the star. The electron capture events create a strong flux of gamma rays and neutrinos powering the SN explosion.

The key classification scheme of core collapse SNe separates the SNe into groups based on spectral features. These spectral features provides information about the outer layer of the star, as seen in the list below.

**Type II** SNe show hydrogen features in their spectra. These are stars that still have their hydrogen envelope.

**Type Ib** SNe show helium features, but no hydrogen features. These stars have lost their hydrogen envelope but still have their helium envelope.

**Type Ic** SNe do not have hydrogen or helium features in their spectra. These stars have lost both their hydrogen and helium envelopes.

Additional sub-classifiers include type II-L and II-P, which are based on the shape of the light curve (linear decline or plateau) of the SN.

### 1.2.4 TYPE IA SNE

The small scatter in the magnitude of SN Ia explosions compared to the scatter of CC SNe and Galactic nova events hint towards a very uniform progenitor system. There is observational evidence that the SN light curve in the optical is powered by radioactive Ni-56, because the decay rate of the SN Ia light curve is consistent with the half life of first Ni-56 to Co-56 decay and later the decay of Co-56 to Fe-56. Optical spectra also show strong absorption features of iron-group elements. The total luminosity of a type Ia SN is equivalent to the energy released when converting a Chandrasekhar mass Carbon-Oxygen White Dwarf (C/O WD) into iron (Wang & Han, 2012; Thielemann et al., 2004). This leads us to believe that the progenitor systems of type Ia SNe must contain a C/O WD near the Chandrasekhar limit. The challenge is now to explain how the C/O WD grows from its initial  $\sim 0.4 M_{\odot}$  to the Chandrasekhar limit of  $\sim 1.4 M_{\odot}$ .

#### SN models

There are multiple of proposed models for how to bring the WD mass to the Chandrasekhar limit, but overall there are two broad classes of models: The so-called single degenerate (SD) and double degenerate (DD) systems.



Figure 1.4 An artist's impression of a single degenerate system. (Credits: NASA/CXC/M. Weiss)

The single degenerate system is a binary system with a WD and a non-degenerate donor star. The donor star can be either a main-sequence (MS) star, a red giant star or even a He star. Most SD models have a chain of events that contain: A Common Envelope (CE) phase and a stable accretion phase.

The CE phase happens early in the evolution of the progenitor system. The first star (labeled A) evolves away from the MS and develops a convective outer envelope which expands. If the outer layer expands beyond the Roche lobe (which happens for close binaries), material will flow from the A star to the MS star (labeled B). This process is unstable as the mass loss changes the moment of inertia. This will decrease the separation allowing for continued mass loss. The mass transfer will therefore continue until the Roche lobe around both stars is full and the CE phase is complete. During the CE phase, the separation between A and B decreases significantly (approximately by a factor of 100) due to drag forces in the CE. The CE phase lasts for on the order of years, and has therefore not been observed yet.

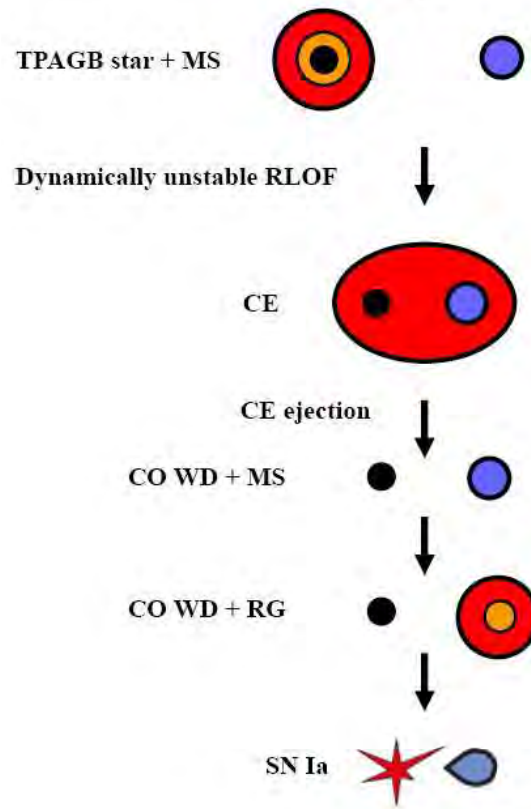


Figure 1.5 A schematic of the phases in the evolution of SD progenitors (adapted from Wang & Han, 2012). The star to the left is labeled A and the star to the right is labeled B. The A star will explode as a type Ia SN.

The accretion phase in the SD models happens towards the final stage of the progenitor system. The primary star A (the accretor) has evolved to a WD and depending on the model the secondary star B (the donor) has now evolved into a red giant, a helium star, or remains a MS star. It is in this phase that the WD is growing from its initial size towards the Chandrasekhar limit by burning the accreted matter into C/O. This stage is therefore crucial in all SD models.

The accretion can not proceed too rapidly as this would set off the accreted outer layer of H or He in a thermonuclear explosion. Such a nova-like event would consume all the accreted matter in the shell and potentially even some of the C/O from the original WD, taking it further away from the Chandrasekhar limit. This fine-balanced accretion needs to be regulated for these models to explain the rate of SN explosions. A proposed mechanism is the so called wind regulation, where a high accretion rate would produce a strong stellar wind from the WD, which serves as negative feedback to regulate the accretion rate.

The double degenerate SN channel consists of a double WD system. Like for the SD scenario, there will be a CE phase (or maybe multiple) when the two stars evolve off the MS and into WDs. The difference with respect to the SD scenario is that this channel does not end in a stable accretion phase, but a merger of the two WDs. The merger happens after enough gravitational waves have been radiated away for the WD to merge.

### 1.2.5 DELAY TIME DISTRIBUTION

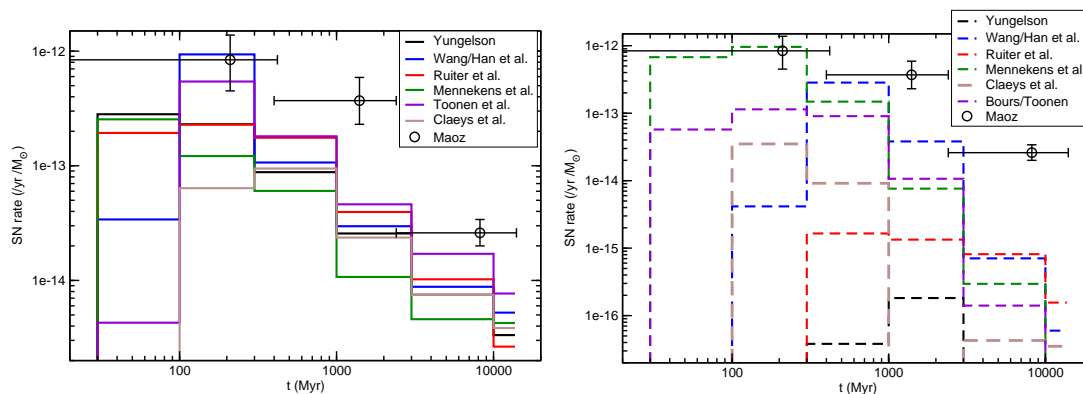


Figure 1.6 Delay time distribution of different double degenerate (left) and single degenerate (right) models (figure from Wang & Han, 2012). The three circles with error bars at the top are measurements of the observed delay times (Maoz et al., 2011).

One of the ways to differentiate between the different models is to measure the time from the formation of the progenitor system to the time the SN explodes, this is called the Delay Time Distribution (DTD). This distribution can then be compared to predictions from the SN models (see Figure 1.6).

In observations, we apply a phenomenological approach and divide the SNe into a prompt ( $< 300$  Myr), intermediate ( $0.3 - 2.3$  Gyr) or delayed ( $> 2.3$  Gyr) population. It is still not known how the models map to these three populations, but from the models plotted in Figure 1.6, it appears that DD models produce SNe on all three timescales. Some SD models on the other hand can only produce SNe on delayed and intermediate timescales.

The observed SN rate is the convolution of star-formation history<sup>4</sup> (SFH) and the DTD,

$$SNR(t) = SFR(t) \otimes DTD(t) = \int_0^t SFR(t - \tau) \cdot DTD(\tau) d\tau. \quad (1.4)$$

There are two approaches to calculate the observed DTD. The first approach is to compare the SN rate to the full SFH of the Universe, as was done by Dahlen et al. (2008b); Strolger et al. (2010); Graur et al. (2011a). Another approach is to use the SFH of the individual galaxies in the sample (Maoz et al., 2011, 2012) in Equation 1.4. In the first approach, the volumetric SN rate is calculated in redshift bins and compared to the volumetric SFH of the Universe (or cosmic SFH). This technique is critically sensitive to the assumed cosmic SFH, especially at high redshift where different measurements of the SFH vary. The approach is computationally more simple, as it only uses the sample of galaxies that host SNe. The second technique, on the other hand fits the SN rate of each galaxy (either zero or one, rarely two) to derive the DTD. This means that the DTD can be determined at any redshift from the survey directly, without relying on a good determination of the cosmic SFH.

<sup>4</sup>SFR as a function of time is referred to as "SFH" whereas "SFR" is the current or instantaneous SFR i.e. a number.

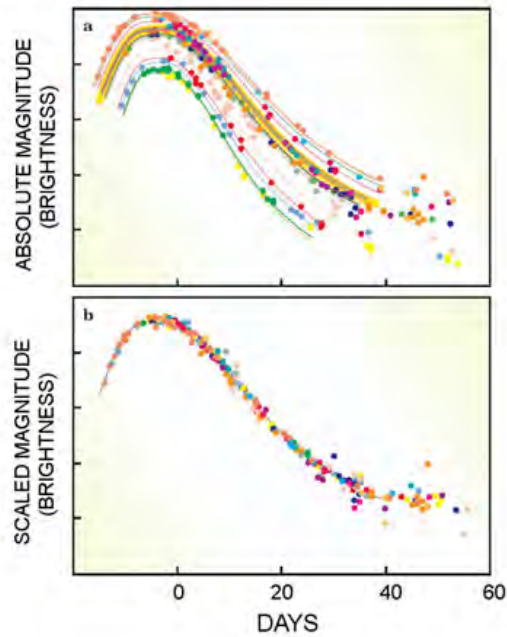


Figure 1.7 SN Ia light curves before and after correction. The broader light curves (slow decline rates) are brighter than the narrow light curves (fast decline rates). After correcting for brightness and stretch all light curves overlap. (Credit: <http://www-supernova.lbl.gov/>)

### 1.2.6 HOST CORRELATIONS

When type Ia SN are used for cosmology, we rely on the fact that SN explosions are standard candles. Phillips (1993) found that SNe with fast declining light curves were intrinsically fainter than the slow declining SNe. This finding, together with a similar relation (Riess et al., 1996) concerning the color of the SN at maximum brightness made it possible to infer a more precise intrinsic brightness of the SN, transforming them from standard candles to more accurate *standardizable* candles.

Hamuy et al. (2000) found that supernova in early-type galaxies are intrinsically fainter than SNe from star-forming galaxies, even after correcting for the light-curve shape and color. This residual correlation was later also observed in samples used to fit cosmology (Kelly et al., 2010; Lampeitl et al., 2010; Sullivan et al., 2010). This was done by determining the best fitting redshift-magnitude relation (a so-called Hubble diagram) and then calculate the magnitude deviation for each SN from the best fitting curve. This is called the Hubble residual of each SN. If all variation was captured by the light curve shape and color corrections, then all Hubble residuals should be distributed randomly around zero and not correlate with other parameters. The Hubble residuals correlate with the properties of the host, most strongly with the stellar mass of the host galaxy. However, the underlying source of this correlation is still unknown.

Hayden et al. (2013) fitted the Hubble residuals to a linear combination of stellar mass and star-formation rate,

$$\mu_{\alpha} = \log M_{*} - \alpha \log SFR, \quad (1.5)$$

where  $\alpha$  is the projection in the mass – SFR plane. When  $\alpha = 0$ ,  $\mu_\alpha$  corresponds to the stellar mass, when  $\alpha = 1$ ,  $\mu_\alpha$  corresponds to one over the specific SFR ( $1/sSFR$ ), which also is an age proxy of the host galaxy. At an intermediate value of  $\alpha = 0.32$ , Mannucci et al. (2011) found  $\mu_\alpha$  to correlate strongest with the gas-phase metallicity of field galaxies. Hayden et al. (2013) found that the strongest correlation with the Hubble residuals occurred at intermediate values of  $\alpha$  consistent with tracing the metallicity of the host galaxy.

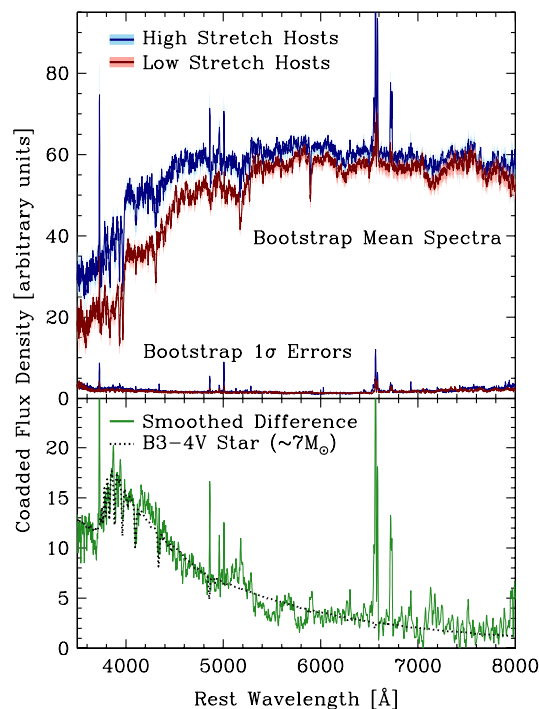


Figure 1.8 Top: Mean spectrum of high- and low-stretch SN host galaxy. Bottom: The difference between the two mean spectra, overplotted with a B-type stellar template. Figure taken from Brandt et al. (2010).

An interesting approach to gauge the difference between the brighter (broad light curves) and fainter (narrow light curves) SNe was done by Brandt et al. (2010). They constructed the mean spectrum of all host galaxies of SN with broad light curves, and subtracted the mean spectrum of all host galaxies of SN with a narrow light curve. The resultant spectrum was identical to a B-type stellar spectrum (Figure 1.8). This leads to the conclusion that the brightest SNe are somehow associated with a very young stellar population as opposed to fainter SNe.

Childress et al. (2013b) has combined all big samples (SDSS, SNLS, and the Nearby Supernova Factory) and finds a smooth step-like shape in the Hubble residuals. When analyzing the three samples as one set the amplitude of this step is  $0.086 \pm 0.016$  magnitudes. This is the first time that the shape of the Hubble-residual curve has been determined, but this now brings forward the question of whether and how the step function evolves with redshift. All this is dependent on what mechanism causes this effect. Childress et al. (2013b) discusses both dust, progenitor age, and metallicity effects, where dust by itself cannot account for the full variation. If the bulk of the variation is due to metallicity effects this can be accounted for by measuring the metallicity of each host and apply a correction derived from SN explosion models. If the

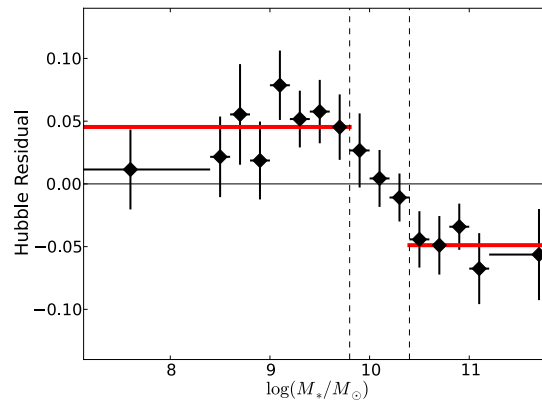


Figure 1.9 Hubble residual as a function of the stellar mass of the host galaxy. Figure from Childress et al. (2013b).

bulk of the variation is due to the change in progenitor ages a correction would rely on the detailed shape and evolution of the DTD.

The conclusion of Childress et al. (2013b) is that the intrinsic dispersion within the SN sample will not be significantly smaller after applying their host correction when used for cosmology, but not corrected for this effect would leave a systematic bias on the order of  $\sim 0.02 - 0.04$  at  $z \sim 1$ .

## 1.3 GALAXY EVOLUTION



Figure 1.10 Picture of a star forming nebula. New stars are emerging from the molecular cloud as small dots at the end of small antennae along the circumference of the cloud. (Credit: NASA/ESA/STScI J. Hester and P. Scowen)

In the context of this thesis I will focus on a specific set of properties that can be derived from the integrated light of a galaxy. I will also focus on the optical and near-IR parts of the spectrum as these are the regions where stars output most of their energy and where the Earth's atmosphere is transparent. The distribution of the energy output of the galaxy as a function of wavelength is called the Spectral Energy Distribution (SED). The shape of the SED is observationally inferred from broad-band photometry and spectra. We can infer properties like the ongoing star formation and the metallicity of the gas between stars by analyzing the emission lines in the rest-frame optical part of the SED. By looking at the overall shape of the continuum we can infer properties like the stellar age and stellar mass of galaxy.

The implied connection between the SNe and their host galaxies makes it interesting to go into the mechanisms that influence the formation of new stars and the enrichment of metals. I will not touch on the morphological aspects of galaxies in the following, I will therefore just consider galaxies merely as containers of stars, gas and dust.

Stars are formed from great clouds of gas and dust called Giant Molecular Clouds as perturbations cause the central regions of the cloud to collapse. The over-density in the cloud grows more compact. Pressure and density grows and a proto star is created. The protostar turns into a main sequence star when the central temperature and density is high enough to start forming hydrogen into helium. The first central stars in a molecular clouds are massive O and B stars that are luminous but short lived. These are called OB complexes, and trigger a second wave of star formation when they burn out and die as CC SN.

As stars burn out and die either as SNe (any type) or planetary nebulae they help enrich the ISM with metals synthesized in the star. These metals are then incorporated into the next generation of stars, thereby enriching the ISM with more and more metals for each generation of stars. The overall metallicity of a galaxy can also change due to the synthesized metals being

expelled by strong SN explosions or diluted by in-falling pristine gas.

### 1.3.1 STAR FORMATION RATE

There are multiple indicators from which we can infer the SFR of a galaxy (Kennicutt, 1998). The first being the flux of the  $H\alpha$  emission line — or any hydrogen recombination line<sup>5</sup>. This is due to the fact that recently formed stars emit much of their energy in the UV. These energetic photons excite and ionize the hydrogen in the vicinity<sup>6</sup> of the star. As the electron settles down into the ground state again it emits the hydrogen recombination lines. The  $H\alpha$  flux is therefore strongly correlated with the amount of ionizing flux and the number of young stars.

Another SFR indicator that relates directly to the energy output of young stars is the UV flux of the entire galaxy. As mentioned above, the young stellar population dominates over the older stellar population in the UV. The total energy output in the UV is therefore strongly correlated with the number of young stars.

So called obscure star formation occurs when the young stars are obscured by dust. This kind of star formation can be measured in the IR, because the young stars are heating the dust and due to energy conservation, this energy is radiated away as thermal radiation. The integrated SED of a galaxy will often have a blackbody-like emission peak at 10–100  $\mu\text{m}$ .

### 1.3.2 MAIN SEQUENCE OF GALAXIES

Among the most important descriptors of the evolutionary state of a galaxy is its stellar mass and SFR. When plotting these two parameters for a large sample of galaxies we would notice that the galaxies are not evenly distributed across this plane. Most galaxies would lie along a band called the Main Sequence (MS) of galaxies approximately along a line of constant sSFR. Galaxies above this sequence have high SFRs i.e strongly star forming or undergoing a star burst event. Galaxies below the MS are dormant and passive in nature and don't produce significant amount of new stars.

The MS evolved with redshift in accordance with the cosmic SFH. The cosmic SFH is increasing progressively at redshifts up to approximately  $z \sim 1 - 3$ . This period has been dubbed the Cosmic High Noon (Grogan et al., 2011). The evolution of the MS is consistent with a scaling of the SFR, maybe with a small change in the slope of the MS.

### 1.3.3 METALLICITY

The metallicity of a galaxy is inferred from two distinct sources. One source is the metals present in the interstellar gas near young stars, the so called gas-phase metallicity, of which oxygen is the main component. The amount of oxygen is inferred from emission-line ratios in the rest frame optical and near-IR. These emission-line ratios must be calibrated though, which is done either by some theoretical photoionization codes (e.g. Kewley & Dopita, 2002) or by empirical correlations (e.g. Pettini & Pagel, 2004). The individual measures of gas-phase metallicity do not always agree and often show systematic shifts between different calibrations. It is therefore necessary to transform metallicities measured in one calibration to another (see Kewley & Ellison, 2008).

The second reservoir of metals that can be inferred from the light of the galaxy resides in the photosphere of the stars themselves. This metallicity is mostly dominated by Iron (Fe) atoms

<sup>5</sup> $\text{Ly}\alpha$  is not well suited, but can technically be used.

<sup>6</sup>The region of fully ionized hydrogen around the star is called the Strömgren Sphere.

that leave absorption features in the stellar continuum. It is this metallicity that enters into the SED modeling described above. The two measures of metallicity need not be equal (measured in solar units), as different mechanisms act on the two phases on different time scales. The two phases are, however, very well correlated.

Metallicity can be a good measure of the evolutionary stage of the galaxy as the metallicity is directly influenced by the number of generations of SNe that have exploded. Both Oxygen and Iron are only released to the surroundings through SN explosions, whereas stars that do not end as SNe lock the synthesized metals into their white dwarf remnant.

### 1.3.4 SPECTRAL ENERGY FITTING

The overall shape and individual features of the galaxy SED contains a lot of information. By modeling the SED we can infer properties such as stellar age, stellar mass and extinction. The many pieces of SED fitting software publicly available all infer the properties of the galaxy in the same way by modeling stellar evolution and attenuation by dust. Some codes can also model other features of the SED like nebular emission lines in the optical or emissions from Polycyclic Aromatic Hydrocarbons (PAH) in the mid-IR. The crucial component is the stellar evolution modeling. The cornerstone in this modeling is the SED of a single stellar population (SSP), which is often calculated by specialized software, like GALAXEV (also known as BC03, Bruzual & Charlot, 2003). In short, the SED is calculated by assuming a population of stars distributed by mass according to an initial mass function (IMF). The population is then evolved along stellar isochrones to a specific point in time.

The SSPs can then either be used to model the starlight of the galaxy directly or be convolved with a star-formation history (SFH) to model a more realistic gradual star formation within a galaxy. From a monolithic collapse model, we expect the SFH to follow an exponentially declining SFR, a so called tau-model,  $SFR(t) \propto \exp(-t/\tau)$ . The true SFH is more stochastic in nature as minor and major merger events interrupt periods of more passive evolution (Lee et al., 2009).

In most practical applications of SED fitting — in particular when one is only fitting broadband photometry — the number of free parameters in the models are far too large to be constrained by the data. This means that we have to make some assumptions on some of the parameters, such as the IMF used or the parameterization of the SFH. All the inferred properties have to be compared in the light of these assumptions. In practice, parameters (e.g. stellar mass) can easily be transformed from one set of assumptions to another (e.g. from Salpeter to Chabrier IMF).

### 1.3.5 FUNDAMENTAL METALLICITY RELATION

Multiple studies have found a connection between the SFR, stellar mass, and gas-phase metallicity (Lara-López et al., 2010; Mannucci et al., 2010, 2011). This has been dubbed the Fundamental Metallicity Relation (FMR) by Mannucci et al. (2010). Lara-López et al. (2013) used Principal Component Analysis to show that there is a plane of lower dimensionality in the space of  $(SFR, M_*, 12 + \log(O/H))$ . This subsurface is usually plotted by projecting the mass-SFR plane onto a single axis  $\mu_\alpha$  using

$$\mu_\alpha = \log M_* - \alpha \log SFR, \quad (1.6)$$

where  $\alpha$  is an angle-of-projection parameter that determines the amount of mixing between the stellar mass and star-formation rate. A value of  $\alpha = 0$  implies  $\mu_\alpha = \log M_*$  and a value of  $\alpha = 1$  implies  $\mu_\alpha = -\log sSFR$  since the specific SFR is SFR per unit stellar mass. Mannucci

et al. (2010, 2011) determine that a value of  $\alpha = 0.32$  correlates strongest with the gas-phase metallicity.

## 1.4 FRONTIER SCIENCE WITH X-SHOOTER

X-shooter is the first of the second-generation instrument at the Very Large Telescope (VLT). The Niels Bohr Institute (NBI) has been a member of the consortium that built the instrument. Researchers at NBI therefore had guaranteed time of observation (GTO) when applying for time on the X-shooter instrument.

The X-shooter instrument is a spectrograph with an exceptionally large wavelength coverage from the atmospheric cut off in the U-band to the near-IR K-band. A very important property of this large wavelength range is that it is possible to derive an emission line redshift for any galaxy that is bright enough to be observed from the ground. For regular optical spectrographs the instrument can only detect emission lines from sources in specific redshift intervals. This is called the redshift desert. The X-shooter instrument can detect emission lines from sources where the lines have been redshifted out of the optical window and into the near-IR.

The CLASH and CANDELS surveys are large *Hubble Space Telescope (HST)* surveys that image the same fields very deep over three years (CLASH targets clusters, CANDELS targets previously well-observed fields). The surveys are conducted such that it is possible to look for transient objects between each visit to each field. For this project my supervisor and I joined the follow-up team of the SN search where we specialized in determining spectroscopic redshifts of the high-redshift sources that where in the redshift desert of optical spectrographs.

During this project we set some ground-breaking records. We determined the spectroscopic redshift of the two highest redshift SN Ia ( $z = 1.55$  and later  $z = 1.91$ ) and the highest redshift CC SN ( $z = 2.37$ ). The fast determination of the redshift for each SN candidate was invaluable for the optimizing and prioritizing of further follow-up with HST, making X-shooter a key player in this SN search.

## 1.5 THESIS OUTLINE AND DESCRIPTION

In this thesis I will investigate the connection between high redshift SNe and their host galaxies.

In the next two chapters (paper I+II) I present the properties of two high redshift SN host galaxies, as inferred from strong emission lines and broadband photometry. In both cases I find young, star forming, metal poor galaxies. The galaxies are above the MS of galaxies defined by SDSS galaxies, but consistent with the MS derived for galaxies at  $z = 1$  and  $z = 2$ . Even though they are consistent with the MS both are on the star forming side of the median relation. The SN Primo host might even be classified as a bursting galaxy depending on the threshold. In the paper we advocate a fixed sSFR cut between regular star forming galaxies and stardust galaxies instead of using the MS as a reference. This is also motivated by the fact that the MS at high redshift is derived from galaxy samples that do not extend down to the mass of the SN Primo host.

Chapter 3 (Paper II) had the added objective of confirming that the detected transient was not due to AGN activity or a low redshift interloper. The Subaru Deep Field (SDF) SN search relies heavily on photometry (and existing catalogs) when classifying the transients and deriving redshifts. The reconstructed SN rates are therefore sensitive to catastrophic outliers (wrong photometric redshift or wrong classification) at high redshift due to low number statistics.

In chapter 4 I present the full sample of high redshift SN hosts found in the CLASH and

CANDELS surveys. I determine stellar parameters such as stellar mass, age, SFR, and extinction. From this sample I determine the ratio between the prompt and delayed population of SN and find that this ratio is consistent with no evolution out to  $z \sim 2$ . I also propose an explanation of why the A+B model determines different parameters for surveys at different redshifts.

From my thesis work I have found that the sSFR of SNe host galaxies on average are 0.5 – 5 times the sSFR MS proposed by Elbaz et al. (2011)<sup>7</sup>. This shows that SN host galaxies are galaxies that are forming stars at average to above average rates. Likewise I show that the metallicity of two of our high redshift SNe host galaxies are consistent with FMR in the same way as regular field galaxies at low redshift. This is in line with what was found for the SN factory (Childress et al., 2013a).

The data presented in my thesis also hints towards a lack of evolution of the shape of the DTD out to a redshift of  $z = 2$ . This can become an important piece of evidence against strong evolutionary effect in the progenitor type or mix of type out to the cosmic high noon ( $z \sim 2$ ).

---

<sup>7</sup>The author classifies everything with a sSFR between 0.5 – 2 times the median relation as MS galaxies and a sSFR above 2 times as a starburst galaxies.



## 2

# THE FIRST SUPERNOVA

*I conclude, therefore, that this star is not some kind of comet or a fiery meteor... but that it is a star shining in the firmament itself one that has never previously been seen before our time, in any age since the beginning of the world.*

Tycho Brahe

**ABSTRACT** – We present VLT/X-shooter observations of a high redshift, type Ia supernova host galaxy, discovered with HST/WFC3 as part of the CANDELS Supernova project. The galaxy exhibits strong emission lines of Ly $\alpha$ , [O II], H $\beta$ , [O III], and H $\alpha$  at  $z = 1.54992^{+0.00008}_{-0.00004}$ . From the emission-line fluxes and SED fitting of broad-band photometry we rule out AGN activity and characterize the host galaxy as a young, low mass, metal poor, starburst galaxy with low intrinsic extinction and high Ly $\alpha$  escape fraction. The host galaxy stands out in terms of the star formation, stellar mass, and metallicity compared to its lower redshift counterparts, mainly because of its high specific star-formation rate. If valid for a larger sample of high-redshift SN Ia host galaxies, such changes in the host galaxy properties with redshift are of interest because of the potential impact on the use of SN Ia as standard candles in cosmology.

## 2.1 INTRODUCTION

Type Ia Supernovae (SNe Ia) are cornerstones of modern cosmology because of their properties as luminous standard candles. The development of these important cosmological tools began in the late 1930's when Zwicky (1938) and Wilson (1939) first suggested that SNe could be used as distance indicators. Theoretical developments in the 1960's suggested that SNe of type Ia form a homogenous class of objects with a measured peak magnitude of  $M_B \approx -19.3 + 5 \log h_{70}$  (for a modern review, see Hillebrandt & Niemeyer, 2000; Kirshner, 2010). To first approximation, the light curves of SN Ia form a one-parameter family of models, driven by the decay of radioactive  $^{56}\text{Ni} \rightarrow ^{56}\text{Co} \rightarrow ^{56}\text{Fe}$ . The amount of radioactive nickel produced in the initial explosion therefore dictates the shape of the light curve. Later observational work showed that the scatter in the peak magnitude is correlated with other SN properties, such as light curve shape and color (Phillips, 1993; Riess et al., 1996; Phillips et al., 1999).

SN cosmology achieved its modern prominence at the close of the millennium with the discovery of the accelerating expansion of the universe, based on just a few dozen objects (Perlmutter et al., 1999; Riess et al., 1998). Nearly 15 years later, modern SNIa samples can now include over 500 well-studied SNe with a dispersion in peak magnitudes of  $\sim 0.16$  magnitudes (e.g., Conley et al., 2011; Suzuki et al., 2012). At this precision, a larger sample size alone will

not improve cosmological constraints, so the limiting factor is our understanding of systematic effects.

Among the major concerns for systematic biases is the fact that we still do not have a complete or conclusive description of the SN Ia progenitor systems. Indeed, there may be several viable progenitor pathways (known as single and double degenerate models, see Wang & Han, 2012, for a review), possibly leading to slightly different explosion characteristics. One might expect different progenitor pathways to be correlated with differences in SN environment, and such correlations with host galaxy properties have recently been observed (Hamuy et al., 2000; Kelly et al., 2010; Lampeitl et al., 2010; Sullivan et al., 2010). Correcting for this effect with measurement of the host galaxy stellar mass brings the dispersion in absolute peak magnitude down to  $\sim 0.1$  magnitudes (Conley et al., 2011; March et al., 2011). This signature of environmental effects calls for further characterization of the host galaxies when SNe are used for cosmography. Riess & Livio (2006) discuss how a change in the progenitor population (like progenitor metallicity and age) at  $1.5 < z < 3.0$  could affect the inferred distance in a way inconsistent with dark energy models. The redshift window  $1.5 < z < 3.0$  is therefore favorable for disentangling systematic effects arising from environment.

The Cosmic Assembly Near-IR Deep Extragalactic Legacy Survey (CANDELS) survey (Grogin et al. 2011) is a Hubble Space Telescope (HST) multi-cycle treasury (MCT) program designed to detect high redshift SNe. The CANDELS collaboration is surveying five well-observed fields (GOODS-N, GOODS-S, COSMOS, EGS and UDF). With this observation strategy CANDELS will find SNe Ia out to redshifts of  $\sim 2$  (see Rodney et al., 2012). The first SN detected in the CANDELS survey was discovered 2010 October 14 in the GOODS-S field and was nicknamed SN Primo. Rodney et al. (2012) present the light curve and grism spectrum of this SN, concluding that SN Primo was of type Ia.

The aim of this paper is to characterize the host galaxy of SN Primo. We derive its spectral properties from spectroscopic emission-line fluxes and fit the spectral energy distribution (SED) based on broad-band photometry to constrain its stellar population. We then compare the properties of the host galaxy of SN Primo with its counterparts at lower redshifts and discuss sources of bias when using high redshift SNe as standard candles.

The paper is structured as follows: In Section 2.2 we present the spectra and photometric data. In Section 2.3 we perform the SED fitting using broad-band photometry to get stellar mass and stellar age and we derive the emission-line fluxes and calculate spectral properties like metallicity and the Lyman- $\alpha$  escape fraction. Finally, a discussion and conclusions are given in Section 2.4. We assume a flat  $\Lambda$ CDM cosmology, with  $H_0 = 70.2 \text{ km s}^{-1} \text{ Mpc}^{-1}$  and  $\Omega_m = 0.274$  (Komatsu et al., 2011). All magnitudes given in this paper are AB magnitudes.

## 2.2 DATA

### 2.2.1 SPECTROSCOPIC DATA

The host of SN Primo is located in the GOODS-S field at R.A. =  $03^{\text{h}}32^{\text{m}}22^{\text{s}}.64$  and decl. =  $-27^{\circ}46'38''.66$  (J2000). The spectroscopic observations were performed on 2010 October 16, using the X-shooter instrument on the ESO Very Large Telescope (VLT) at Paranal Observatory, Chile (D’Odorico et al., 2006; Vernet et al., 2011). X-shooter is a cross-dispersed Echelle spectrograph with a large wavelength coverage from the UV to the Near IR (300 – 2500 nm). This is achieved by splitting the light beam into three wavelength regions and sending them into three different spectrographs (so-called arms) designated UVB (for UV and Blue,  $\sim 300 - 550 \text{ nm}$ ), VIS (for Visual,  $\sim$

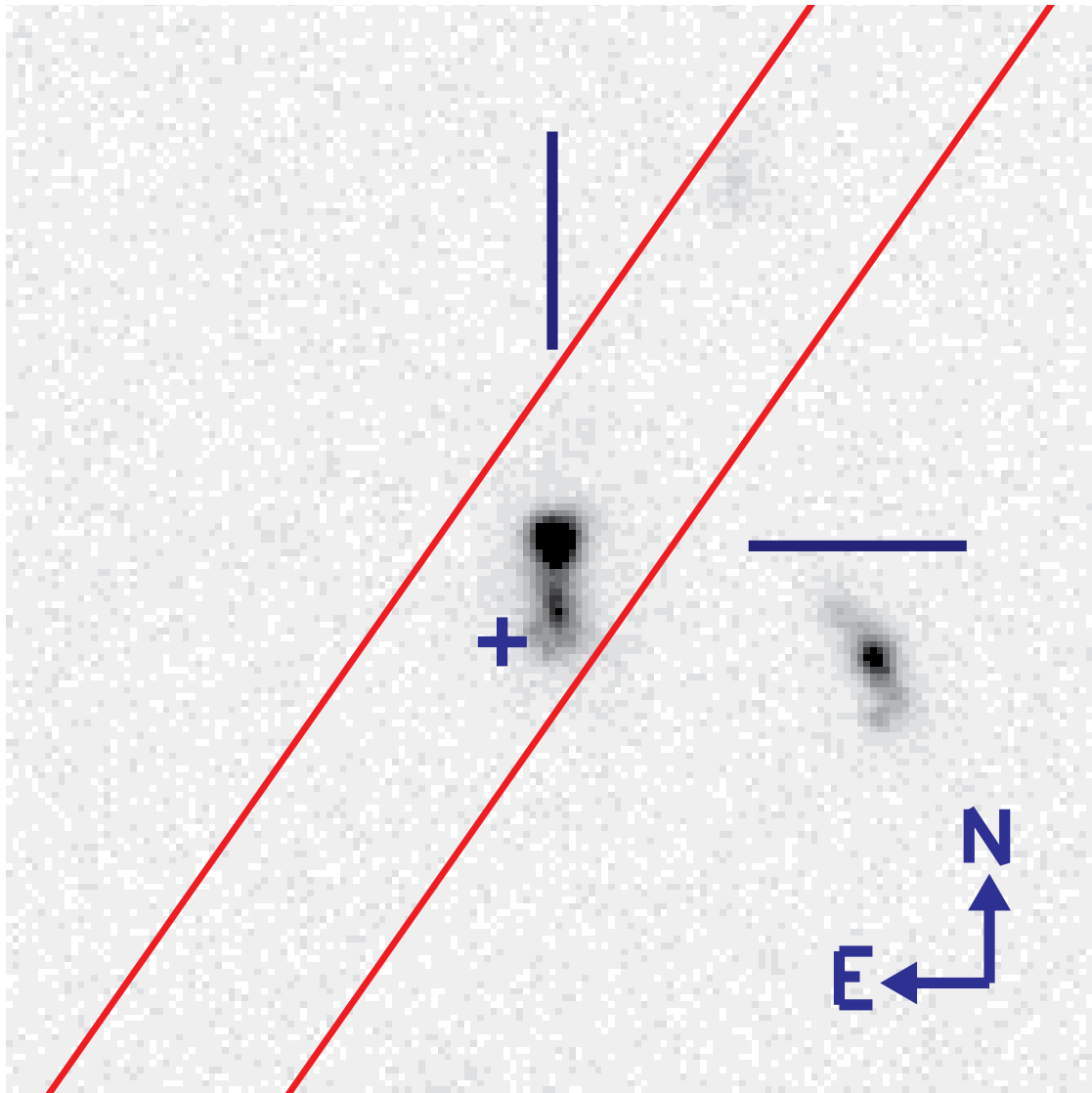


Figure 2.1 Pre-explosion *HST* F775W (i-band, rest frame u-band) image with the X-shooter slit configuration overlaid (red). The peak luminosity of the host galaxy is marked by ticks (blue). The size of the tick marks is  $1''$ , corresponding to 8.6 kpc at the redshift of SN Primo. The faint part to the south is also part of the galaxy (see Rodney et al., 2012). The location of the SN is marked by a plus (blue).

550 – 1000 nm), and NIR (for Near IR,  $\sim 1000 - 2500$  nm). For the observation we used an ABAB on-source nodding template with an exposure time of 1.3 hr ( $4 \times 1200$  sec). A  $0.''9$  slit<sup>1</sup> with a PA of  $-35^\circ$  E of N was placed to cover both the host and the SN (see Figure 2.1). The observations were conducted under photometric conditions, with a median seeing<sup>2</sup> of  $0.''54$ .

The X-shooter spectra were reduced using the official X-shooter pipeline<sup>3</sup> v1.3.7. We achieved

<sup>1</sup>A  $1.''0$  slit in the UVB arm.

<sup>2</sup>As measured by the Paranal on-site seeing monitor

<sup>3</sup>See, <http://www.eso.org/sci/software/pipelines/>

resolving powers of  $R = 5400 \pm 360$  (UVB),  $R = 7450 \pm 300$  (VIS), and  $R = 5800 \pm 180$  (NIR). The extraction of the object spectra was conducted with our own IDL script, and flux calibration was done using the *HST* flux standard star, GD71<sup>4</sup>.

Even though the SN was still bright it was not detected in the spectrum (see Figure 2.3); only narrow emission lines from the host galaxy were visible with no trace of any continuum emission from either host or SN.

## 2.2.2 FLUX CALIBRATION QUALITY

We checked the quality of the flux calibration using a telluric standard star (HIP 018926) taken prior to the science exposure. The telluric standard star was of stellar type B3V, and has a high signal-to-noise ratio ( $\sim 50$ – $300$  per wavelength bin,  $0.04$ – $0.1$  nm per bin). The telluric standard star was reduced, extracted and flux calibrated in the same way as the science exposure. The flux calibrated spectrum agrees with the published photometric data points. A model spectrum of a B3V star was scaled to the photometric data and compared to the flux calibrated spectrum. The agreement between the model and the spectrum was within 5–10%, consistent with the expected quality of the flux calibration for X-shooter<sup>5</sup> at the wavelengths of the lines detected in the science exposures (except at the location of Ly $\alpha$ ). At an observed wavelength of 310 nm Ly $\alpha$  is close to the spectral lower limit of the UVB arm (300 nm). The discrepancy between the model and the telluric spectrum is  $\sim 40\%$ , i.e., the conversion factor between counts and cgs units is too large and will overestimate the flux of Ly $\alpha$ . We are therefore cautious when drawing conclusions based on the flux of the Ly $\alpha$  line.

## 2.2.3 PHOTOMETRIC DATA

To construct the SED for the host of SN Primo, we use photometry from the F160W filter (H-band) selected TFIT catalogue. The photometry in each band is carried out using the TFIT algorithm (Laidler et al., 2007). This method performs point-spread function (PSF) matched photometry uniformly across different instruments and filters, despite their large variations in PSFs and pixel scales. The final catalogue has photometry in VLT/VIMOS (U-band), *HST*/ACS (F435W, F606W, F775W, and F850LP), *HST*/WFC3 (F105W, F125W, and F160W), VLT/ISAAC ( $K_s$ ), and two *Spitzer*/IRAC channels ( $3.6 \mu\text{m}$  and  $4.5 \mu\text{m}$ ). The SN search uses the *HST*/WFC3 bands. To get SN free photometry in these bands a set of pre-explosion images from another *HST*/WFC3 survey (GO-11563, PI:Illingworth, see e.g. Oesch et al., 2010) was used. The photometry is listed in Table 1. The *HST* (WFC3) observations are performed as a part of CANDELS project and are further described in Grogin et al. (2011) and Koekemoer et al. (2011). More details on the rest of the filters and observations are given in Dahlen et al. (2010).

## 2.3 ANALYSIS

### 2.3.1 BROAD-BAND SED FITTING

The broad-band SED of the host of SN Primo (Table 2.1) covers rest frame UV to near-IR (200 – 2000 nm). We use the SED fitting code FAST (Kriek et al., 2009) to derive properties such as stellar mass,  $M_*$ , and stellar age,  $t_*$ . The photometric data is corrected for the strong emission lines detected in the spectrum by subtracting the line flux from the corresponding filters. The

<sup>4</sup>See, <http://www.eso.org/sci/observing/tools/standards/spectra/gd71.html>

<sup>5</sup><http://www.eso.org/sci/facilities/paranal/instruments/xshooter/doc/>

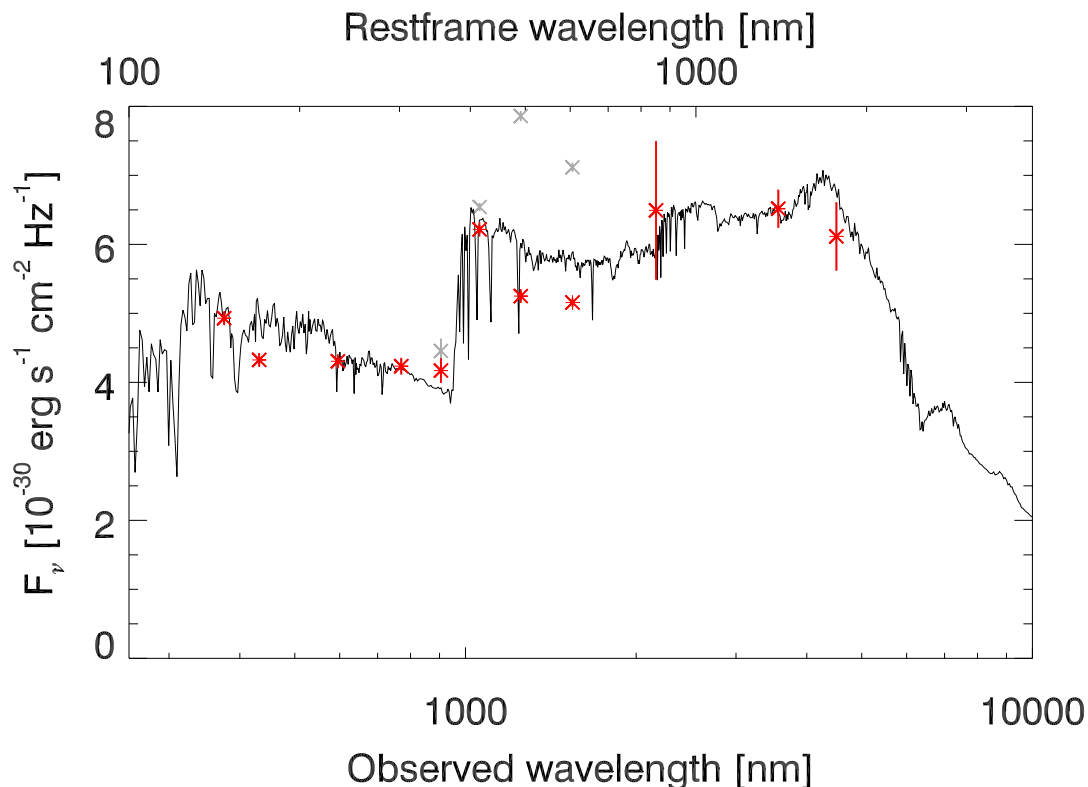


Figure 2.2 The SED of the SN Primo host derived from broad-band photometry. In red (gray) are the photometric points after (before) the subtraction of the emission-line flux. Overplotted is the best-fitting model SED from FAST.

strong emission lines are not modeled by the stellar population synthesis models of Bruzual & Charlot (2003) used by FAST. For each filter that has strong emission lines the flux is corrected as

$$F_{\nu}^{(\text{corr})} = F_{\nu} - \frac{F_{\text{line}}}{\Delta\nu}, \quad (2.1)$$

where  $F_{\nu}$  is the flux density in the broad-band filter,  $F_{\text{line}}$  is the flux in the emission line, and  $\Delta\nu = \int T(\nu) d\nu \cdot T(\nu_{\text{line}})^{-1}$  is the integral of the filter curve, corrected for the transmission of the filter at the location of the emission line. We use the same transmission function that is used in FAST for each filter.

The emission-line-subtracted SED is corrected for Galactic extinction (Schlegel et al., 1998,  $E(B - V) = 0.008^6$ ) using a Galactic extinction-law (Cardelli et al., 1989) and  $R_V = 3.1$ . We use FAST to fit the corrected SED assuming a Chabrier (2003) initial mass function (IMF) and three different star-formation histories (SFH, see Table 2.2 and Figure 2.2). The masses, ages and star-formation rates (SFR) derived in Table 2.2 assuming different SFH agree within the  $1\sigma$  uncertainties.

We also run the SED fitting without any correction to the broad-band SED, but excluding the J and H band to get a second measure of the physical parameters. This second measure quantifies the systematic shift that the correction procedure can put on the physical parameters.

<sup>6</sup>Quoted from the NASA/IPAC Extragalactic Database (NED) website: <http://ned.ipac.caltech.edu/>

We check that the best fitting parameters of this second fit is within the  $1\sigma$  error bars. For reference the shift in  $\log(M_*)$  is 0.07 higher for the second fit, compared to the upper error bar of 0.13 on our main SED fit.

### 2.3.2 RESAMPLING OF THE X-SHOOTER SPECTRUM

We correct the spectrum for Galactic extinction in the same manner as the broad-band photometry. To obtain a robust estimate of the uncertainties in the spectral quantities such as the metallicity or line ratios, we re-sample the X-shooter spectrum 10 000 times. For each wavelength bin we resample the flux using the error spectrum (assuming gaussian error). In each iteration the spectral lines are fitted with a gaussian line profile and the centroid, the Full Width at Half Maximum (FWHM), and the total flux is calculated (see Table 2.3 and Figure 2.3). The redshift is determined from  $H\alpha$ , [O II]  $\lambda 3729$ , [O III]  $\lambda\lambda 4959, 5007$  in each iteration. All reported values that are derived from the spectrum are the median values and 68% error bars of the 10 000 samplings. The heliocentric velocity correction is  $6.54 \text{ km s}^{-1}$ , calculated using the IRAF task `rvcorrect`.

Special care is taken when fitting [O II]  $\lambda\lambda 3726, 3729$  and  $H\beta$  in each resampling: The blue component of the [O II] doublet, [O II]  $\lambda 3726$ , is located on top of a sky line. After masking out the sky line it is impossible to fit the peak of [O II]  $\lambda 3726$ . We therefore fit a double-gaussian line-profile to [O II]  $\lambda\lambda 3726, 3729$ . We fix the peak of the blue components,  $\lambda_{\text{blue}}$ , to the peak of the red component,  $\lambda_{\text{red}}$ , by requiring  $\lambda_{\text{blue}}/\lambda_{\text{red}} = 372.6032\text{nm}/372.8815\text{nm}$ . The flux ratio of the two components is left as a free parameter.

$H\beta$  is also located on top of a sky line with the wings visible. We remove the sky line in the same manner as for [O II]  $\lambda 3726$  and fix the wavelength,  $\lambda_0$ , and FWHM of the fit.  $\lambda_0$  is fixed to  $\lambda_{H\beta}(1+z)$ , where  $\lambda_{H\beta} = 486.1325\text{nm}$ . The FWHM is fixed to the measured FWHM of  $H\alpha$  in velocity units. The instrumental broadening of spectral lines is constant if measured in velocity units and therefore affects  $H\alpha$  and  $H\beta$  equally. The derived flux may be biased if a gaussian line profile is not a correct description of the line. Due to the uncertainties in the  $H\beta$  detection we will not use the derived flux, other than for constraining the Balmer decrement. For all other purposes we set the flux of  $H\beta$  equal to the flux of  $H\alpha$  divided by 2.86 (see discussion in Section 2.3.3).

We do not detect [N II]  $\lambda 6583$  in the spectrum. To derive an upper limit of the flux, we measure the standard deviation of the flux density at the location of the line,  $\lambda_{\text{NII}}(1+z) \pm 2\Delta\lambda$ , where  $\lambda_{\text{NII}} = 658.346\text{nm}$  and  $\Delta\lambda = \lambda/R$  is the size of one resolution element. Table 2.3 lists the  $5\sigma$  upper limit of the non-detection.

### 2.3.3 HOST EXTINCTION

We correct the X-shooter spectrum for Galactic extinction in the same manner as for the broad-band SED. We test if the  $A_V$  from SED fitting is consistent with the spectrum. To gauge the intrinsic extinction from the spectrum we measure the Balmer decrement,  $H\alpha/H\beta$ . By comparing the measured Balmer decrement,  $B$ , with the expected  $B_0 = 2.86$  given in Osterbrock & Ferland (2006) (case B recombination,  $T_e = 10^4 \text{ K}$ ), we calculate the extinction as

$$A_V = -2.5 \log \left( \frac{B}{B_0} \right) \frac{k(V)}{k(H\alpha) - k(H\beta)}, \quad (2.2)$$

where  $k(\lambda) = A_\lambda/E(B-V)$ :  $k(V) \equiv R_V = 3.1$ ,  $k(H\alpha) = 2.468$ , and  $k(H\beta) = 3.631$  (Calzetti, 2001). We assume  $R_V = 3.1$  because the SED and the spectrum probe the luminosity weighted

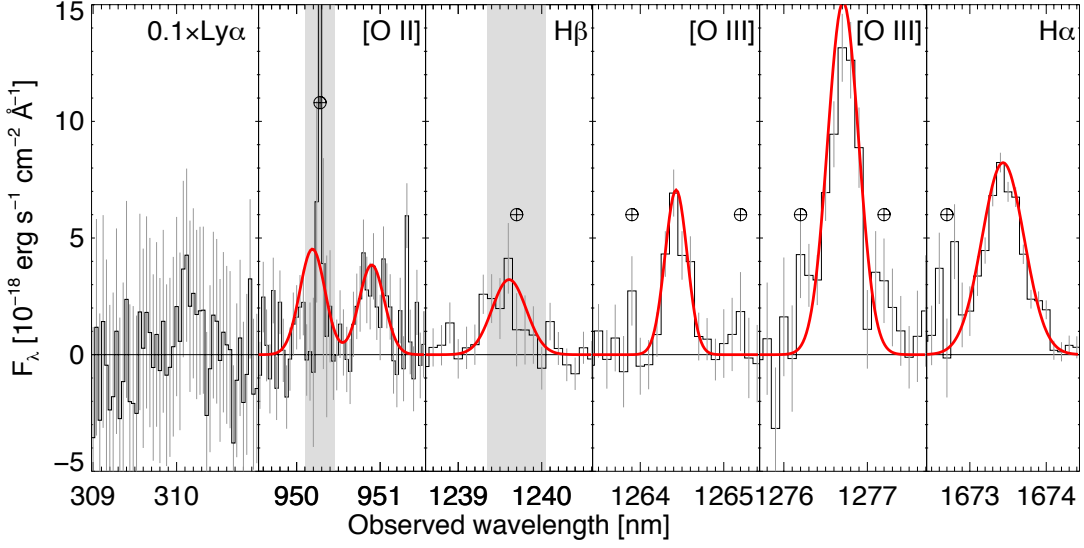


Figure 2.3 The detected emission lines in the X-shooter spectrum of the host of SN Primo. The spectrum is flux-calibrated and corrected for Galactic extinction. The solid (red) line shows the best fitting gaussian line profiles. The [O II]  $\lambda\lambda 3726, 3729$  line is fitted with a double gaussian line profile. The gray bands mark regions excluded due to sky lines. In the  $H\beta$  fit the line center was fixed to  $\lambda_{H\beta}(1+z)$ , where  $\lambda_{H\beta} = 486.1325$  nm and  $z$  is the redshift.  $Ly\alpha$  is detected, but located close to the Earth’s atmospheric UV cutoff.

average  $R_V$  of the host of SN Primo and not just the SN sight line, where a lower  $R_V$  (down to  $\sim 1.7$ ) can be measured (Phillips, 2012).

The value  $A_V = 0.6^{+1.1}_{-0.7}$  derived from the Balmer decrement is consistent with the value derived from the SED fitting. The large uncertainty in  $A_V$  is due to the difficulty in estimating the  $H\beta$  flux (see Section 2.3.2). For reference, the extinction derived from the SN light curve is  $A_V = 0.14 \pm 0.14$  (Rodney et al., 2012), but it does not have to be linked to the (luminosity weighted) average of the galaxy as a whole.

### 2.3.4 METALLICITY

Given that we do not detect [N II] or [S II] lines in our spectrum we will use the line ratio,

$$R_{23} = \log \left( \frac{[\text{O II}]_{\lambda\lambda 3726, 3729} + [\text{O III}]_{\lambda\lambda 4959, 5007}}{H\beta} \right), \quad (2.3)$$

to determine the metallicity. We take the average of the two  $R_{23}$  calibrations (McGaugh, 1991; Kobulnicky & Kewley, 2004) as used in Kewley & Ellison (2008) whose procedure we follow.

The  $R_{23}$  diagnostic has the problem of being double valued, meaning that from a measured  $R_{23}$  value two metallicities can be inferred (see Figure 2.4). We therefore need an independent measure to break this degeneracy. The upper limit on [N II]  $\lambda 6586$  gives an upper limit on

$$\log \left( \frac{[\text{N II}]_{\lambda 6586}}{[\text{O II}]_{\lambda\lambda 3726, 3729}} \right) < -1.0. \quad (2.4)$$

This constrains the metallicity to the low metallicity branch of  $R_{23}$  (see Kewley & Dopita, 2002, their Figure 3). The low metallicity branch of  $R_{23}$  changes with ionization parameter,  $q$ . To

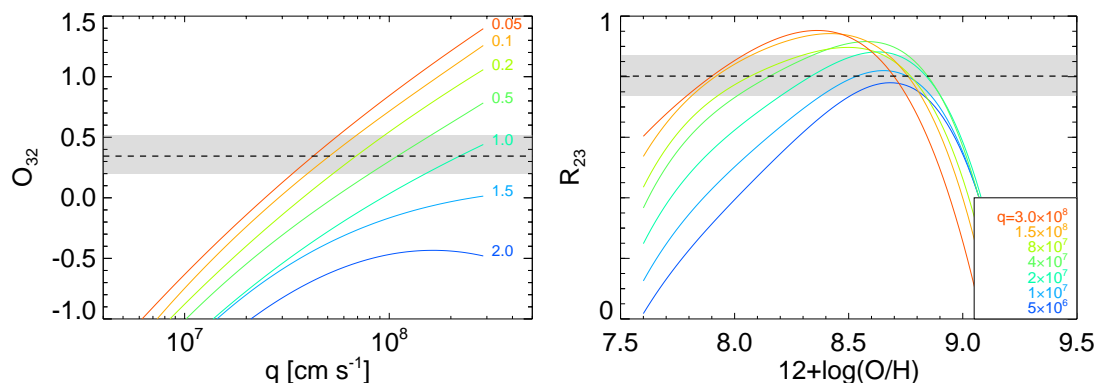


Figure 2.4 The  $O_{32}$  and  $R_{23}$  line ratios of the host of SN Primo together with the photo-ionization models of Kewley & Dopita (2002). The dashed lines and gray bands show the line ratios and  $1\sigma$  error bars derived from the spectrum. Left:  $O_{32}$  (Equation 2.5) versus the ionization parameter  $q$ . From top down the metallicities are  $Z = 0.05, 0.1, 0.2, 0.5, 1.0, 1.5,$  and  $2.0 Z_{\odot}$ . Right:  $R_{23}$  (Equation 2.3) versus the metallicity. From the top down  $q = 30, 15, 8, 4, 2, 1, 0.5 \times 10^7 \text{ cm s}^{-1}$ .

break the  $q$ -degeneracy, we need the line ratio

$$O_{32} = \log \left( \frac{[\text{O III}]_{\lambda 5007}}{[\text{O II}]_{\lambda \lambda 3726, 3729}} \right), \quad (2.5)$$

see Figure 2.4. The procedure of Kobulnicky & Kewley (2004) is to iterate back and forth between the two plots of Figure 2.4 until the estimates of metallicity and  $q$  converge. In Kobulnicky & Kewley (2004) convergence is achieved after three iterations. We use 10 iterations in our implementation as this makes the convergence independent of the choice of initial guess. The metallicities derived from the two techniques are within the 0.1 dex of each other, which is the expected scatter of the two techniques (Kewley & Dopita, 2002; Kewley & Ellison, 2008). The metallicity of the SN Primo host is  $12 + \log(\frac{\text{O}}{\text{H}}) = 8.12^{+0.09}_{-0.10}$  or  $Z = 0.27 \pm 0.06 Z_{\odot}$ , assuming a solar abundance of  $12 + \log(\frac{\text{O}}{\text{H}}) = 8.69$  (Asplund et al., 2009).

### 2.3.5 STAR FORMATION

We check whether the emission lines of the host of SN Primo are powered by star formation or AGN activity by plotting  $\log([\text{N II}] \lambda 6586/\text{H}\alpha)$  versus  $\log([\text{O III}] \lambda 5007/\text{H}\beta)$  in a BPT diagnostics diagram (Baldwin, Phillips, & Terlevich, 1981). The host of SN Primo is located in the star-forming region of Figure 2.5. We therefore conclude that the  $\text{H}\alpha$  flux is powered by star formation. We derive the SFR from the  $\text{H}\alpha$  luminosity. We report the SFR for different IMFs for comparison (Kennicutt, 1998; Brinchmann et al., 2004; Mannucci et al., 2010). Using the stellar mass from SED fitting we calculate the specific SFR,  $\text{sSFR} = \text{SFR}/M_*$  from the spectrum and obtain a value of  $\sim 10^{-8} \text{ yr}^{-1}$ , independent of the IMF and SFH, making the host of SN Primo a starburst galaxy. Our definition of a starburst is based on the sSFR (see, e.g. Sullivan et al., 2006, for a review), see Section 2.4 for discussion on other definitions.

### 2.3.6 LYMAN- $\alpha$

We detect  $\text{Ly}\alpha$  emission at  $2.8\sigma$  in the spectrum (see Figure 2.6). This is possibly the lowest redshift ground-based detection of a cosmological  $\text{Ly}\alpha$  emitter. The significance of the detection

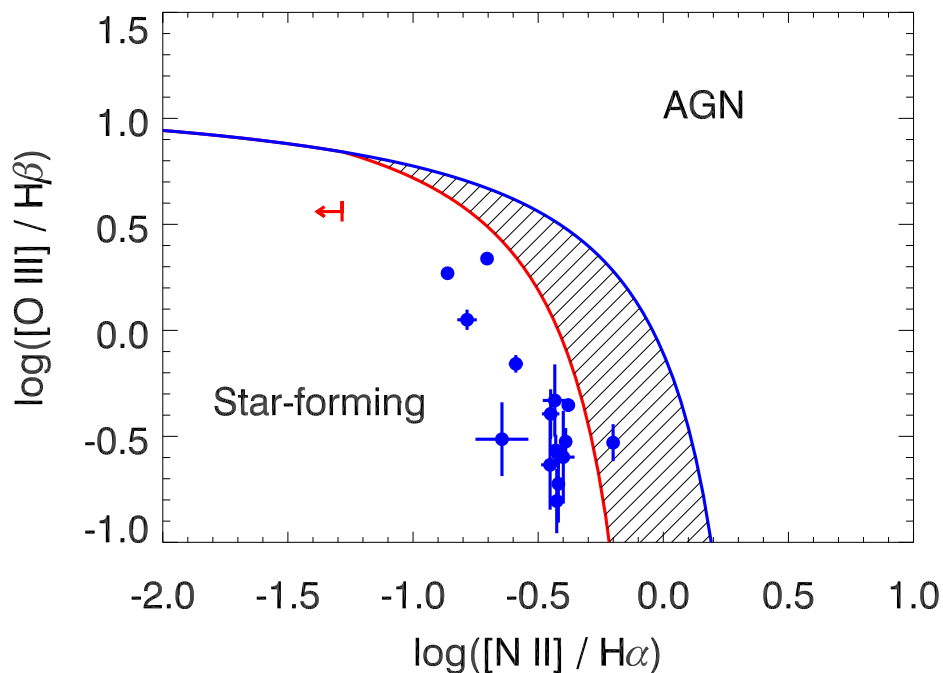


Figure 2.5 BPT diagnostic diagram (Baldwin, Phillips, & Terlevich, 1981). The x-axis denotes the ratio  $\log([\text{N II}] \lambda 6586 / \text{H}\alpha)$  and the y-axis the ratio  $\log([\text{O III}] \lambda 5007 / \text{H}\beta)$ . The data point marks the host galaxy of SN Primo, with the arrow denoting the upper-limit of the ratio derived from the non-detection of  $[\text{N II}] \lambda 6586$ . The vertical bar denotes the  $1\sigma$  error bar of the ratio. For illustrative purposes we overplot the 15 emission-line hosts from the Lampeitl et al. (2010) sample of SN Ia host galaxies with SDSS spectra.

is independent of the systematic error in conversion factor between counts and cgs units (i.e. the flux calibration) at  $\text{Ly}\alpha$  (Section 2.2.2).

Given the low significance of the detection we can only give an order-of-magnitude estimate of the  $\text{Ly}\alpha$  escape fraction (as defined in Atek et al., 2009; Hayes et al., 2011, among others),

$$f_{esc} = \frac{F_{\text{Ly}\alpha}}{8.7F_{\text{H}\alpha}}. \quad (2.6)$$

We derive the line flux  $F_{\text{Ly}\alpha}$  by co-adding the flux in all pixels from  $\lambda = 309.97 - 310.68$  nm (corresponding to  $v = 0-600$  km s $^{-1}$ ). The derived flux estimate is corrected for extinction in the host galaxy. The deviation from the expected value of 8.7 (case B recombination, Brocklehurst, 1971) will be due to conditions in the interstellar medium (ISM) like the presence of dust, ISM clumpiness or due to geometric effects that will suppress or enhance the amount of  $\text{Ly}\alpha$  photons that can escape the galaxy. At a redshift of  $z = 1.5$  the universe is fully ionized, absorption of  $\text{Ly}\alpha$  in the intergalactic medium is therefore not important. We will not try to distinguish between these different scenarios. We include a systematic uncertainty of 40% in the derived  $\text{Ly}\alpha$  escape fraction, due to the uncertainty in the conversion factor between counts and cgs units at the  $\text{Ly}\alpha$  wavelength.

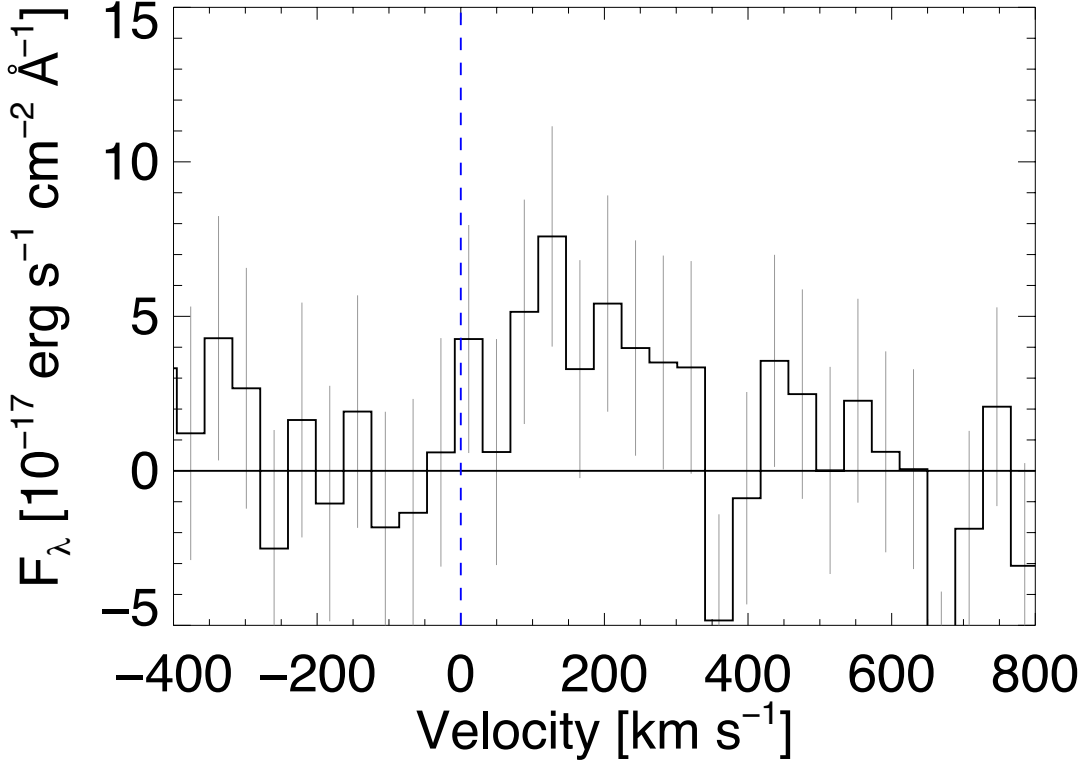


Figure 2.6 The Lyman- $\alpha$  line in the SN Primo host spectrum. The systemic velocity is determined from  $H\alpha$ ,  $[O\text{ III}] \lambda\lambda 4959, 5007$ , and  $[O\text{ II}] \lambda 3729$ .

## 2.4 DISCUSSION & CONCLUSIONS

We have performed a photometric and spectroscopic study of the SN Primo host galaxy. We find a young Large Magellanic Cloud (LMC) sized ( $\sim 4.5$  kpc) galaxy with LMC-like ( $\sim \frac{1}{3}Z_{\odot}$ ) metallicity and low intrinsic extinction. We confirm that the emission lines are generated by star formation and derive a SFR of almost one order of magnitude larger than that of the LMC. The stellar mass derived from SED fitting is one order of magnitude lower than the LMC. From the  $\text{Ly}\alpha$  line we estimate a high escape fraction of  $\text{Ly}\alpha$  photons. All host properties are summarized in Tables 2.2 and 2.4.

In Figure 2.7 we plot the SFR vs. stellar mass for the host of SN Primo in comparison to both a low redshift (Lampeitl et al., 2010,  $z < 0.21$ ) and two high redshift samples from HST (Thomson & Chary, 2011,  $0.95 < z < 1.8$ ) and SNLS (Sullivan et al., 2010,  $0.2 < z < 1.0$ ) samples. The host of SN Primo clearly stands out from the low- $z$  sample, due to its high specific star-formation rate. The relation between SFR and stellar mass is expected to evolve with redshift as seen in observations (Daddi et al., 2007; Elbaz et al., 2007). If SN host galaxies are representative of field galaxies the blue points in Figure 2.7 are expected to shift upwards in the same way as the green dashed lines (signifying  $z = 0, 1$ , and 2). It is hard to see that trend from the SNLS and HST samples due to the scatter (HST) and degeneracies (SNLS) in the data. The degeneracies (at constant sSFR) in the SNLS data is due to shortcomings in the SED fitting in Sullivan et al. (2010).

Its derived metallicity is not unusually low for galaxies in general, but the metallicity is very

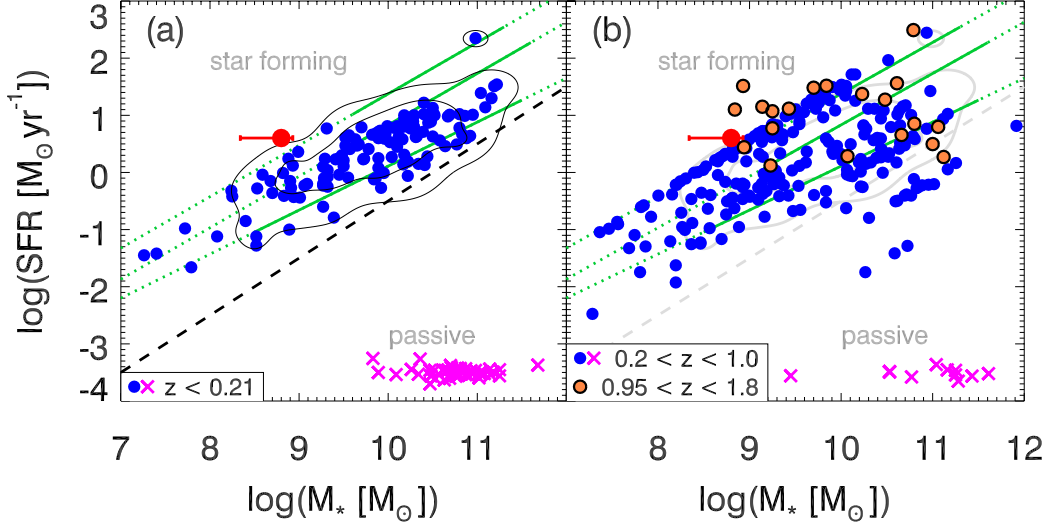


Figure 2.7 The SFR-mass relation for SN Ia host galaxies. The (red) asterisk denotes the host of SN Primo with error bars. Filled (blue) circles mark star-forming hosts in each sample. The (magenta) crosses marks the passive hosts in each sample. The solid and dotted (green) lines show the correlation between SFR and stellar mass for  $z \sim 0$  (bottom),  $z = 1$  (middle), and  $z = 2$  (top) from Daddi et al. (2007,  $z = 2$ ) and Elbaz et al. (2007,  $z \sim 0$  and  $z = 1$ ). The solid section of each line marks the range of validity of the relations. (a) The low redshift sample ( $z < 0.21$ ) from SDSS (Lampeitl et al., 2010). The dashed line marks the cut,  $\log(sSFR) = -10.6$ , between star forming and passive galaxies. The contours mark the region enclosing 68% and 95% of the star-forming sample. (b) The high redshift samples from HST (Thomson & Chary, 2011,  $0.95 < z < 1.8$ , open (orange) circles) and SNLS (Sullivan et al., 2010,  $0.2 < z < 1.0$ , filled (blue) circles / (magenta) crosses). The apparent upper diagonal ridge-line for the Sullivan et al. (2010) data is due to shortcomings in their SED fitting.

low for SN Ia host galaxies (Gallagher et al., 2005; Prieto et al., 2008). We plot the metallicity-luminosity relation for the sample of Prieto et al. (2008,  $z < 0.04$ ). The host of SN Primo has a lower metallicity than any of the low- $z$  galaxies (see Figure 2.8). The host of SN Primo also falls below the mass-metallicity relation (Tremonti et al., 2004). We check why this could be the case by comparing the host of SN Primo to the Fundamental Metallicity Relation (FMR) of star-forming galaxies (Lara-López et al., 2010; Mannucci et al., 2010) which relates metallicity, stellar mass, and SFR. Mannucci et al. (2011) updated the low-mass slope of the FMR relation using GRB host galaxies. The metallicity predicted by the FMR relation is within the error bars of the measured metallicity. The residual between SN Primo and the FMR relation is  $\Delta[12 + \log(\frac{O}{H})] = 0.07 \pm 0.15$ . The host of SN Primo is therefore consistent with the FMR relation defined in Mannucci et al. (2011). The FMR relation is consistent with a simple model (Dayal et al., 2013) where the balance of gas infall, outflow, and star formation brings out the relation between SFR, metallicity and stellar mass seen in the FMR relation.

The stellar age of  $\sim 10^{8.6}$  years (Table 2.2) could give an upper limit on the delay time of SN Primo, assuming there is no underlying old stellar population. This would put SN Primo in the prompt progenitor distribution (see Sullivan et al., 2006, for a review). There are however caveats to the values derived from our SED fitting. It is assumed that there is no underlying old

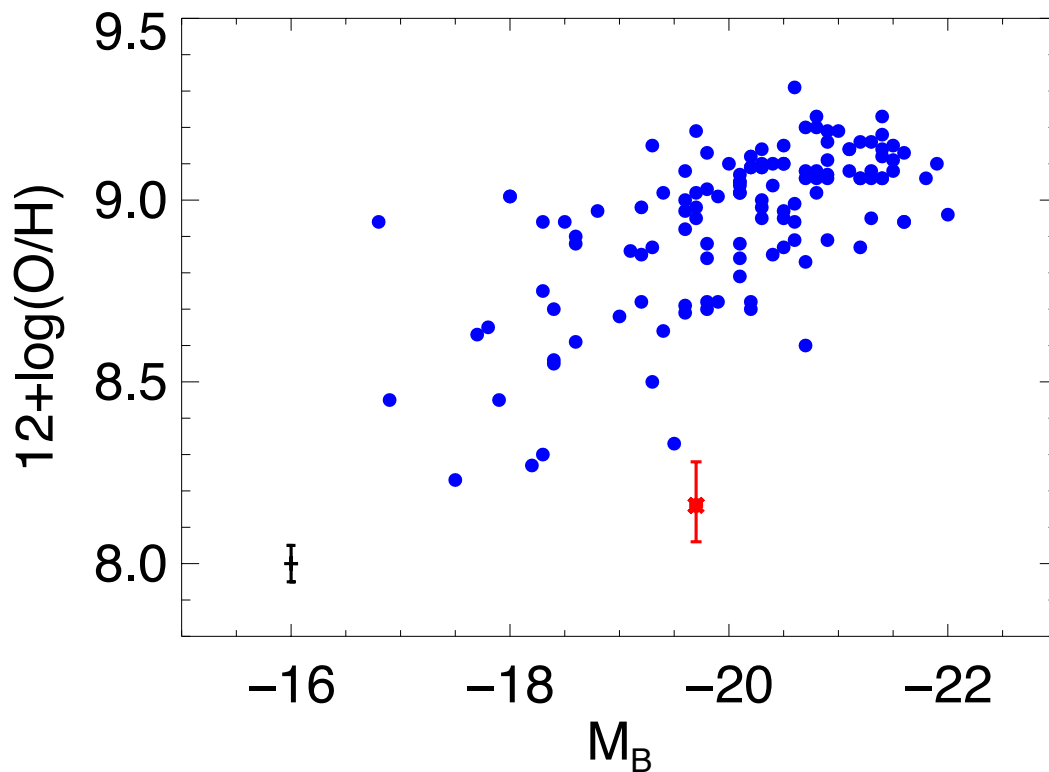


Figure 2.8 Metallicity–luminosity relation for SN Ia host galaxies. The (red) asterisk denotes the host of SN Primo with error bars. The (blue) filled circles denotes the sample of Prieto et al. (2008,  $z < 0.04$ , median error bar plotter to the lower left).

stellar population, which can not be ruled out. This is also seen in Table 2.2 where ages up to  $\sim 10^9$  are still consistent within  $1\sigma$ .

In this paper we have used a redshift independent definition of a starburst based on the value of the sSFR ( $\log(sSFR) > -9.5$ , Sullivan et al., 2006). Alternatively a starburst can be defined based on the SFR and  $M_*$  of galaxies at the same redshift — the so called main-sequence (MS) of galaxies (indicated in Figure 2.7a). The evolution of the MS with redshift, however, is not fully settled (see Daddi et al., 2007; Wuyts et al., 2011; Whitaker et al., 2012, among other). As indicated in Figure 2.7a the MS fits at  $z = 1$  and  $z = 2$  would have to be extrapolated down to the mass of the host of SN Primo.

Gallagher et al. (2005) showed that the light-curve shape correlates with the Hubble type of the host galaxy and Meyers et al. (2012) showed that both light-curve shape and SN peak color are different between early-type and late-type galaxies. Sullivan et al. (2011) showed by splitting up the SNLS3 sample of SNe Ia into a high and low sSFR sample, that the host galaxy has an influence on the mean SN peak brightness and the correction of light-curve shape and color correction. Galaxy evolution models find that sSFR increases with redshift out to at least  $z = 2$ . Using the mass of the host of SN Primo the “host term” of Kelly et al. (2010) is 0.3 mag (super-luminous SN). These dependencies highlight that the bulk of the training sample of SNe Ia lies below  $z < 1$  where the host galaxies are older and in general have a smaller sSFR. As a consequence, this could introduce a potential bias in the distances derived to the high sSFR

Table 2.1. Photometry of the host of SN Primo

Filter	Instrument	$\lambda_{\text{eff}}$ (nm)	Magnitude <sup>a</sup> (AB mag)	Corrected <sup>b</sup> (AB mag)
U-band	VLT/VIMOS	375.3	$24.69 \pm 0.02$	...
F435W (B)	<i>HST</i> /ACS	432.8	$24.84 \pm 0.02$	...
F606W (V)	<i>HST</i> /ACS	595.8	$24.84 \pm 0.02$	...
F775W (i)	<i>HST</i> /ACS	770.6	$24.86 \pm 0.03$	...
F850LP (z)	<i>HST</i> /ACS	905.3	$24.80 \pm 0.04$	$24.88 \pm 0.04$
F105W (Y)	<i>HST</i> /WFC3	1059	$24.50 \pm 0.01$	$24.56 \pm 0.01$
F125W (J)	<i>HST</i> /WFC3	1252	$24.27 \pm 0.01$	$24.71 \pm 0.01$
F160W (H)	<i>HST</i> /WFC3	1544	$24.36 \pm 0.01$	$24.71 \pm 0.01$
K <sub>s</sub> -band	VLT/ISAAC	2168	$24.47 \pm 0.17$	...
Channel 1	<i>Spitzer</i> /IRAC	3563	$24.43 \pm 0.05$	...
Channel 2	<i>Spitzer</i> /IRAC	4511	$24.49 \pm 0.09$	...

<sup>a</sup>The magnitudes before subtraction of the emission-line fluxes.

<sup>b</sup>The magnitudes after subtraction of the emission-line fluxes.

host galaxies, when not explicitly including the host correction. As the sample of high redshift and high sSFR SNe grows the size of this effect can be investigated further.

We thank Robert Kirshner, Mark Dickinson, Peter M. Garnavich, Brian Hayden, Giorgos Leloudas for comments and discussions. We thank the anonymous referee for valuable comments that helped improve this manuscript. We thank Martin Sparre for providing his X-shooter meta-pipeline, which has simplified the reduction of the X-shooter spectra significantly. This work is based on observations taken by the CANDELS Multi-Cycle Treasury Program with the NASA/ESA HST, which is operated by the Association of Universities for Research in Astronomy, Inc., under NASA contract NAS5-26555. The Dark Cosmology Centre is funded by the Danish National Research Foundation. This research has made use of the NASA/IPAC Extragalactic Database (NED) which is operated by the Jet Propulsion Laboratory, California Institute of Technology, under contract with the National Aeronautics and Space Administration.

Table 2.2. Summary of SED fitting using FAST.

Parameter <sup>a</sup>	Exponential <sup>b</sup>	Delayed <sup>c</sup>	Truncated <sup>d</sup>
$\log(t_*[\text{yr}])$	$8.50^{+0.28}_{-1.41}$	$8.60^{+0.51}_{-1.25}$	$8.65^{+0.13}_{-1.20}$
$\log(\tau[\text{yr}])$	$8.80^{+2.20}_{-2.30}$	$8.30^{+2.70}_{-1.62}$	$9.40^{+1.60}_{-1.96}$
$Z$	$0.020^{+0.023}_{-0.016}$	$0.020^{+0.021}_{-0.016}$	$0.020^{+0.015}_{-0.016}$
$A_V$	$0.00^{+0.71}_{-0.00}$	$0.00^{+0.71}_{-0.00}$	$0.00^{+0.70}_{-0.00}$
$\log(M_*[M_\odot])$	$8.80^{+0.13}_{-0.46}$	$8.81^{+0.16}_{-0.34}$	$8.84^{+0.07}_{-0.39}$
$\log(SFR[M_\odot\text{yr}^{-1}])$	$0.33^{+0.77}_{-0.87}$	$0.32^{+0.84}_{-0.49}$	$0.35^{+0.73}_{-0.99.35}$
$\log(sSFR[\text{yr}^{-1}])$	$-8.47^{+1.07}_{-0.61}$	$-8.49^{+1.15}_{-0.27}$	$-8.50^{+1.06}_{-0.50}$
$\log(t_*/\tau)$	$-0.30^{+1.05}_{-3.25}$	$0.30^{+0.50}_{-3.60}$	$-0.75^{+0.80}_{-2.75}$
$\chi^2$	19.9	19.8	19.8

<sup>a</sup>We have assumed a Chabrier IMF

<sup>b</sup>Exponential star-formation history:  $SFR(t) \propto \exp(-t/\tau)$ ,  $\tau > 0$

<sup>c</sup>Delayed star-formation history:  $SFR(t) \propto t \cdot \exp(-t/\tau)$

<sup>d</sup>Truncated star-formation history:  $SFR(t) = \text{constant}$ ; for  $t \in [t_*, t_* + \tau]$ , else

0

Table 2.3. Emission lines detected in the spectrum of the host of SN Primo.

Line	Wavelength [nm]	Observed FWHM [nm]	FWHM [km s <sup>-1</sup> ]	Flux <sup>a</sup> [10 <sup>-17</sup> erg s <sup>-1</sup> cm <sup>-2</sup> ]
H $\alpha$ $\lambda$ 6563	$1673.43^{+0.01}_{-0.02}$	$0.65^{+0.05}_{-0.04}$	$117^{+8}_{-7}$	$< 5.1^{+0.3}_{-0.3}$
[O III] $\lambda$ 5007	$1276.71^{+0.02}_{-0.02}$	$0.44^{+0.07}_{-0.05}$	$103^{+16}_{-11}$	$< 6.0^{+0.6}_{-0.5}$
[O III] $\lambda$ 4959	$1264.43^{+0.04}_{-0.03}$	$0.31^{+0.07}_{-0.08}$	$75^{+16}_{-17}$	$< 2.1^{+0.4}_{-0.4}$
H $\beta$ $\lambda$ 4861 <sup>b</sup>	-	-	-	$< 1.4^{+0.4}_{-0.5}$
[O II] $\lambda$ $\lambda$ 3726,3729 <sup>c</sup>	$950.90^{+0.08}_{-0.05}$	$0.35^{+0.27}_{-0.07}$	$112^{+86}_{-21}$	$< 2.6^{+1.0}_{-0.8}$
[N II] $\lambda$ 6586 <sup>d</sup>	-	-	-	$< 0.3$
Ly $\alpha$ $\lambda$ 1216 <sup>e</sup>	-	-	-	$< 11.2^{+4.0}_{-3.9}$

<sup>a</sup>Fit of the observed flux corrected for Galactic extinction ( $E(B - V) = 0.008$ ).

<sup>b</sup>In each resampling the following fit was performed: The central-wavelength of the line was fixed to  $\lambda_{H\beta}(1+z)$ , where  $\lambda_{H\beta} = 486.1325\text{nm}$  and  $z$  is the redshift.  $\text{FWHM}(H\beta)$  was fixed to  $\text{FWHM}(H\alpha)$  in velocity units. Only the peak intensity was allowed to vary.

<sup>c</sup>The wavelength is that of [O II]  $\lambda$ 3729 (the red component) only, the flux is the sum of both components.

<sup>d</sup> $5\sigma$  upper limit of the non-detection.

<sup>e</sup>The Ly $\alpha$  flux is the co-added flux from  $v = 0 - 600 \text{ km s}^{-1}$ . The error bars only cover the statistical errors. The systematic error is  $\sim 40\%$ .

Table 2.4. Spectroscopic summary.

Parameter	Value	Assumed IMF
Redshift (heliocentric)	$z = 1.54992^{+0.00008}_{-0.00004}$	
Metallicity	$12 + \log\left(\frac{O}{H}\right) = 8.12^{+0.09}_{-0.10}$ $Z = 0.27^{+0.06}_{-0.06} Z_{\odot}$ <sup>a</sup>	
Extinction	$A_V = 0.6^{+1.1}_{-0.7}$ mag	
Ly $\alpha$ escape fraction	$f_{esc} = 0.25 \pm 0.09$ ( $\pm 0.10$ ) <sup>b</sup>	
Star-formation rate:		
	$SFR = 6.4 \pm 0.3 M_{\odot} \text{ yr}^{-1}$	Salpeter
	$SFR = 4.3 \pm 0.2 M_{\odot} \text{ yr}^{-1}$	Kroupa
	$SFR = 3.8 \pm 0.2 M_{\odot} \text{ yr}^{-1}$	Chabrier
Specific star-formation rate:		
	$\log(sSFR[\text{yr}^{-1}]) = -7.8 \pm 0.2$	Salpeter
	$\log(sSFR[\text{yr}^{-1}]) = -8.0 \pm 0.2$	Kroupa
	$\log(sSFR[\text{yr}^{-1}]) = -8.1 \pm 0.2$	Chabrier

<sup>a</sup>Assuming a solar oxygen abundance of 8.69 (Asplund et al., 2009)<sup>b</sup>The value in parenthesis covers the systematic uncertainty on the flux of Ly $\alpha$  of 40%.



# 3

## THE TWIN IN THE SUBARU DEEP FIELD

*The most exciting phrase to hear in science, the one that heralds new discoveries, is not “Eureka!” but “That’s funny...”*

Isaac Asimov

**ABSTRACT – Context:** *The Subaru Deep Field (SDF) Supernova Survey discovered 10 Type Ia supernovae (SNe Ia) in the redshift range  $1.5 < z < 2.0$ , as determined solely from photometric redshifts of the host galaxies. However, photometric redshifts might be biased, and the SN sample could be contaminated by active galactic nuclei (AGNs).*

**Aims:** *We aim to obtain the first robust redshift measurement and classification of a  $z > 1.5$  SDF SN Ia host galaxy candidate*

**Method:** *We use the X-shooter (U-to-K-band) spectrograph on the Very Large Telescope to allow the detection of different emission lines in a wide spectral range.*

**Results:** *We measure a spectroscopic redshift of  $1.54563 \pm 0.00027$  of hSDF0705.25, consistent with its photometric redshift of  $1.552 \pm 0.018$ . From the strong emission-line spectrum we rule out AGN activity, thereby confirming the optical transient as a SN. The host galaxy follows the fundamental metallicity relation defined in Mannucci et al. (2010, 2011) showing that the properties of this high-redshift SN Ia host galaxy is similar to other field galaxies.*

**Conclusions:** *Spectroscopic confirmation of additional SDF SN hosts would be required to confirm the cosmic SN rate evolution measured in the SDF.*

### 3.1 INTRODUCTION

The nature of the progenitor stellar systems of Type Ia supernovae (SNe Ia) remains a mystery (see Howell 2011, Maoz & Mannucci 2012 and Maoz et al. 2013 for reviews). While both circumstantial and direct lines of evidence point to a carbon-oxygen white dwarf (WD; Nugent et al. 2011; Bloom et al. 2012 and see Leibundgut 2000 for a review) as the progenitor, the otherwise stable WD must be ignited. The current consensus is that the carbon in the core of the WD is ignited due to the buildup of pressure, or temperature, resulting from mass accretion from a companion star in a binary system. The two leading scenarios for the nature of the progenitor binary system are the single degenerate scenario (SD; Whelan & Iben 1973; Nomoto 1982), which contends that the WD accretes mass from a main-sequence, helium, or giant star; and the double degenerate scenario (DD; Iben & Tutukov 1984; Webbink 1984), in which the WD merges with a second CO WD through loss of angular momentum and energy to gravitational waves.

Volumetric SN rates provide strong constraints on SN progenitor models. An important discriminator between explosion scenarios is the delay time distribution (DTD), which quantifies the distribution of times from progenitor formation to explosion.

A SN survey in the Subaru Deep Field (SDF) was conducted with the Subaru 8.2-m Telescope. Graur et al. 2011b (G11) discovered 150 candidate SNe, of which 28 (10) were classified as  $1 < z < 1.5$  ( $z > 1.5$ ) SNe Ia. Each SN candidate in the SDF was observed in one of four independent epochs, in the  $R$ ,  $i'$ , and  $z'$  bands. Consequently, variable active galactic nuclei (AGNs) can be mistaken for SNe. G11 identified interloping AGNs using a catalog of known variable AGNs in the SDF (provided by T. Morokuma) and by culling SN candidates that appeared in more than one of the four survey epochs (see their section 3.1 for a detailed description). However, lacking spectroscopy, the possibility that some of the  $z > 1.5$  SDF SNe Ia are in fact AGNs could not be ruled out.

Combining the measured SN rates with SN rates at other redshifts, and comparing to different realizations of the cosmic star-formation history, G11 set constraints on the SN Ia DTD, which in turn impacts on the progenitor question. However, the classification of the SNe discovered in the SDF is purely photometric and depends on the redshift of the host galaxy. The redshifts of most of the SDF SN host galaxies, including those at  $z > 1.5$ , are photometric redshifts (photo- $z$ 's). These photo- $z$ 's are based on photometry in 11 bands, from the far-ultraviolet (UV) to the near-infrared (IR), trained on hundreds of galaxies in the field with spectroscopy. Yet, because of the inherent difficulty in obtaining spectroscopic redshifts for early-type galaxies due to the lack of strong emission lines, training the photo- $z$  method used by G11 at high redshift is difficult. There could be systematic biases in the redshift estimates in that range, biases that are not accounted for in the formal uncertainty. Because of the small number of SN candidates, even a few 'catastrophic' photo- $z$  failures or contamination by unidentified AGNs could strongly distort the inferred DTD. In order to determine whether the G11  $z > 1.5$  rate suffers from such systematic biases, the host galaxies of the SN candidates must be observed spectroscopically.

The  $i' = 24$  mag host galaxy of SNSDF0705.25, denoted hSDF0705.25, was typed as a Sbc galaxy with a sharp redshift probability distribution function ( $z$ -PDF) that peaked at  $z_p = 1.552 \pm 0.018$ . In Figure 3.1 we show the photometry of hSDF0705.25, along with the best-fitting galaxy spectral-energy distribution and resultant  $z$ -PDF.

In this research note we present a VLT/X-shooter emission-line spectrum, derive the spectroscopic redshift and classify AGN vs. star-formation activity of the SN host galaxy hSDF0705.25. We also place constraints on the metallicity and star-formation rate of the host galaxy. From broad-band photometry we determine the stellar mass to place the host on the fundamental metallicity relation (FMR; Mannucci et al., 2010, 2011). Throughout this research note we assume a flat  $\Lambda$ CDM cosmology with  $H_0 = 70 \text{ km s}^{-1}$  and  $\Omega_m = 0.3$ .

## 3.2 DATA

The spectrum of hSDF0705.25 was obtained on 2012 April 23 with the X-shooter spectrograph (D'Odorico et al., 2006; Vernet et al., 2011) at the Very Large Telescope (VLT) at Cerro Paranal, Chile. We used an ABBA on-source nodding template with an exposure time of 1.3 hr ( $4 \times 1200$  sec) and a  $0''.9$  slit.<sup>1</sup> The spectrum was obtained under clear conditions. For details on high-redshift emission-line spectroscopy with X-shooter, see Frederiksen et al. (2012).

<sup>1</sup>A  $1''.0$  slit in the UVB arm.

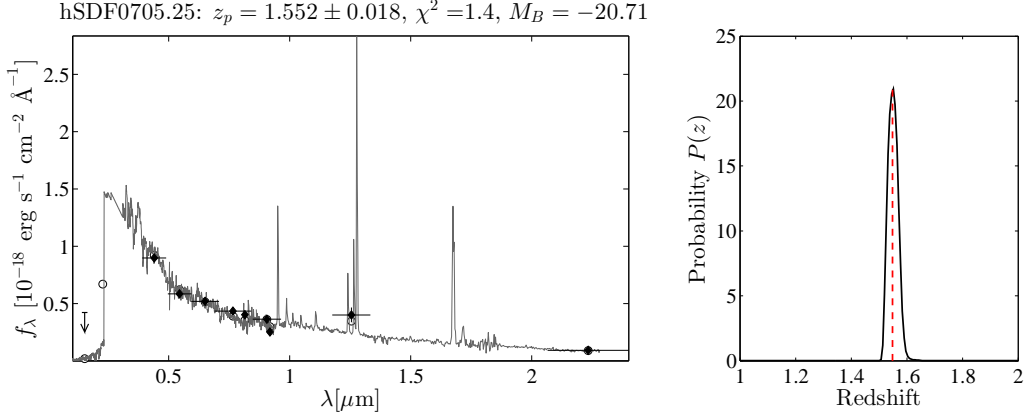


Figure 3.1 ZEBRA fit and resultant  $z$ -PDF of hSDF0705.25. The left panel shows the actual photometry (filled circles), the best-fitting galaxy template (solid line), and its synthetic photometry (empty circles). The vertical error bars denote the photometric uncertainty, and the horizontal error bars show the width of the filter. The  $1\sigma$  upper limit on the photometry in the *GALEX FUV* band is shown as the downturned arrow. The header gives the designation of the SN host galaxy, most probable photo- $z$  ( $z_p$ ), the  $\chi^2$  per degree of freedom of the fit, and the absolute  $B$ -band magnitude the galaxy would have at  $z_p$ . The right panel shows the resultant  $z$ -PDF peaking at  $z_p = 1.552 \pm 0.018$ . The red line marks the spectroscopic redshift obtained in this work.

The X-shooter spectra were reduced using the official X-shooter pipeline<sup>2</sup> v1.3.7. The extraction of the object spectrum was conducted with our own IDL script, and flux calibration was done using the flux standard star, LTT 3218.<sup>3</sup>

The broad-band photometry was taken from G11.

### 3.3 ANALYSIS

The flux-calibrated spectrum is corrected for Galactic extinction and slit loss. The Galactic extinction along the line of sight to hSDF0705.25 is  $A_V = 0.042 \text{ mag}^4$  (Schlafly & Finkbeiner, 2011) and we assume the Galactic extinction law of Fitzpatrick (1999). The slit loss correction assumes a  $\lambda^{-0.2}$  variation in seeing.<sup>5</sup>

In the available atmospheric transmission windows, we detect a strong emission line at 1671.88 nm which we identify as  $\text{H}\alpha$  at  $z = 1.54563 \pm 0.00027$ . This identification is supported by the detection of  $\text{H}\beta$ ,  $[\text{N II}]$  6583, and  $[\text{S II}]$  6716,6731 at the same redshift. We do not detect  $[\text{O III}]$  4959,5007 in the spectrum and can therefore only derive upper limits on its flux. We also detect  $[\text{O II}]$  3726,3729 in the VIS arm of X-shooter, but the blue part of the doublet is obscured by a skyline. Without the detection of  $[\text{O III}]$  5007 we cannot derive a metallicity from the  $R_{23}$ -ratio. We therefore only consider the emission lines present in the NIR arm as presented in Figure 3.2. The detected emission lines in the spectrum are fitted individually with a Gaussian

<sup>2</sup>See, <http://www.eso.org/sci/software/pipelines/>

<sup>3</sup>See <http://www.eso.org/sci/observing/tools/standards/spectra/ltt3218.html>

<sup>4</sup>Quoted from the NASA/IPAC Extragalactic Database (NED) website: <http://ned.ipac.caltech.edu/>

<sup>5</sup>The standard star itself was observed with a 5 slit, making slit losses negligible.

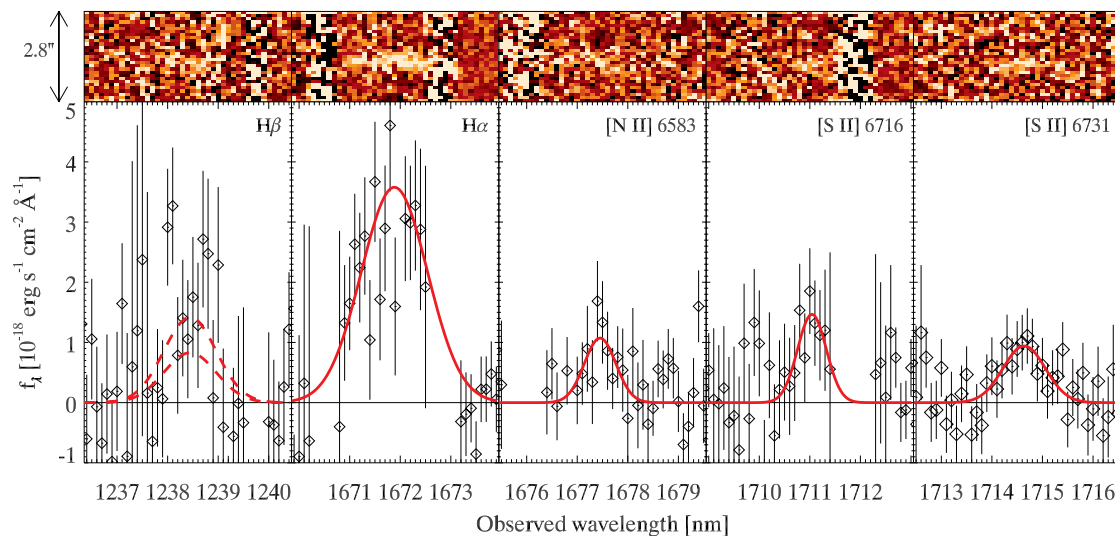


Figure 3.2 X-shooter 1D and 2D spectrum of hSDF0705.25. The spectrum has been corrected for Galactic extinction. The solid (red) line shows the fit to the emission lines assuming a Gaussian line profile. The dashed line shows a scaled version of the  $H\alpha$  line assuming the same FWHM (in velocity units) and extinction in the host of  $E(B - V) = 0$  mag (upper) and  $E(B - V) = 0.5$  mag (lower). Color version available online.

line profile and the flux is calculated from the fit. The  $H\beta$  line is severely affected by noise and therefore not fitted. The  $H\alpha$  line seems to have a larger line width than other lines, which might be an artifact due to the masked skylines on either side of the line. The masked skylines allow for a wider fit and the central part of the line does not constrain the fit to a more narrow profile. For  $H\beta$ , we plot in Figure 3.2 a scaled-down version of the  $H\alpha$  line assuming case-B recombination, central wavelength and FWHM (in velocity units) as for  $H\alpha$ , and intrinsic reddening in the host of  $E(B - V)$  of zero or 0.5 mag (Calzetti, 2001) to illustrate the variation allowed by the spectrum.

The emission line ratios  $N2 = \log([\text{N II}] 6583/H\alpha)$  and  $O3 = \log([\text{O III}] 5007/H\beta)$  are among the main diagnostics for discriminating between star formation and AGN activity by way of the Baldwin, Phillips, & Terlevich (1981, BPT) diagram. The  $N2$  diagnostic places the host in the star forming region of the BPT diagram. This is also supported by the  $O3$  diagnostic, which provides an upper limit. The upper limit on  $O3$  is calculated using the  $3\sigma$  upper limit on  $[\text{O III}]$  and the predicted  $H\beta$  flux from the  $H\alpha$  flux. We calculate the  $H\beta$  flux assuming  $E(B - V) = 0$  or 0.5 mag to make sure the classification does not depend on the assumed amount of extinction in the host galaxy. ( $N2 = -0.88$ ,  $O3 < 0.28$ , see e.g. Frederiksen et al., 2012, their Figure 5). The lack of a broad-line component in the emission lines (see Table 3.1) and the absence of strong emission from C IV 1550 and Mg II 2799 also supports the conclusion that the line-flux is dominated by star formation and not AGN activity.

From the  $N2$  line ratio we derive a metallicity of  $8.40 \pm 0.18$  (Pettini & Pagel, 2004, PP04). We use the emission-line calibrations of Kewley & Dopita (2002, KD02) to constrain the metallicity. (In addition we get a constraint on the ionization parameter  $q$ .) We make use of the emission-line ratios  $N2$  and  $N2O3 = \log([\text{N II}] 6583/[\text{O III}] 5007)$ . The  $N2$  ratio (like the PP04 metallicity) places the host galaxy in the low-metallicity regime at  $12 + \log(O/H) < 8.55$ . The  $N2O3$  ratio

Table 3.1 Spectroscopic summary

Line	Wavelength (nm)	Obs. FWHM <sup>a</sup> (km s <sup>-1</sup> )	Int. FWHM <sup>a</sup> (km s <sup>-1</sup> )	Flux (10 <sup>-18</sup> erg s <sup>-1</sup> cm <sup>-2</sup> )
H $\alpha$	1671.88 $\pm$ 0.09	117 $\pm$ 18	103 $\pm$ 18	58.8 $\pm$ 10.4
[N II] 6583	1677.45 $\pm$ 0.07	47 $\pm$ 14	...	7.7 $\pm$ 3.1
[S II] 6716	1711.04 $\pm$ 0.11	50 $\pm$ 21	...	10.4 $\pm$ 5.0
[S II] 6731	1714.64 $\pm$ 0.09	73 $\pm$ 16	47 $\pm$ 16	9.9 $\pm$ 2.8
[O III] 5007 <sup>b</sup>	...	...	...	< 23.2 $\pm$ 10.4
[O III] 4959 <sup>b</sup>	...	...	...	< 9.1 $\pm$ 10.4

a) The instrumental resolution is 57 km s<sup>-1</sup>. b) This is the 3 $\sigma$  upper limit on the flux.

Table 3.2 Derived properties of the SN host galaxy hSDF0705.25

Property	Value
Redshift	$z = 1.5456 \pm 0.0003$
Star-formation rate <sup>ab</sup>	$SFR = 4.0 \pm 0.7 M_{\odot} \text{ yr}^{-1}$
Metallicity (PP04)	$12 + \log(O/H) = 8.4 \pm 0.2$
Metallicity (KD02)	$12 + \log(O/H) < 8.0$
Ionization parameter (KD02)	$q < 4 \times 10^7 \text{ cm s}^{-1}$
Stellar mass <sup>c</sup>	$\log(M_* [M_{\odot}]) = 9.46_{-0.08}^{+0.23}$
Specific SFR <sup>d</sup>	$\log(\text{sSFR} [\text{yr}^{-1}]) = -8.86_{-0.24}^{+0.11}$
Host extinction <sup>c</sup>	$A_{V,\text{host}} = 0.4_{-0.4}^{+0.7} \text{ mag}$
Stellar age <sup>c</sup>	$\log(t_* [\text{yr}]) = 7.9_{-0.6}^{+0.3}$

a) Assuming a Chabrier (2003) IMF. b) SFR is a lower limit as extinction in the host galaxy would make the intrinsic SFR higher by 34% ( $A_V = 0.4$ ). c) Using an exponentially declining star-formation history, redshift fixed to the spectroscopic redshift, and metallicity fixed to  $Z = 0.008$  (i.e.  $12 + \log(O/H) \sim 8.4$ ). d) Assuming  $A_V = 0.4$  corresponds to a shift of  $\Delta \log(\text{sSFR}) = +0.127$ .

gives us an upper limit of  $12 + \log(O/H) < 8.0$  (and ionization parameter  $q < 2 \times 10^7 \text{ cm s}^{-1}$ ).

We convert the rest-frame H $\alpha$  luminosity into a star-formation rate (SFR) using the calibration of Kennicutt (1998), rescaled to a Chabrier (2003) initial mass function (IMF). The observed SFR,  $4.0 \pm 0.7 M_{\odot} \text{ yr}^{-1}$ , represents a lower limit to the intrinsic SFR of the host galaxy, due to the unconstrained extinction in the host galaxy.

The photo- $z$  fitter ZEBRA (Feldmann et al., 2006) is not suited for deriving stellar parameters like the mass of the galaxy. We therefore fit the Subaru+UKIRT ( $B, V, R, i', z', J$  and  $K$ ) photometric measurements (corrected for foreground extinction in the same way as the spectrum) using the FAST SED fitter (Kriek et al., 2009). We derive the intrinsic extinction, stellar mass, and stellar age of the host galaxy (see Table 3.2). The extinction in the host is not very well constrained ( $0 < A_V < 1.1$ ) so we assume  $A_V = 0$  in our further analysis. We calculate the specific SFR (sSFR, see Table 2) using the H $\alpha$  SFR and the stellar mass from FAST.

### 3.4 DISCUSSION

We find a highly star-forming (i.e., high sSFR), low-metallicity SN host galaxy (see Frederiksen et al., 2012, for the discussion of another high SF low metallicity SN host at similar redshift). The

derived SFR may be affected by extinction in the host galaxy, but due to the low signal-to-noise ratio of the  $H\beta$  line we are not able to place any strong constraints on it. Likewise, the extinction derived from SED fitting does not provide a strong constraint. If we use the best fit SED value of  $A_V = 0.4$  mag the SFR would increase by 34%.

The stellar mass and SFR of hSDF0705.25 places it midway between the  $z = 1$  and  $z = 2$  main-sequence of star-forming galaxies defined in Daddi et al. (2007) and Elbaz et al. (2007). As hSDF0705.25 falls on the main sequence at its redshift, it can be classified as an average star-forming galaxy at its redshift. Alternatively, the sSFR can be used to define whether a galaxy is passive, star forming or a starburst galaxy. Using the definition of Sullivan et al. (2006, see their Figure 6), the high sSFR of hSDF0705.25 makes it a starburst galaxy. Such galaxies are representative of the “prompt” population of the DTD of SNe Ia (Mannucci et al., 2005; Scannapieco & Bildsten, 2005; Maoz & Mannucci, 2012).

The combination of SFR, stellar mass, and metallicity of hSDF0705.25 is fully consistent with the FMR defined in Mannucci et al. (2010, 2011). In Figure 3.3, we plot the metallicity against the projection parameter  $\mu_{0.32} = \log(M_*) - 0.32 \log(SFR)$  defined in Mannucci et al. (2010). The SFR is not corrected for host extinction. For  $A_V = 0.4$  mag, the correction would amount to a difference of 0.04 dex in  $\mu_{0.32}$ . The metallicity in Figure 3.3 is derived from the  $[N II]/H\alpha$  ratio and translated from the PP04-calibration to the KD02-calibration using Kewley & Ellison (2008). At metallicities above 8.4 the KD02-calibration is consistent with the calibration of Maiolino et al. (2008) used in Mannucci et al. (2010, 2011). The hSDF0705.25 and the host of SN Primo at  $z = 1.55$  (Frederiksen et al., 2012) are the two SNe Ia above  $z > 1$  for which a measurement of gas-phase metallicity has been obtained. For comparison we also plot the sample of gamma-ray burst (GRB) host galaxies at  $0.01 < z < 1$  from Mannucci et al. (2011) and a sample of lensed galaxies presented in Richard et al. (2011,  $1.5 < z < 3.5$ ) and Christensen et al. (2012,  $1.5 < z < 3.5$ ). The fact that high-redshift SN Ia host galaxies follow the FMR relation suggests that they follow the same evolutionary path as regular field galaxies.

### 3.5 CONCLUSIONS

Our derived spectroscopic redshift,  $z = 1.54563 \pm 0.00027$ , is in full agreement with the G11 photometric redshift of  $z = 1.552 \pm 0.018$  (Figure 3.1). We also exclude AGN activity as the source of the emission-line flux. From the flux of the  $H\alpha$  line we derive an observed SFR and from the emission line ratios we constrain the host-galaxy metallicity.

The SN Ia rates at high redshift are dominated by small-number statistics. The three  $z > 1.4$  SNe Ia found with the *Hubble Space Telescope* (HST) in the HST/GOODS survey (Dahlen et al., 2008a) belong to host galaxies with measured spectroscopic redshifts and no AGN activity. On the other hand, the larger Subaru/SDF sample includes ten SNe Ia at  $z > 1.5$ , but their classification as SNe Ia relies on photometric redshifts which, at high redshifts, might be systematically offset. Two ongoing HST Multi-Cycle Treasury programs, the Cluster Lensing and Supernova survey with Hubble (Postman et al., 2012) and the Cosmic Assembly Near-IR Deep Extragalactic Legacy Survey (Grogin et al., 2011; Koekemoer et al., 2011) and the upcoming Frontiers Fields will find new SNe out to  $z \approx 2.5$  (Rodney et al., 2012; Jones et al., 2013; Graur et al., 2013), but their samples will still be small and will suffer from the same classification challenges faced by the GOODS and SDF surveys. For example, in the HST/CLASH survey, 2 of 4  $z > 1.2$  SN Ia with light curves in multiple filters have spectroscopic redshifts (Graur et al., 2013). It is thus important to test the robustness of the SDF SN Ia rate measurements by spectroscopically measuring the redshifts of the SN host galaxies, and ascertaining whether the SN sample was con-

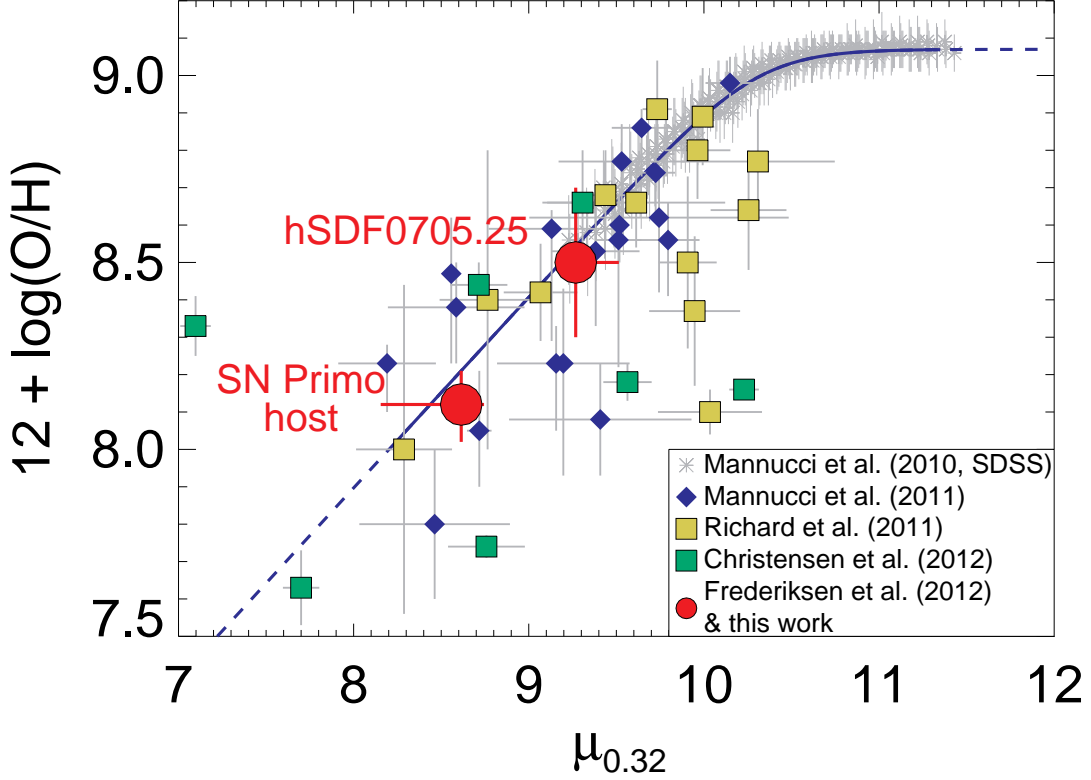


Figure 3.3 The Fundamental Metallicity Relation (FMR). The parameter  $\mu_{0.32} = \log(M_*) - 0.32 \log(SFR)$  is the projection in the stellar mass, SFR plane. The two circles (red) are the two high-redshift SN Ia host galaxies with measured gas-phase metallicity, hSDF0705.25 and SN Primo (Frederiksen et al., 2012). The crosses are the binned data from the Sloan Digital Sky Survey (York et al., 2000, SDSS) used in Mannucci et al. (2010). The diamonds (blue) are GRB host galaxies used to calibrate the low metallicity slope in Mannucci et al. (2011,  $z < 1$ ). The squares are lensed galaxies from Christensen et al. (2012, yellow,  $z > 1$ ) and Richard et al. (2011, green,  $z > 1.5$ ). The dark (blue) line is the parameterization of Mannucci et al. (2011) (solid in the range of validity, extrapolation in dashed blue, high metallicity as constant, low metallicity as straight line). The two SN Ia host galaxies ( $z = 1.5$ ) are fully consistent with the FMR of star-forming field galaxies.

taminated by unclassified AGNs. The confirmation of the photometric redshift of hSDF0705.25, and its classification as a star-forming, non-AGN-hosting galaxy, represents the first step in this endeavour. hSDF0705.25 is the brightest of the high-redshift SDF SN Ia host galaxies, so to investigate other high-redshift SDF SNe hosts will require longer exposure times on ground based near-IR spectrographs (like X-shooter). The study of early-type galaxies at these redshifts is currently beyond the capabilities of single object, ground based IR spectrographs, and will require observations from the future generation of ground based and space based instruments.

We thank Martin Sparre for providing his X-shooter meta-pipeline, which simplified the reduction of the X-shooter spectra significantly. The Dark Cosmology Centre is funded by the Danish National Research Foundation. DM and OG acknowledge support by a grant from

the Israel Science Foundation. This research has made use of the NASA/IPAC Extragalactic Database (NED) which is operated by the Jet Propulsion Laboratory, California Institute of Technology, under contract with the National Aeronautics and Space Administration.

# 4

## HIGH REDSHIFT SN HOST SAMPLE

**ABSTRACT** – *Characterizing the environment of type Ia supernovae allow us to get more insight into their progenitors. We therefore present the characteristics of 21 high-redshift ( $z > 1$ ) SN host galaxies (14 SN Ia, 5 core-collapse SN, and 2 of unknown type). Among the sources for which we determine the spectroscopic redshifts are the highest redshift SN Ia and CC SN. We perform SED fitting to available UV-to-near-IR photometry to determine stellar parameters. From the stellar age we determine the stellar main-sequence mass of the progenitors of the fastest prompt SN Ia population at  $z = 1.5 - 2.0$  to be  $\sim 5 - 8 M_{\odot}$ . We discuss the implications of three major findings:*

- 1) *We analyze the prompt-to-delayed SN-ratio using the A+B model. We determine the ratio of the two parameters A and B and show that this ratio changes as a function of redshift out to  $z \sim 2$ . This is consistent with no evolution of the Delay Time Distribution (DTD) of type Ia SNe.*
- 2) *We propose a new parameterization of the A+B model that is derived from the assumption that the DTD is not evolving.*
- 3) *We find a fraction of SN Ia with very short delay times (i.e. prompt) of  $0.50 - 0.71$ . This is consistent with the findings of Rodney et al. (2013). They find that the very prompt part of the DTD is consistent with a powerlaw of slope  $-1$ .*

### 4.1 INTRODUCTION

Thermonuclear supernova explosions (SN Ia) have become the most important tool for probing the expansion history of the Universe in recent decades.

The Wide Field Camera III's Infrared detector (WFC3/IR) onboard the *Hubble Space Telescope* (HST) has made it possible to detect SNe Ia at redshifts up to  $z \sim 2$ . At these very high redshifts we can start to disentangle evolutionary effects from cosmological effects (Riess & Livio, 2006). Furthermore we can compare how the host galaxy population compares to the general field population. If the progenitor (or mix of progenitor types) changes over cosmic time then the host galaxies will also change as a function of redshift. So by characterizing how the population of SN Ia hosts change as a function of redshift we are able to indirectly characterize the SN progenitor population itself.

One promising measurement that would shed light on the explosion mechanisms of SNe is the so-called delay time. The delay time denotes the time from the progenitor star is born until it explodes as a SN. The distribution of all delay times in a SN population is called the Delay-time distribution (DTD),

$$R(t) = \frac{r(t)}{M_*}, \quad (4.1)$$

where  $r(t)$  has units of SNe per year and  $R(t)$  has units of SNe per year per unit stellar mass. The DTD corresponds to the observed SN rate (per unit stellar mass) after a hypothetical single burst of star formation creating an amount of stars equal to  $M_*$ . Scannapieco & Bildsten (2005) and Mannucci et al. (2005) proposed that the SN Ia rate in galaxies could be inferred from the stellar mass and star-formation rate (SFR) of the galaxy,

$$r = A \cdot M_* + B \cdot SFR \quad (4.2)$$

This fits very well with the fact that star forming galaxies have a much higher rate of SN Ia per stellar mass than passive galaxies. Passive galaxies on the other hand still have a non-zero SN rate. This model was called the A+B model. The A+B model corresponds to a DTD with only two delay-time bins. The prompt delay times dominate the young stellar populations where many new stars are created, whereas the SNe with long delay times are dominant in old stellar populations where there are no new stars formed.

Several studies have measured the shape and normalization of the DTD. Strolger et al. (2010) assumed that the DTD could be described by a generalized skew-normal function with width and skewness as free parameters. This analysis found the SN Ia DTD to have most power at 3 – 4 Gyr. Other determinations yield a powerlaw behavior with a slope consistent with  $-1$  (see Maoz & Mannucci, 2012, for a review). A powerlaw-like DTD is expected from double-degenerate SN models (see Chapter 1 Figure 1.6).

In this chapter we present and describe the sample of high redshift SN host galaxies from the CLASH and CANDELS surveys. We present stellar parameters (like stellar masses, stellar ages, SFR, and extinction) derived from SED fitting. We will in the discussion especially focus on three areas of interest that are impacted by our analysis:

- Evolution (or lack thereof) of the shape of the DTD as a function of redshift
- A new formulation of the "A+B model".
- The fraction of SNe explosions with very short delay times (Prompt SNe).

We assume a flat  $\Lambda$ CDM cosmology with  $H_0 = 71.2 \text{ km s}^{-1}$  and  $\Omega_m = 0.264$  (Hinshaw et al., 2012, WMAP9). All magnitudes are reported in AB magnitudes unless explicitly stated otherwise.

## 4.2 DATA & SAMPLE SELECTION

Our host galaxy sample is compiled from the transients detected in the CLASH and CANDELS surveys from 2010–2012, and where the transients are classified as SNe (using light curve and color information). As of March 2013 this list was frozen. The full list is presented in Table 4.2. In case of multiple host candidates the most probable host was chosen based on the angular separation, magnitude of the SN, and the redshifts of the potential host candidates. From this raw sample we construct our sample using the following selection criterion:

- (A) We select high redshift host galaxies depending on the redshift quality.
- i) If the host has a spectroscopic redshift above  $z > 1$  it is included in the sample.
  - ii) If no spec- $z$  is available we require a well-constrained phot- $z > 1$  (well-constrained means  $\Delta z / (1 + z) < 0.2$ , hosts that fail this criterion are marked by “(-)” in table 4.2)
  - iii) If the phot- $z$  is not well-constrained we require that the 95% confidence interval completely lies above  $z > 1$  (i.e.  $z - \Delta z > 1$ ).

(B) We apply a magnitude cut of  $J < 25$  or if  $J$  is not available  $Z < 26$  to make sure we can do follow-up from ground.

Our final sample is listed in Table 4.3.

As a consequence of the freezing of the list, the few SNe that had only a preliminary classification or where there was some ambiguity about the classification might therefore be subject to change in future works.

#### 4.2.1 SPECTROSCOPIC DATA

The SN hosts selected using the above stated selection criteria were followed up with the VLT/X-shooter spectrograph<sup>1</sup> (as described in Frederiksen et al., 2012) unless a spectroscopic redshift was already determined or the object was not visible from the VLT.

#### 4.2.2 PHOTOMETRIC DATA

All host galaxies in our high- $z$  sample (satisfying criteria A, and B, see Table 4.3) are located in four CANDELS fields (GOODS-S+N, EGS and UDS) and five CLASH fields (A383, MACS0416, A2261, RXJ2129, MS2137, MACS2129).

In the CANDELS GOODS-S field we make use of photometry from CTIO/MOSAIC (U-band), VLT/VIMOS (U-band), VLT/ISAAC (J+H+K<sub>s</sub>-band), *Spitzer*/IRAC (Channel 1-4), *HST*/ACS (F435W, F606W, F775W, F850LP), and *HST*/WFC3 (F105W, F125W, F160W). In the CANDELS GOODS-N field we make use of photometry from KPNO/Mosaic (U-band), *Spitzer*/IRAC (Channel 1-4), *HST*/ACS (F435W, F606W, F775W, F850LP), UKIRT/WFCAM (J, K<sub>s</sub>-band). In the CANDELS EGS field we make use of photometry from CFHT/MegaCam (u\*, g', r', i', z'), UKIRT/WFCAM (J, K<sub>s</sub>-band), *Spitzer*/IRAC (Channel 1-4). In the CANDELS UDS field we make use of photometry from SUBARU/SuprimeCam (B, V, R', i', z'), UKIRT/WFCAM (K<sub>s</sub>-band), *HST*/ACS (F606W, F814W), *HST*/WFC3 (F125W, F160W).

In most CLASH clusters there is only photometry from SUBARU/SuprimeCam (B, V, R', i', z'), but for some hosts follow-up photometry is available from *HST*/WFC3 (F125W, F160W) where the galaxy light is not contaminated with SN light.

### 4.3 ANALYSIS

The detailed reduction procedure of the X-shooter spectra is described in Frederiksen et al. (2012, see Chapter 2).

#### 4.3.1 SED FITTING

For determining physical parameters of our host sample we use the SED fitting code GalMC (Acquaviva et al., 2011). We assume a Chabrier (2003) Initial Mass Function, and we use the 2007 update of the Bruzual & Charlot (2003) stellar libraries. The extinction in the host galaxy is modeled using a Calzetti et al. (2000) extinction law.

The available photometry is first corrected for galactic extinction using the updated Schlegel maps (Schlafly & Finkbeiner, 2011)<sup>2</sup>. For most targets in most bands the extinction is comparable or lower than the errors on the magnitudes. We add 0.05 magnitudes in quadrature to the photometric error in all bands to account for template mismatches (see Dahlen et al., 2010). We

<sup>1</sup>ESO Program ID: 088A-0708, 089A-0739, 090A-0726

<sup>2</sup>Taken from the NED website, <http://ned.ipac.caltech.edu/>

discard any bands that might probe the rest frame Mid-IR ( $\lambda > 3\mu\text{m}$ ) as these can contain unmodeled PAH emissions. For our sample this affects *Spitzer*/IRAC channel 3 and 4 for objects with redshifts  $z < 1.3$  (Ch. 3 + 4) or  $z < 2.3$  (Ch. 4 only).

We run GalMC MCMC<sup>3</sup> chains for 25 000 – 50 000 steps depending on the number of parameters<sup>4</sup>. For some chains the initial guess was far from the best fit and the chain therefore didn't converge within 25 000 – 50 000 steps. A new chain was therefore started at the best fit point and allowed to run for 25 000 – 50 000 steps. This approach has ensured that the burn-in phase for most objects are just a few thousand steps. See Figure 4.17 – 4.26 for detailed plots on each of the chains. For objects that only have a phot-z we also let the redshift vary and later marginalize over the redshift.

To gauge the effect of assuming different SFH, we perform four separated fits to the photometry: One fit using a single burst model (simple stellar population, SSP), one using a constant SFH (CSF), and one using an exponential SFH ( $\tau$ -model, with  $\tau$  as a free parameter). We also gauge the presence of an underlying second population by fixing the age of the best fitting single burst model and then fit a second burst with the age- and mass-ratio between the two populations left as free parameters ( $2\times\text{SSP}$ ). For each fit we calculate the Bayesian Information Criterion (BIC),

$$BIC = -2 \ln L + k \ln N, \quad (4.3)$$

where  $L$  is the likelihood function,  $k$  is the number of parameters and  $N$  is the number of photometric data points. The BIC penalizes the extra free parameters. We choose the SFH with the lowest BIC value for each host galaxy. See the full list of BIC values in Table 4.4.

The star-formation rate (SFR) is derived from the observed flux corresponding to the rest frame UV (1500–2800Å). The observed flux is converted to UV luminosity and corrected for host extinction using the Calzetti et al. (2000) extinction law and the  $E(B - V)$  values from the MCMC chain. We use Kennicutt (1998) to convert UV luminosity to SFR.

### 4.3.2 EMISSION LINE REDSHIFTS

For the three hosts Quayle, Wilson, and Cleveland (see Tabel 4.1) we have determined the redshift from strong emission lines using X-shooter (along with the Primo host already presented in Chapter 2 of this thesis). See Table 4.1 for a list of all SN hosts targeted by this program. SN Wilson (Jones et al., 2013) is the highest redshift SN Ia with a spectroscopic redshift ( $z = 1.91$ ), likewise Quayle is the highest redshift CC SN with a spectroscopic redshift ( $z = 2.37$ ). For Quayle and Cleveland we detect multiple lines (see Table 4.3) and can derive an un-ambiguous redshift. The spectra are presented in Figures 4.1 & 4.2.

For the Wilson host we only detect one strong line. This leads to two plausible redshift solutions at  $z \sim 1.2$  and  $z \sim 1.9$ . We therefore have to deduce the most proper redshift solution from low signal-to-noise lines and lack of strong lines. In host galaxies like the Wilson host we expect to see  $H\alpha$ ,  $H\beta$ , [O III] 4959,5007, and [O II] 3726,3729. In Figure 4.3 we plot the emission lines that fall in the atmospheric transmission window at the two redshift solutions. The solid lines in each panel show best fit line shapes and dashed lines show predicted line shapes. The high-redshift solution is consistent with low signal-to-noise expected emission lines. The low-redshift solution does not show strong emission of [O III] 4959,5007 as would be expected. We therefore conclude that the high-redshift solution is most consistent with the spectrum, whereas the low-redshift solution is unlikely, but we can not rule this solution out from the spectrum

<sup>3</sup>MCMC: Markov Chain Monte Carlo

<sup>4</sup>If the redshift is free to vary or a second population is present the MCMC chain will need to run for longer.

Table 4.1 All triggered sources under our program.

Name	Exp. time	Cont. <sup>a</sup>	Em.line <sup>b</sup>	Notes
Primo	1.3 h	–	✓	$z = 1.55$
Washington	1.3 h	–	–	No lines detected
Wilson	4.0 h	–	✓	$z = 1.91$
Cleveland	3.3 h	–	✓	$z = 1.41$
Caligula	1.3 h	–	–	No lines detected
Geta	2.7 h	✓	–	Continuum consistent with photometry
Trajan	0.7 h	–	–	No lines detected
Vespasian	1.3 h	✓	–	Very-low-S/N Continuum detected
Quayle	3.3 h	–	✓	$z = 1.91$
Tiberius	0.7 h	–	–	(Telescope error)
Jackson	1.3 h	–	✓	$z = 0.66$
Vitellius	1.3 h	–	✓	(Transient disappeared. SN? $z = 1.54$ )
Noah	5.3 h	–	–	(Transient not a SN)
Rose*	1.3 h	–	–	SN spectrum contaminated by intra-cluster light.

\* Rose is the only target where we targeted the SN directly, instead of the host.

a) Continuum emission detected in the spectrum.

b) Strong emission lines detected in the spectrum.

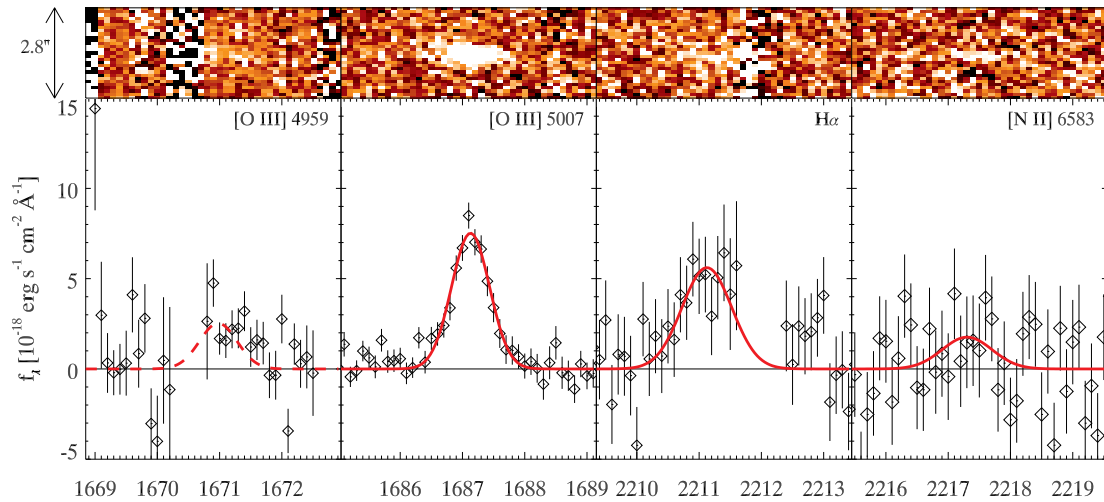


Figure 4.1 The emission line spectrum of the host of SN Quayle at  $z = 2.370$ . The solid lines show the best-fitting Gaussian line profiles. When fitting the  $H\alpha$  and  $[N II] 6583$  line the width is fixed to the width of the  $[O III] 5007$  line (in velocity units). The dashed line shows the predicted line profile of  $[O III] 4959$  assuming a line ratio of the  $[O III] 4959, 5007$  doublet of 1 : 3.

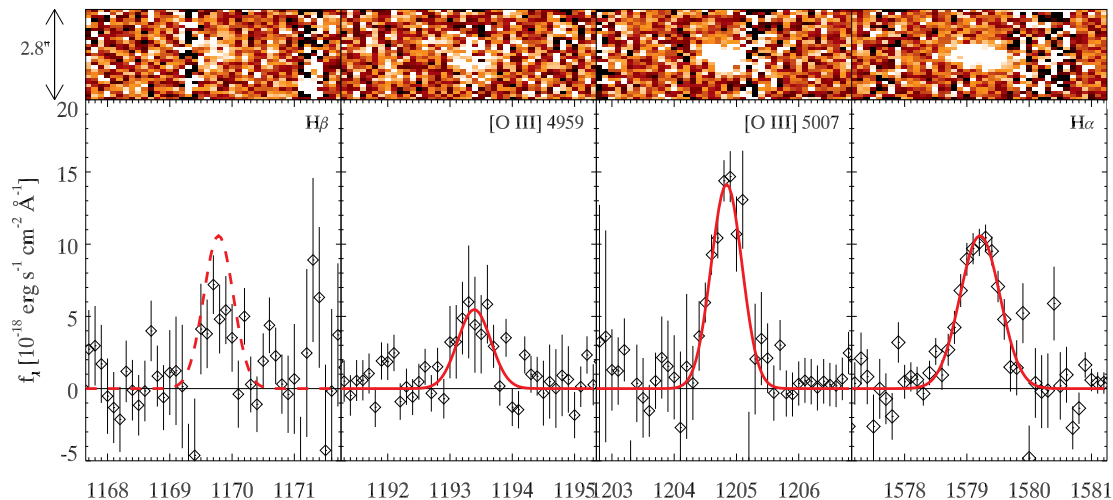


Figure 4.2 The emission line spectrum of the host of SN Cleveland at  $z = 1.406$ . The solid lines show the best-fitting Gaussian line profiles. The dashed line shows the expected line shape of  $H\beta$  calculated from the  $H\alpha$  line, assuming Case-B recombination and no host extinction. The over prediction  $H\beta$  flux, is most probably due to extinction in the host of SN Cleveland.

alone. SED fits to the broadband photometry of the host presented in Jones et al. (2013) and in our analysis both prefer a high-redshift solution.

### 4.3.3 PHOTOMETRIC REDSHIFT TEST

Approximately half of all SN Ia in the sample does not have a spec- $z$ . We therefore need to make sure that the redshift used by GalMC is un-biased. We check this by fitting all object with a spec- $z$  for a photo- $z$  and compare the two. The residual is usually quantified by the ratio  $\frac{\Delta z}{1+z_s}$ , where  $\Delta z = z_{ph} - z_s$  is the difference between the phot- $z$ ,  $z_{ph}$ , and the spec- $z$ ,  $z_s$ . Figure 4.4 shows the cumulative distribution of the residual. Most phot- $z$  (except two) lie within 10% of the spec- $z$ . The two outliers are Polk (leftmost curve) and Obama (right-most curve). Polk is a very red galaxy with large error bars<sup>5</sup>. The fit therefore has a broad distribution which is not centred on the spec- $z$ . The broad-band photometry of Obama shows an overall powerlaw behavior which makes it hard for the code to identify a break.

The outlier fraction in this test is  $f_{out} = 2/12 = 16.7\%$ . After excluding the outliers the phot- $z$  bias is  $b = 0.018 = 1.8\%$ . The spread in the phot- $z$  estimates (average of lower and upper 65% error bars) is  $\sigma_{ph} = (0.0677 + 0.0847)/2 = 0.076 = 7.6\%$ .

This test shows that GalMC fits are not skewed when no spec- $z$  is present, but when evaluating the quality of a GalMC fit we also keep the phot- $z$  from other sources in consideration as to minimize catastrophic outliers like Polk and Obama. In CANDELS a phot- $z$  estimate is calculated using GOODZ (Dahlen et al., 2010) and in CLASH a phot- $z$  is calculated using BPZ (Benítez, 2000).

<sup>5</sup>The large errorbars are due to contamination from diffraction spikes from a nearby star in all HST bands.

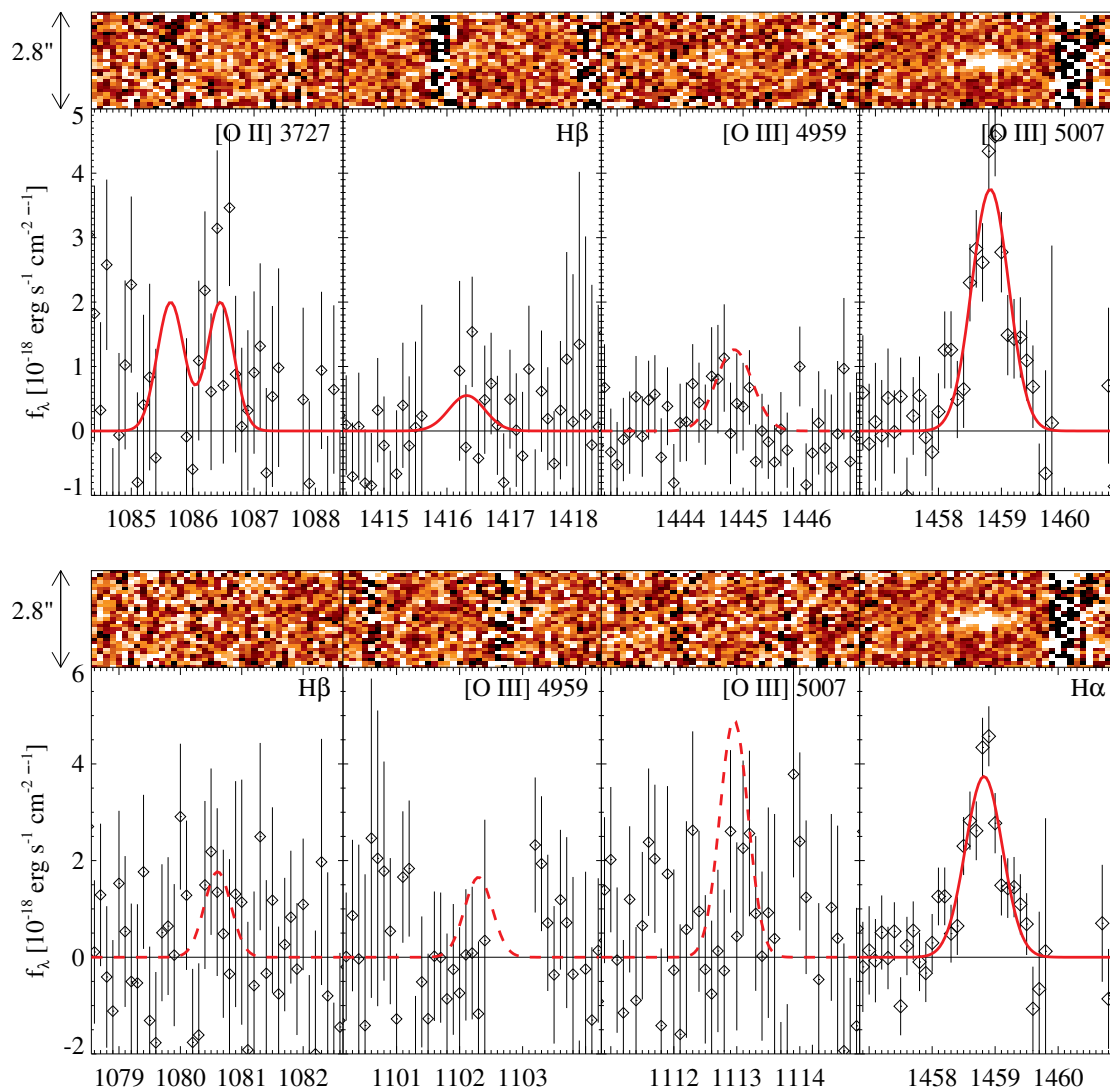


Figure 4.3 The emission line spectrum of the host of SN Wilson. Top: Identifying the strong emission line as [O III] 5007 ( $z = 1.91$ ). The other expected emission lines have very low signal-to-noise. When fitting [O II] 3726,3729 and  $H\beta$  we fix the line width to the width of [O III] 5007 (in velocity units). The [O II] 3726,3729 doublet is fitted with a double gaussian profile, with fixed 1 : 1 line ratio and a fixed ratio between the wavelength of the red and the blue peak. Bottom: Identifying the strong emission line as  $H\alpha$  ( $z = 1.22$ ). The dashed lines are the predicted  $H\beta$  and [O III] 4959,5007 line shapes. For the  $H\beta$  line we assume Case-B recombination and no extinction in the host galaxy. For the [O III] 4959,5007 we assume a line ratio of 1 : 3 and that the [O III] 5007 and  $H\alpha$  lines have comparable (equal) line fluxes (as seen in the hosts of SN Primo, Cleveland and Quayle). The [O III] 4959,5007 doublet seems inconsistent with the low-redshift solution.

#### 4.3.4 SPECIAL CASES

When going through the SED fitting results we noticed that objects like Vespasian and Trajan had a large inferred amount of extinction. The initial fit of Vespasian converged on a young

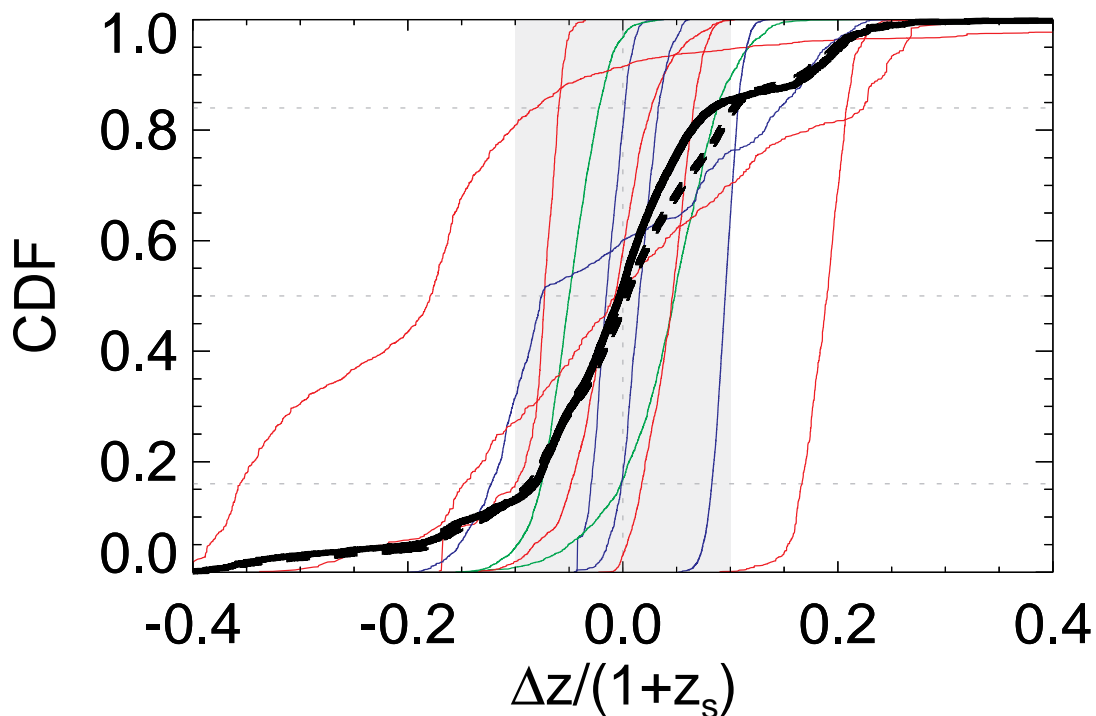


Figure 4.4 Cumulative distribution of the residual between the phot- $z$  and spec- $z$ . The thin lines (SN Ia: red, CCSN: blue, Unknown: green) show the distribution of each individual host galaxy, where all but two are within 10%. Thick solid line shows the combined distribution of all hosts (the bias is 1.8%) and the dashed line shows the distribution after excluding the two outliers. The two outliers are Polk (left-most curve) and Obama (right-most curve).

population at low redshift with a large amount of extinction,  $E(B - V) > 1$  magnitude.

When fitting Polk, the fit also converged on a low- $z$ , young, highly extinct population which made Polk a catastrophic outlier in the phot- $z$  test. Such high values of extinction are also clearly outliers to the rest of the sample which all have  $E(B - V) < 0.5$ . The X-shooter spectra of Geta, Trajan, and Vespasian, all show continuum emission but no emission lines. We therefore know that these three hosts can not be dusty young galaxies. A very dusty galaxy may also have extinguished the SN below detectability. We therefore impose an extinction prior to all objects in the sample and for all SFHs, but the prior primarily has an effect on objects with very red colors and is crucial for objects without a spec- $z$ .

Aside from the red objects Vespasian and Trajan, Colfax is also a special case. The Colfax host does not have a spec- $z$ , but from the (medium-band) colors of the SN itself the redshift range has been narrowed down to  $z = 2.1 \pm 0.2$ . We therefore constrain the redshift to this range in the SED fit. This is not the same as using the phot- $z$  derived from other codes as priors for the redshift as that would use the the same data twice (photometry of the galaxy). This prior is based on the photometry (colors) of the SN and is therefore independent of the photometry of the host galaxy.

### 4.3.5 A REFERENCE SAMPLE

We want to compare stellar masses and stellar ages from our sample to a sample of generic galaxies. We use the NEWFIRM Medium-Band Survey (Whitaker et al., 2011, NMBS) as a reference sample. The NMBS survey provides a catalog of stellar parameters, with masses and stellar ages. We use the same selection criteria to select a subsample of the NMBS that matches our SN-selected sample.

The stellar-parameters catalog is prepared using FAST (Kriek et al., 2009). To make sure that the stellar age derived using FAST ( $\log t_F$ ) is comparable to the ages derived using GalMC ( $\log t_G$ ) we determine the mathematical transform that transforms the GalMC age distribution into the FAST age distribution. The transformation between two probability distributions is

$$F_G(\log t_G) = F_F(\log t_F), \quad (4.4)$$

where  $F_G$  and  $F_F$  are the cumulative distribution functions (CDFs) of the stellar ages derived by GalMC and FAST, respectively. We write this as  $\log t_G = T(\log t_F)$ , where the transform is defined as

$$T(x) = F_G^{-1}(F_F(x)). \quad (4.5)$$

We calculate the empirical transform,  $T(\cdot)$ , by fitting all our host galaxies using FAST with the same settings as in the NMBS catalog. We then determine a crude continuous CDF from the 68% and 95% confidence intervals of each fitted object. The sum of all the individual CDFs then approximates  $F_F(\cdot)$ . The individual GalMC CDFs are calculated directly from the MCMC chains of GalMC.  $F_G(\cdot)$  is then, like  $F_F(\cdot)$ , the sum of the individual CDFs. The final plot of  $T(\cdot)$  is shown in Figure 4.5. The empirical transform is fitted with a fourth order polynomial,

$$\log t_G = T(x) = -310.049 + 102.501x - 10.2077x^2 + 0.206103x^3 + 0.0110430x^4, \quad (4.6)$$

with  $x = \log t_F$  which is used in the computations (range of validity:  $7.6 < \log t_F < 9.7$ ). It is worth noting that GalMC ages are systematically younger than the ages computed by FAST. The youngest ages are offset by 1 dex.

The disadvantage of choosing the NMBS survey is that it is a ground based survey that is only complete to a depth of  $\sim 23.5$  AB mag which is more shallow than our faintest objects at  $K \sim 24.5$  mag.

## 4.4 DISCUSSIONS

In figure 4.6, we see that all the CCSN (in blue) lie above or on the MS for  $z = 1 - 2$ . The SN Ia (in red) are more evenly dispersed across the SFR-Mass plane. This is in line with the prediction that CCSN stem from young star-forming populations and SNIa can stem from both young and more evolved populations.

We take a closer look at the three youngest hosts (Caligula, Primo, and Wilson,  $z = 1.5 - 2.0$ ) which all have stellar ages younger than  $\log t_* < 8.0$  and single stellar populations (See Figure 4.9 for age distribution of the full sample). We use these SN hosts to probe the most prompt population of type Ia SN. At ages this young stars do not have time to evolve off the MS at masses below  $\sim 10 M_\odot$ . Due to the age-extinction degeneracy the derived stellar ages for these young hosts might be underestimated. In Figure 4.9 we show how the effect of assuming no extinction in the three young hosts affect the distribution of stellar ages.

The best fitting age range is converted to a stellar MS mass. This gives us an estimate of the mass range of the progenitors of prompt SN Ia at  $z = 1.5 - 2.0$ . The fastest of the prompt

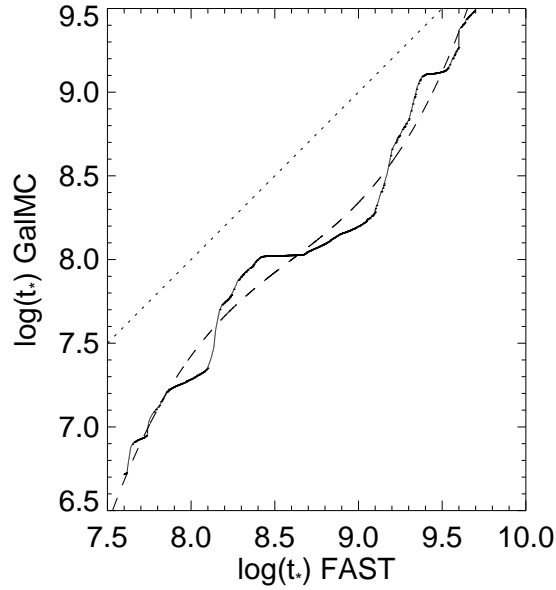


Figure 4.5 Transformation function between stellar ages derived using FAST and GalMC. The solid line is the empirical transformation derived from the SN sample. The dotted line is the one-to-one line. The dashed line is a fourth-order polynomial fit to the empirical transform.

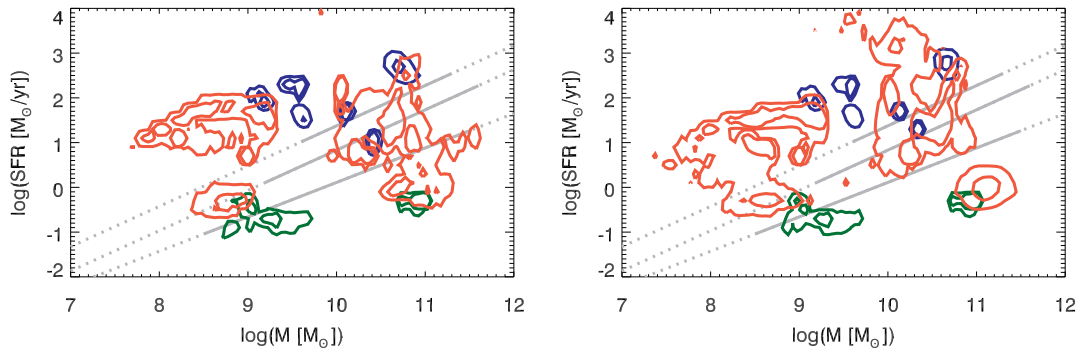


Figure 4.6 SFR vs stellar mass. The solid lines mark the 68% and 95% contours. Red contours show the distribution of SN Ia, blue contours show CC SN and green contours show unknown classifications. Left: Assuming the best fitting SFH (see Table 4.4). Right: Assuming an exponential SFH.

SN Ia population seems to come from progenitors  $\sim 8 M_{\odot}$  if we use the age derived by GalMC and  $\sim 5 M_{\odot}$  for the FAST age. A similar calculation can be performed for Vespaian, which is the older SN Ia with only a single stellar population. This gives a MS mass of  $1.3 - 1.6 M_{\odot}$  (independent of the code used). It is assumed that the delay time is dominated by the timescale it takes to produce a WD and thereby not including the accretion timescale (SD) or the inspiraling timescale (DD), which makes these estimates lower bounds on the MS mass.

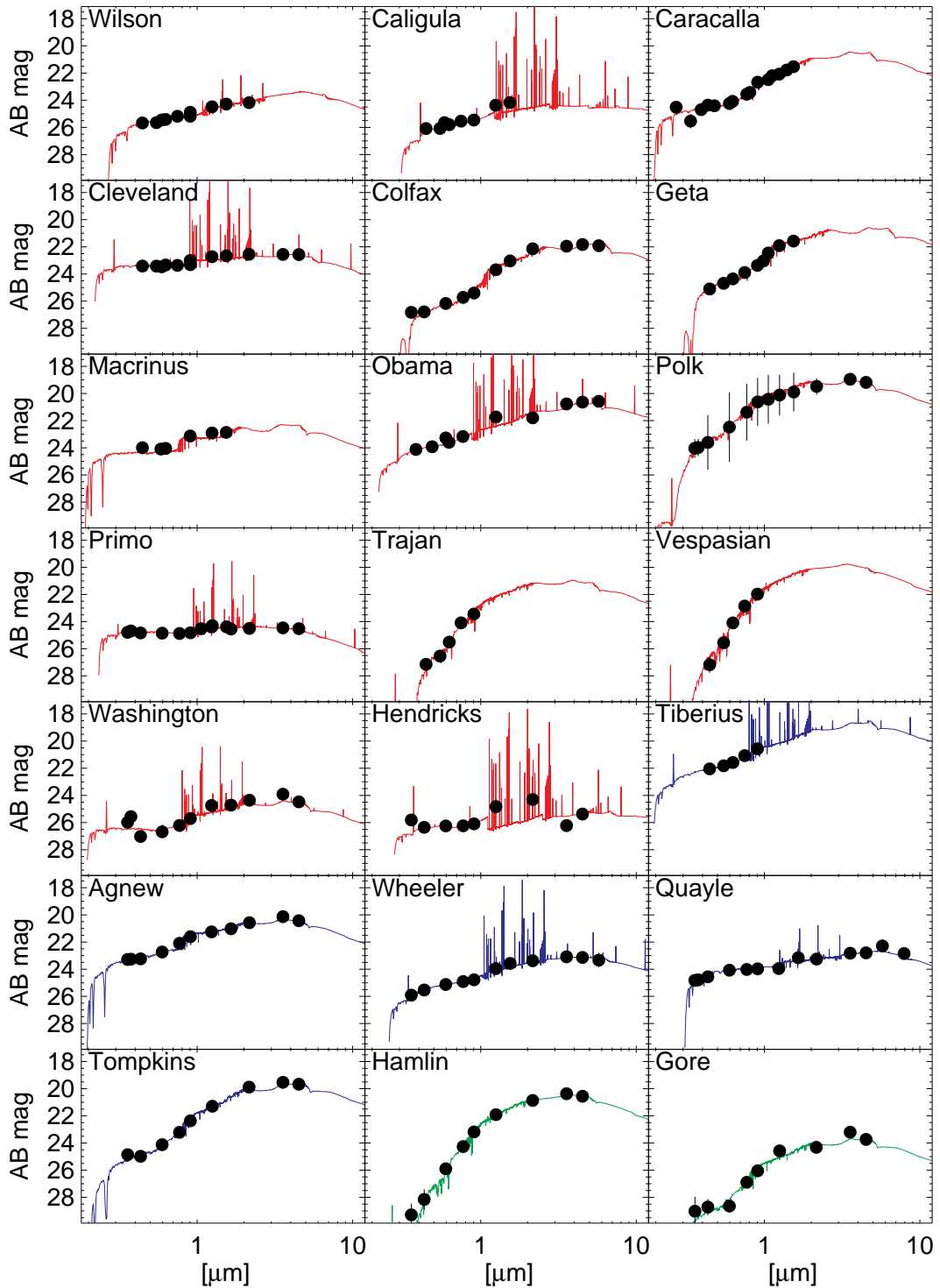


Figure 4.7 Spectral Energy Distribution of all the SN host galaxies. The black points mark the photometry and the solid curve marks the best fitting SED. Red curves mark fits to SN Ia hosts, the blue curves mark CC SN hosts, and the green curves mark hosts of SN with unknown classification.

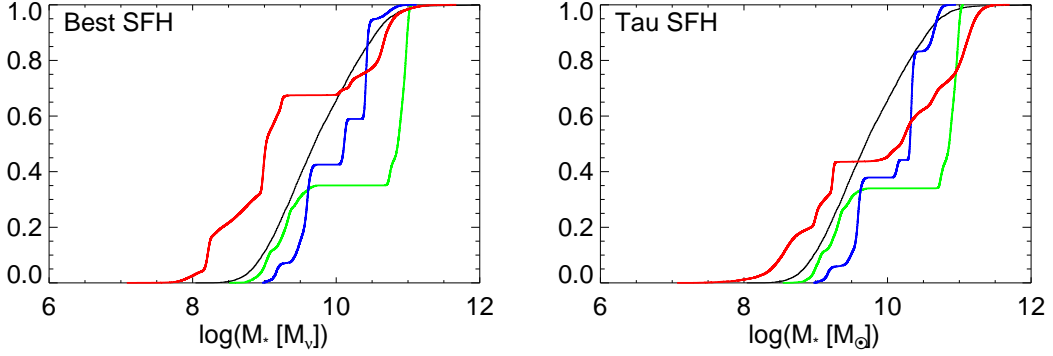


Figure 4.8 Cumulative distribution of stellar masses. The red curve marks the distribution of SN Ia hosts, the blue curve marks CC SN hosts, and the green curve marks hosts of SN with unknown classification. The solid black line shows a comparative sample of field galaxies (NMBS). To show the effect of changing SFH we plot the cumulative distribution under the assumption of both individual best SFH (left) and tau-model SFH (right) for all hosts.

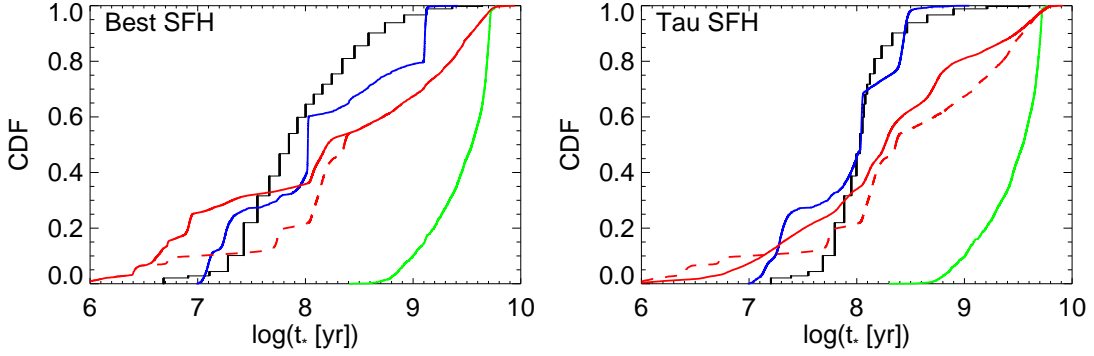


Figure 4.9 Cumulative distribution of stellar masses. Colors as in Figure 4.8. Individual best SFH (left) and tau-model SFH (right)

#### 4.4.1 DTD EVOLUTION

In the following sections the term "SN" will only refer to "SN Ia" unless explicitly stated otherwise. The volumetric SN Ia rate is not part of this study (this will be presented in separate papers by the CLASH+CANDELS SN collaboration, for the CLASH sample only see Graur et al., 2013). Therefore we can not infer the DTD from our sample, but we can constrain the relative distribution of prompt vs. delayed SN. For this we assume a very simple 2-point form for the DTD with only a prompt and a delayed component,

$$R(t) = \begin{cases} R_A & t_{\min} < t < t_{\text{split}} \\ R_B & t_{\text{split}} < t < t_{\max} \end{cases}, \quad (4.7)$$

where the boundaries  $(t_{\min}, t_{\max})$  correspond to the minimum and maximum delay time to create a SN Ia. The delay time  $t_{\text{split}}$  correspond to the transition from prompt to delayed SNe. This split is to some extent arbitrary, but we will use a value of  $t_{\text{split}}$  that will allow us to use the

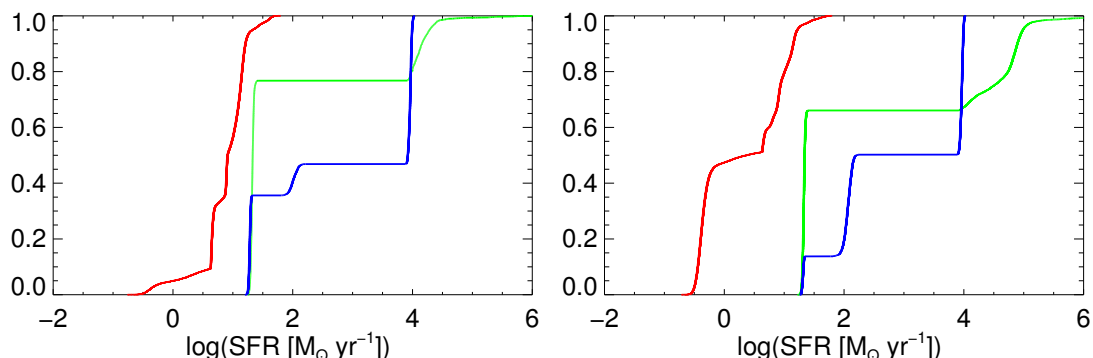


Figure 4.10 Cumulative distribution of star-formation rate. Colors as in Figure 4.8. Individual best SFH (left) and tau-model SFH (right)

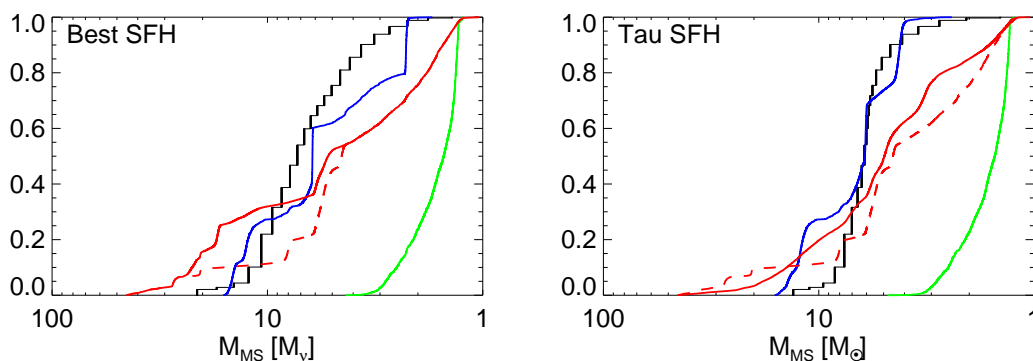


Figure 4.11 Distribution of stellar main sequence mass. Colors as in Figure 4.8. Individual best SFH (left) and tau-model SFH (right). The dotted line marks the distribution when the three youngest SN Ia hosts are forced to have no extinction (i.e. age-extinction degeneracy).

A+B model to describe this DTD. This means that the prompt bin has to correlate strongly with the SFR term in the A+B model. We use the rest frame UV flux to estimate the SFR, which has a timescale of  $\sim 10^8$  yr.

The two parameters of the A+B model represent the SN rate per unit stellar mass and SN rate per unit SFR, respectively. We will explicitly split the rate into the prompt rate,  $r_B$  and delayed rate  $r_A$ .

$$r = r_A + r_B = A \cdot M_* + B \cdot SFR, \quad (4.8)$$

where  $r$  is the total SN rate in SNe per yr,  $A$  is the parameter that governs the delayed component and  $B$  is the parameter that governs the prompt component.

The DTD has units of SN rate per unit stellar mass, we therefore make the distinction between the SN rate (written lower case  $r$ ) and SN rate per stellar mass (written upper case  $R$ ). In the following we will derive a new parameterization of the A+B model based on the assumption that the shape of the DTD is universal across all redshifts (i.e. the relative rates between

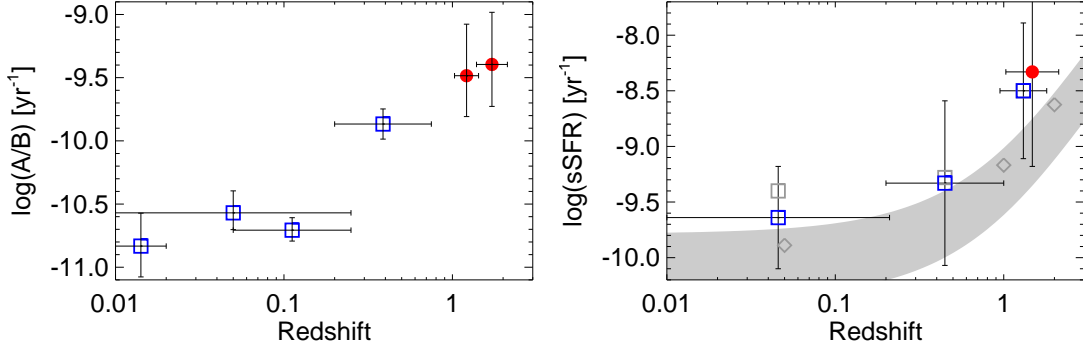


Figure 4.12 Left: The evolution of the A/B ratio as a function of redshift. The data points in increasing order of redshift are Mannucci et al. (2005); Dilday et al. (2008); Smith et al. (2012); Sullivan et al. (2006); and this work (two red bins). The three low redshift points are derived from SDSS SNe samples, and the medium redshift point is from SNLS SNe. Right: The evolution of the specific SFR within SN samples of Lampeitl et al. (2010, SDSS, low- $z$ ), Sullivan et al. (2010, SNLS, medium- $z$ ), Thomson & Chary (2011, high- $z$ ), and our sample (high- $z$ ). The gray band shows the evolution of the cosmic sSFR predicted by Elbaz et al. (2011) and the gray diamonds show the MS of field galaxies from Elbaz et al. (2007,  $z \sim 0$  and  $z = 1$ ) and Daddi et al. (2007,  $z = 2$ ). All SN samples are consistent with the MS within the uncertainties, but show a general tendency to be more star forming on average than the MS.

prompt and delayed SNe is constant). The two rates  $r_x$  and  $R_x$  ( $x = A$  or  $B$ ) are related by

$$R_x = \frac{r_x}{\sum_i^{\text{survey}} (M_*)_i} = \frac{\sum_i^{\text{survey}} (r_x)_i}{\sum_i^{\text{survey}} (M_*)_i}, \quad (4.9)$$

where  $(r_x)_i$  is the SN rate (of either prompt or delayed SNe) of each galaxy, and  $(M_*)_i$  is the stellar mass of each surveyed galaxy. From this definition we get

$$\frac{r_A}{r_B} = \frac{R_A}{R_B}, \quad (4.10)$$

as the surveyed galaxies are the same for both the prompt and delayed SNe. We calculate the delayed-to-prompt ratio by summing all prompt SN rates and delayed SN rates over all galaxies in the survey,

$$\frac{r_A}{r_B} = \frac{\sum_i^{\text{survey}} (r_A)_i}{\sum_i^{\text{survey}} (r_B)_i} = \frac{A}{B} \cdot \frac{\sum_i^{\text{survey,A}} (M_*)_i}{\sum_i^{\text{survey,B}} SFR_i}. \quad (4.11)$$

We assume that the A and B subsamples of SN hosts are a fair sample of all young (B) and old (A) galaxies in the survey, respective. We specifically assume that the mean specific SFR of the SN hosts is the same as for the whole survey (for the A and B subsamples separately),

$$\frac{\sum_i^{\text{hosts,x}} SFR_i}{\sum_i^{\text{hosts,x}} (M_*)_i} = \frac{\sum_i^{\text{survey,x}} SFR_i}{\sum_i^{\text{survey,x}} (M_*)_i}, \quad (4.12)$$

where  $x$  is either the A or B sample. Extending from the fair-sample argument we also require that the ratio between the A and B samples are equal for the SN hosts and the survey as a whole:

$$\frac{\sum_i^{\text{hosts,A}} (M_*)_i}{\sum_i^{\text{hosts,B}} (M_*)_i} = \frac{\sum_i^{\text{survey,A}} (M_*)_i}{\sum_i^{\text{survey,B}} (M_*)_i}. \quad (4.13)$$

With these two assumptions we are able to rewrite Equation (4.11) to only sum over the SN host sample instead of the whole survey sample. We start by eliminating the survey SFR from the denominator of Equation (4.11) using Equation (4.12),

$$\frac{r_A}{r_B} = \frac{A}{B} \cdot \frac{\sum_i^{\text{survey,A}} (M_*)_i}{\sum_i^{\text{survey,B}} (M_*)_i} \cdot \frac{\sum_i^{\text{hosts,B}} (M_*)_i}{\sum_i^{\text{hosts,B}} SFR_i}. \quad (4.14)$$

We now use the Equation (4.13) to change the mass ratio to a sum over the SN hosts.

$$\frac{r_A}{r_B} = \frac{A}{B} \cdot \frac{\sum_i^{\text{hosts,A}} (M_*)_i}{\sum_i^{\text{hosts,B}} (M_*)_i} \cdot \frac{\sum_i^{\text{hosts,B}} (M_*)_i}{\sum_i^{\text{hosts,B}} SFR_i}. \quad (4.15)$$

Canceling the two mass-sums over "hosts, B" and isolating  $A/B$  we get

$$\frac{A}{B} = \frac{r_A}{r_B} \cdot \frac{\sum_{i=1}^{N_B} SFR_i}{\sum_{i=1}^{N_A} (M_*)_i}. \quad (4.16)$$

The ratio of delayed-to-prompt SNe,  $N_A/N_B$ , is equal to

$$\frac{N_A}{N_B} = \frac{r_A \cdot T}{r_B \cdot T} = \frac{r_A}{r_B}, \quad (4.17)$$

where we use the fact that the number of SNe is proportional to the SN rate,  $r_A$  and  $r_B$ , (in SN/yr) and the survey time,  $T$ . The survey time is the same for both delayed and prompt SNe and therefore cancels out. This gives us the final simplification of Equation (4.16),

$$\frac{A}{B} = \frac{N_A}{N_B} \cdot \frac{\sum_{i=1}^{N_B} SFR_i}{\sum_{i=1}^{N_A} (M_*)_i}, \quad (4.18)$$

where,  $N_A$  and  $N_B$  is the number of delay and prompt SNe respectively,  $SFR_i$  is the SFR of the host of the  $i^{\text{th}}$  prompt SN, and  $(M_*)_i$  is the stellar mass of the host of the  $i^{\text{th}}$  delayed SN.

We will shorthand the last fraction of the last equation to

$$\overline{sSFR^*} = \frac{\sum_{i=1}^{N_B} SFR_i}{\sum_{i=1}^{N_A} (M_*)_i}. \quad (4.19)$$

The "stared" specific SFR is approximately equal to the usual mean specific SFR

$$\overline{sSFR} = \frac{\sum_{i=1}^{N_A} SFR_i + \sum_{i=1}^{N_B} SFR_i}{\sum_{i=1}^{N_A} (M_*)_i + \sum_{i=1}^{N_B} (M_*)_i} \approx \frac{\sum_{i=1}^{N_B} SFR_i}{\sum_{i=1}^{N_A} (M_*)_i} = \overline{sSFR^*}, \quad (4.20)$$

as the numerator is dominated by the SFR of the prompt (young) hosts and the denominator is dominated by the delayed (old passive) hosts. We calculate  $\overline{sSFR}$  and  $\overline{sSFR^*}$  for all galaxies in our sample (i.e. hosts of SN Ia, CC SN, and unknown types). The value of  $\overline{sSFR^*}$  is one third of a dex lower than  $\overline{sSFR}$ , because the average SFR of the delayed SN hosts are smaller, but not negligible compared to the average SFR of the prompt SN hosts. We are not able to calculate  $\overline{sSFR^*}$  for literature data and therefore use  $\overline{sSFR}$  when comparing to other works. The discrepancy between the two measures of specific SFR can have some dependance on redshift as the cosmic SFR of the Universe rises out to  $z \sim 2$ . The rise in cosmic SFR also makes the delayed SN hosts more star forming which is the major source of the difference between  $\overline{sSFR}$  and  $\overline{sSFR^*}$ .

From the definition in Equation (4.7) we see that the shape of the DTD is independent of redshift if the ratio  $R_A/R_B$  (or  $N_A/N_B$ , see derivation above) is also independent of redshift. From the derivation we also see that this is equivalent to  $A/B \propto \overline{sSFR}^*$  having no explicit redshift dependence. Figure 4.12 presents the determinations of  $A$  and  $B$  from the literature (SDSS and SNLS samples) and the median  $SFR$  from both SDSS, SNLS, and high- $z$  SN samples. There seems to be a clear trend with increasing  $A/B$  ratio with redshift. We argue that that is due to that fact that higher redshift samples probe a more star-forming sample of galaxies. In Figure 4.13 we plot the  $A/B$  ratio against the average  $\overline{sSFR}$  of each sample. All samples seem to be consistent with the relation,

$$A/B \approx k \cdot \overline{sSFR}, \quad (4.21)$$

where the value of  $k$  is determined below. This is consistent with little to no evolution of the slope of the DTD out to  $z = 2$ , only the lower SDSS points tend to be lower than the others. This might be due to the fact that we estimate the sSFR of all the SDSS samples from Lampeitl et al. (2010), as we do not have access to the measured SFRs and stellar masses of the other SDSS works. The value of the proportionality constant  $k$  is directly related to the shape of the DTD. Comparing Equation (4.21) with Equation (4.18) we can see that

$$k = \frac{N_A}{N_B} = \frac{r_A}{r_B} = \frac{R_A}{R_B}. \quad (4.22)$$

#### 4.4.2 A NEW A+B MODEL

Our analysis is just a simple approximation and among others assumes that the age of the host galaxy (on average) is a valid proxy of the delay time of the SN. The stellar age of the host is only used to sort each SN into the prompt and delayed bins. We test the sensitivity of  $k$  to the value of  $t_{\text{split}}$  and by extension the sensitivity of the classification as prompt or delayed hosts to the value of  $t_{\text{split}}$ . For each possible value of  $t_{\text{split}}$  we calculate  $k_{\text{min}}$  and  $k_{\text{max}}$  assuming that all ambiguous hosts are put into the prompt bin (lower limit) or the delayed bin (upper limit). The ambiguous hosts are either hosts containing two stellar populations - one on each side of the split - or hosts with constant SFHs that have a stellar age above  $t_{\text{split}}$ . The values of  $k_{\text{min}}$  and  $k_{\text{max}}$  mark the extremes of the true value of  $k$  (see Figure 4.14). The value of  $k$  is insensitive to small changes in  $t_{\text{split}}$ .

Assuming a universal shape of the DTD (or more correctly a constant  $k$ ), we can use the  $A/B = k \cdot sSFR$  relation to construct a better empirical relation for the two-point DTD (i.e. a "new A+B model"). We start by hypothesizing that it is the value of  $B$  that is dominating the change in the  $A/B$  ratio. From a time-scale argument it is most likely that the prompt component will respond more to changes in the sSFR than the delayed component.

The  $B$  parameter in the A+B model controls the slope of the SNR-sSFR relation. Our hypothesized new model suggests that the slope is changing i.e. the SNR-sSFR relation has a curvature. This can be stated as a simple differential equation,

$$\frac{dR}{dsSFR} = B(sSFR) = \frac{A}{k \cdot sSFR}. \quad (4.23)$$

This equation has the solution

$$R = \begin{cases} \frac{A}{k} \ln\left(\frac{sSFR}{sSFR_0}\right) + A & \text{if } sSFR > sSFR_0 \\ A & \text{else} \end{cases}, \quad (4.24)$$

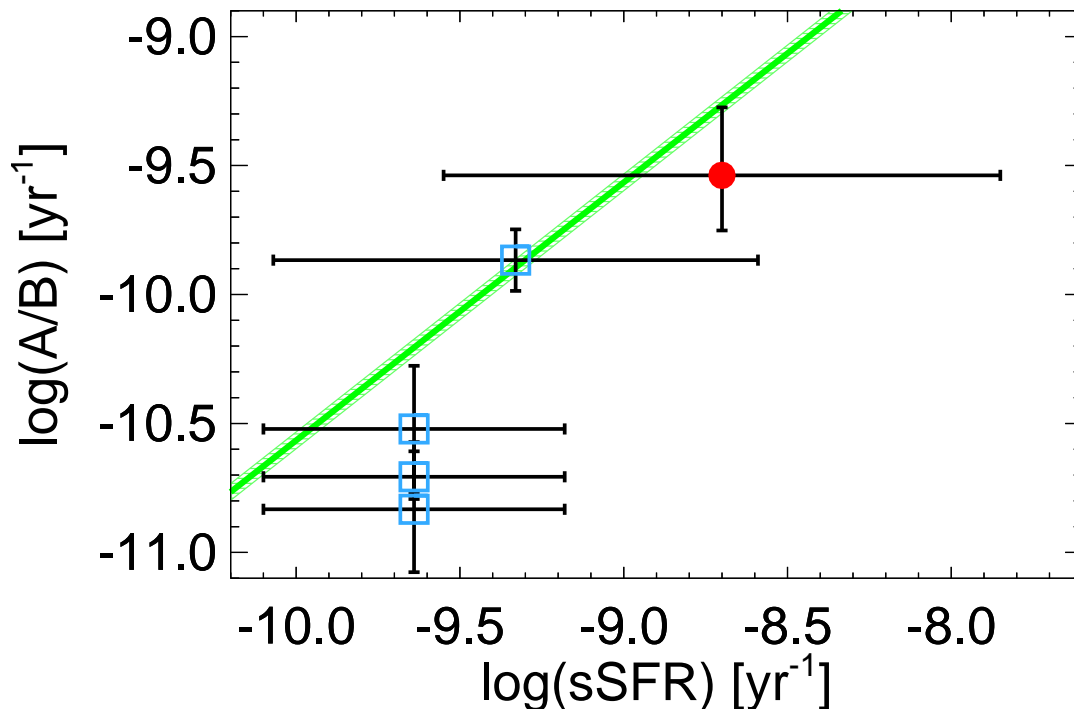


Figure 4.13  $A/B$ -ratio vs.  $sSFR$  range of literature samples. The lower square data-points are SDSS samples where the  $A/B$ -ratios are taken from Mannucci et al. (2005); Dilday et al. (2008); Smith et al. (2012) respectively and the range  $sSFR$  of SDSS SNe is estimated from Lampeitl et al. (2010). The middle data-point is the SNLS SN samples with the  $A/B$ -ratio from Sullivan et al. (2006) and the  $sSFR$ -range from Sullivan et al. (2010). The upper circles data-point is from this study. The solid lines and hashed regions mark the relation in Equation 4.21 using  $k$  from Equation 4.25 (horizontally hashed, green).

where  $A$ , like above, is the SN rate per stellar mass in passive galaxies,  $sSFR_0$  is the constant-of-integration and it marks the transition where the  $sSFR$  term starts to take effect, and  $k$  is the ratio of the prompt-to-delayed SN rate as described above.

We fit Equation (4.24) to literature data (Sullivan et al., 2006; Smith et al., 2012; Gao & Pritchett, 2013) and find the following parameter values

$$\begin{aligned}
 A &= 4.18 \pm 0.37 \cdot 10^{-14} \text{ SN yr}^{-1} \text{ M}_{\odot}^{-1} \\
 k &= 0.272 \pm 0.042 \\
 sSFR_0 &= 3.82 \pm 0.76 \cdot 10^{-11} \text{ yr}^{-1}
 \end{aligned}
 \tag{4.25}$$

In Figure 4.15 we plot Equation (4.24) against the literature data (including Mannucci et al., 2005) using the above parameters.

#### 4.4.3 FRACTION OF PROMPT SUPERNOVAE

Rodney et al. (2013, hereafter R13) used the volumetric SN rates at  $z < 2.5$  to constrain the shape of the DTD. This was done by convolving the cosmic (volumetric) SFH with a model of

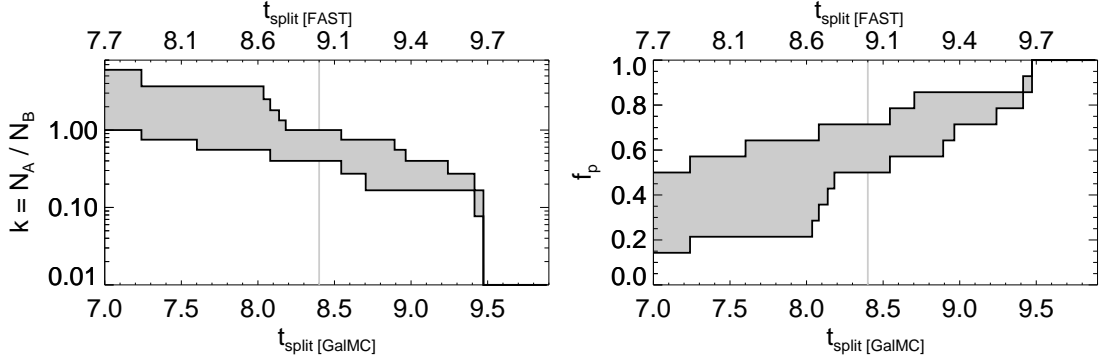


Figure 4.14 Left: The delay-to-prompt ratio,  $k$ , and its dependence on the value of  $t_{\text{split}}$ . For each value of  $t_{\text{split}}$  we calculate the maximum and minimum value of  $k$  by assuming that all ambiguous SN hosts belong either to the prompt or delayed bin of the DTD. Ambiguous hosts are hosts with two stellar populations, one in each bin, or hosts with a constant SFH that have a stellar age larger than  $t_{\text{split}}$ . The value of  $k$  is insensitive to small changes in  $t_{\text{split}}$ . Right: Prompt fraction calculated from the delay-to-prompt ratio (see Equation 4.27).

the DTD. They found that a DTD with a powerlaw slope of  $-1$  was consistent with the measured SN rates. They also tried to fit a two component DTD,

$$R(t) = \begin{cases} 0 & t < 40 \text{ Myr} \\ \eta \cdot K \cdot \frac{f_p}{1-f_p} & 40 \text{ Myr} < t < 0.5 \text{ Gyr} \\ \eta \cdot \left(\frac{t}{1 \text{ Gyr}}\right)^{-1} & t > 0.5 \text{ Gyr} \end{cases} \quad (4.26)$$

with a powerlaw shape ( $t^{-1}$ ) for long delay times and an independent bin for very short delay times (see schematic in Figure 4.16). They found that the fraction of prompt SNe ( $\sim 45\%$ ) was consistent with the powerlaw continuing all the way down to the shortest delay times (40 Myr).

In this analysis we use the SFH of each individual host galaxy to put constraint on the shape of the DTD without relying on the cosmic SFH. Our partition between prompt and delayed ( $\log t = 8.4$ ) almost coincides with the value of 0.5 Gyr ( $\log t = 8.7$ ) used in R13. Their prompt bin is equivalent with our B-bin and the averaged powerlaw at long delay times corresponds to our delayed bin (i.e. the A-bin). The delay-to-prompt ratio determined above can be translated to a prompt fraction,  $f_p$ , as used in R13 using

$$f_p = \frac{N_B}{N_A + N_B} = \frac{1}{k + 1}, \quad (4.27)$$

where  $k$ , is the delay-to-prompt ratio defined above (see also Figure 4.14, right). We plot our 2-bin DTD in comparison to the R13 DTD in Figure 4.16. We plot the their DTD using the best fit parameters of R13 ( $K = 7.132$ ,  $f_p = 0.45$ ,  $\eta = 1.98 \cdot 10^{-4} \text{ SNe yr}^{-1} M_\odot$ ). We had to put an absolute scaling on our DTD. The absolute scaling is chosen such that the time-integrated ( $\int DTD dt$ ) value of both DTDs is the same (i.e. integrated from 30 Myr — approx. age of youngest host — to 13.9 Gyr). From our analysis we get  $k = 1.0 - 0.4$  or equivalently  $f_p = 0.50 - 0.71$ .

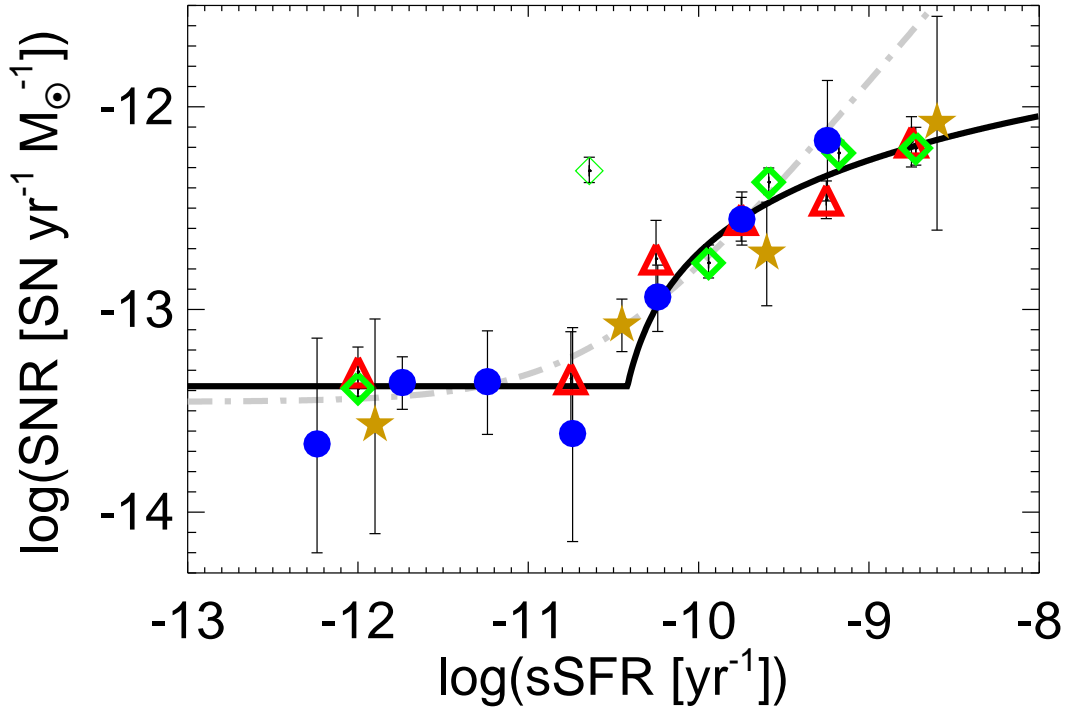


Figure 4.15 The SN rate as a function of sSFR. The measurements of Mannucci et al. (2005); Sullivan et al. (2006); Smith et al. (2012); Gao & Pritchett (2013) (yellow stars, red triangles, green diamonds, and blue circles, respectively). The black line show Equation 4.24 fitted to the data (except Mannucci et al., 2005). The gray dash-dotted line show the A+B model of Gao & Pritchett (2013).

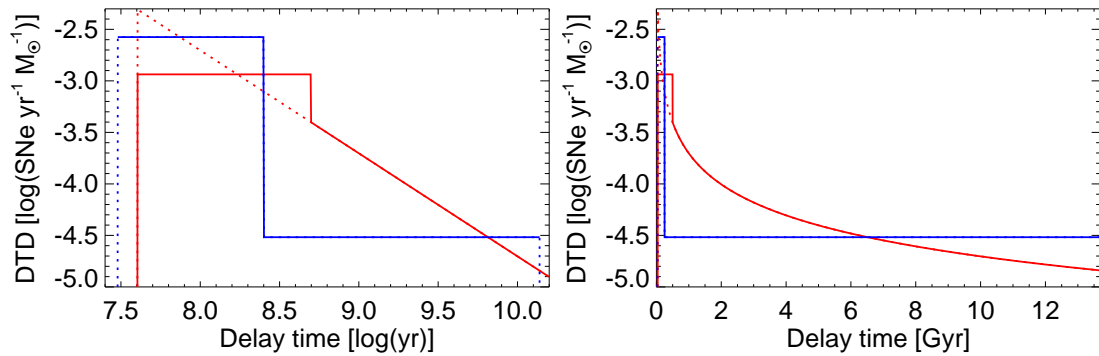


Figure 4.16 Schematic of the DTD model of Rodney et al. (2013, red; dotted line: powerlaw only) and the one used in our analysis (blue). (Left: log-log scale, Right: log-linear scale.) The 2-bin DTD (A+B model) used in our analysis is not fixed to any absolute scale, we therefore choose to set the scale such that the area under the curve (i.e. the time-integrated SN rate) is equal to the Rodney et al. (2013) curve. The upper and lower bounds marked by blue dashed lines correspond to the stellar age of the youngest and oldest host.

## 4.5 CONCLUSIONS & OUTLOOK

In this chapter we have analyzed the host galaxies of  $z > 1$  SNe from the CLASH and CANDELS surveys. We have performed careful SED fitting to broadband photometry of the SN hosts to determine stellar parameters like masses, ages, extinction and star formation. On the basis of this dataset we are able to conclude:

- We infer that the shape of the DTD is consistent with only little evolution out to  $z \sim 2$ , but leaving the possibility that DTD inferred from low redshift samples like SDSS might be different from higher redshift samples (like SNLS or HST). This was done by comparing the A/B ratio to the specific SFR of different literature datasets. A proper reanalysis of the literature data, with SFR and stellar masses for each SN host would be able to put stronger constraints on any DTD evolution using this method.
- We have proposed a new parameterization of the SN rate as a function of the specific SFR. The model is derived from a simplified 2-bin DTD inspired by the empirical A+B model. The model predicts that the slope of the SNR(sSFR)-graph becomes more flat at high specific SFRs. The curvatures at high specific SFRs is related to the shape of the DTD. Even assuming a constant DTD shape (even though it might not be) this parameterization gives a better prediction of the SN rate for high-sSFR galaxies than the empirical A+B model (which over-predicts the SN rate at high specific SFR).
- The fraction of prompt SN,  $f_p = 0.45 \pm 0.1$ , measured by Rodney et al. (2013, R13) is confirmed by our analysis,  $f_p = 0.50 - 0.71$ . Our analysis is an independent measure of  $f_p$  even though the R13 sample coincides with our CANDELS SNe. Our use of the star-formation histories (SFH) of the individual host galaxies compared to the cosmic SFH used by R13 makes the two measurements independent.

The sample of high redshift SNe is constantly increasing. The 14 SNe used in this analysis does not include the SN found in 2013 (see Section 4.2). The CLASH and CANDELS surveys are now concluded, but a new survey called the Frontiers Fields (FF) has been approved to survey six strong lensing clusters. Due to the strong lensing effects of the clusters the FF survey will be able to survey very deep. This survey will also have a SN search components to enlarge the sample of high redshift SNe. The SN found behind strong-lensing clusters in FF will also help improve the lensing models of each cluster by providing a measure of the local magnification (and thereby the local mass density) at the SN location. This is possible because the SNe are good enough standard candles. This can provide constraints on the mass model in the weak lensing regime.

Childress et al. (2013b) was the first to build a big enough SN sample to infer the precise shape of the Hubble residuals as a function of the stellar mass of the host. The next question that we need to answer is what causes this effect, and how does this effect affect the usability of high redshift SNe to infer cosmology. The size of the "step" is 0.077 magnitudes, and is therefore smaller than the intrinsic dispersion of 0.1 magnitude seen in most SN samples. But this effect introduces a small systematic offset that we need to quantify. We also need to study how the size of the step evolves with redshift.

Table 4.2: Full list of all SN-like transients in the CANDELS and CLASH surveys

SN name	Redshift ( $z > 1$ )	Host V	Host Z ( $Z < 26$ )	Host J ( $J < 25$ )	Crit.			SN Type
					A	B	AB	
<i>CANDELS SNe</i>								
UDS10Gra (Grant)	0.211 <sub>s</sub>	22.7	22.4	22.4	–	B	–	decliner
UDS10Joh (Johnson)	1.3 ± 1.3 <sub>p</sub>	30.4	27.5	26.4	(–)	–	–	decliner
UDS11Gar (Garfield)	0.651 <sub>s</sub>	24.3	24.6	24.2	–	B	–	
UDS10Wil (Wilson)	1.914 <sub>s</sub>	25.5	25.2	24.5	A	B	✓	Ia
uds02j (Cleveland)	1.406 <sub>s</sub>	23.5	23.0	22.7	A	B	✓	decliner
UDS10Pie (Pierce)	0.6 ± 0.2 <sub>p</sub>	25.3	—	22.9	–	B	–	decliner
UDS10Ben (Benjamin)	—	31.5	—	24.7	–	B	–	decliner,AGN?
GSA12Roc (Rockefeller)	0.4 ± 0.2 <sub>p</sub>	26.3	—	—	–	–	–	
gsa02b (Jefferson)	0.311 <sub>s</sub>	19.8	—	—	–	–	–	decliner
GSA11Wor (Workman)	0.654 <sub>s</sub>	23.5	—	21.3	–	B	–	
GSA12Qua (Quayle)	2.370 <sub>s</sub>	24.1	24.0	23.9	A	B	✓	CC?
GSA11For (Ford)	0.578 <sub>s</sub>	22.8	—	20.8	–	B	–	
GSA12Hum (Humphrey)	2.343 <sub>s</sub>	26.8	26.6	—	A	–	–	CC?
GSA10Tum (Tumbleweed)	0.124 <sub>s</sub>	19.1	—	17.6	–	B	–	CC?
gsa06c (Madison)	0.988 <sub>s</sub>	23.4	23.0	22.9	–	B	–	decliner
GSA11Van (VanBuren)	0.7 ± 0.2 <sub>p</sub>	25.9	24.2	23.9	–	B	–	CC
GSA11Ada (Adams)	0.735 <sub>s</sub>	22.7	21.9	21.7	–	B	–	
GSA11Was (Washington)	1.0 ± 0.2 <sub>p</sub>	26.7	25.7	24.7	A	B	✓	Ia
GSA12Agn (Agnew)	1.095 <sub>s</sub>	22.7	21.6	21.2	A	B	✓	CC
GSA11Pol (Polk)	1.090 <sub>s</sub>	23.8	21.8	20.2	A	B	✓	decliner
GSA11Buc (Buchanan)	0.679 <sub>s</sub>	22.9	—	21.1	–	B	–	
GSA11Lin (Lincoln)	0.8 ± 0.2 <sub>p</sub>	25.1	—	24.0	–	B	–	
GSA11Har (Harrison)	0.681 <sub>s</sub>	21.2	20.3	20.0	–	B	–	
GSA11Roo (Roosevelt)	0.655 <sub>s</sub>	23.1	22.5	22.4	–	B	–	CC?
GSA11Jac (Jackson)	0.659 <sub>s</sub>	24.7	23.9	23.7	–	B	–	
GSA10Pri (Primo)	1.550 <sub>s</sub>	24.8	24.8	24.4	A	B	✓	Ia
GSA11Bus (Bush)	1.8 ± 0.7 <sub>p</sub>	28.8	28.3	27.0	(–)	–	–	
gsa04b (McKinley)	0.195 <sub>s</sub>	23.6	—	22.3	–	B	–	decliner
GSA11Tay (Taylor)	0.535 <sub>s</sub>	22.2	—	20.5	–	B	–	
COS12Car (Carter)	1.2 ± 0.2 <sub>sn</sub>	—	—	—	A	–	–	Ia
COS12Aid (Aidan)	0.731 <sub>s</sub>	24.7	—	—	–	–	–	CC?
COS12Cli (Clinton)	0.187 <sub>s</sub>	19.8	—	18.0	–	B	–	CC
cos02b (FDR)	0.729 <sub>s</sub>	26.1	25.2	26.5	–	–	–	decliner
COS12Mon (Mondale)	0.777 <sub>s</sub>	22.7	—	22.0	–	B	–	CC
COS12Mik (Mikulski)	0.927 <sub>s</sub>	23.9	22.2	22.0	–	B	–	Ia?
COS12Rea (Reagan)	0.679 <sub>s</sub>	23.8	—	21.8	–	B	–	CC
COS12Ken (Kennedy)	0.371 <sub>s</sub>	22.3	—	22.2	–	B	–	CC
COS12Tru (Truman)	0.234 <sub>s</sub>	23.2	21.8	21.6	–	B	–	CC
COS12LBJ (LBJ)	0.782 <sub>s</sub>	27.3	26.6	25.3	–	–	–	CC? (decliner)
COS12Her (Herbert)	0.4 ± 0.1 <sub>p</sub>	25.0	—	23.8	–	B	–	CC
gna07g (Fairbanks)	0.332 <sub>s</sub>	25.4	25.3	24.5	–	B	–	CC

gna02d (Cheney)	0.213 <sub>s</sub>	21.0	20.5	20.2	–	B	–	decliner
gna02c (Gore)	1.020 <sub>s</sub>	28.6	26.0	24.6	A	B	✓	
gna04a (Wheeler)	1.9 ± 0.5 <sub>p</sub>	25.1	24.8	23.9	(–)	B	✓	
gna07c (Burr)	0.5 ± 0.2 <sub>p</sub>	25.7	25.1	25.2	–	–	–	
gna02b (Barkley)	0.457 <sub>s</sub>	20.0	18.8	18.2	–	B	–	decliner
gna02e (Colfax)	2.1 ± 0.2 <sub>sn</sub>	26.2	25.4	23.7	A	B	✓	
gna07d (Amara)	0.518 <sub>s</sub>	22.3	21.3	20.8	–	B	–	
gna04f (Tompkins)	1.141 <sub>s</sub>	24.1	22.4	21.3	A	B	✓	
gna07f (Hendricks)	1.6 ± 0.6 <sub>p</sub>	26.2	26.1	24.8	(–)	B	✓	decliner
gna02f (Hamlin)	1.220 <sub>s</sub>	25.9	23.2	22.1	A	B	✓	
gna07b (Thomas)	3.0 ± 3.0 <sub>p</sub>	26.2	26.0	26.5	(–)	–	–	
gna02a (Wallace)	0.457 <sub>s</sub>	23.6	23.0	22.8	–	B	–	decliner
gna04b (Breckenridge)	1.8 ± 1.5 <sub>p</sub>	26.6	26.8	26.9	(–)	–	–	
gna04c (Calhoun)	0.940 <sub>s</sub>	24.4	23.4	23.0	–	B	–	
gna04d (King)	1.9 ± 0.4 <sub>p</sub>	28.8	28.0	25.1	A	–	–	
gna07a (Gerry)	0.9 ± 0.1 <sub>p</sub>	25.2	24.2	24.2	–	B	–	
gna05a (Morton)	1.1 ± 0.5 <sub>p</sub>	24.5	24.0	24.1	(–)	B	–	
gna07e (John)	0.212 <sub>s</sub>	21.7	21.2	20.8	–	B	–	
EGS11Per (Perriello)	0.915 <sub>s</sub>	—	—	—	–	–	–	
egs02c (Coolidge)	1.8 ± 0.5 <sub>p</sub>	26.5	27.0	25.8	(–)	–	–	decliner
egs02b (Arthur)	0.436 <sub>s</sub>	—	—	—	–	–	–	decliner
EGS11Tho (Thor)	0.350 <sub>s</sub>	—	—	—	–	–	–	
egs02e (Taft)	0.717 <sub>s</sub>	—	22.8	—	–	B	–	decliner
EGS11Tyl (Tyler)	2.7 ± 2.0 <sub>p</sub>	26.7	—	26.1	(–)	–	–	
EGS11Oba (Obama)	1.409 <sub>s</sub>	—	23.2	21.7	A	B	✓	
EGS11Nix (Nixon)	—	—	—	—	–	–	–	
<i>CLASH SNe</i>								
CLA10Cal (Caligula)	1.7 ± 0.2 <sub>p</sub>	26.1	25.5	24.4	A	B	✓	Ia
CLA10Ner (Nero)	0.362 <sub>s</sub>	22.0	20.4	—	–	B	–	Ia
CLA11Tib (Tiberius)	1.141 <sub>s</sub>	21.9	20.6	—	A	B	✓	CC
CLA11Gal (Galba)	0.275 <sub>s</sub>	18.4	16.5	—	–	B	–	
CLB11Oth (Otho)	0.962 <sub>s</sub>	23.7	21.9	—	–	B	–	Ia
CLB11Sca (Scarlet)	0.354 <sub>s</sub>	21.1	19.4	—	–	B	–	
CLC11Tit (Titus)	0.839 <sub>s</sub>	23.5	22.6	—	–	B	–	Ia
CLD11Cla (Claudius)	0.3 ± 0.1 <sub>p</sub>	21.7	21.4	—	–	B	–	CC
CLE11Aug (Augustus)	0.329 <sub>s</sub>	21.1	20.5	—	–	B	–	CC
CLF11Ves (Vespasian)	1.220 <sub>s</sub>	25.4	21.9	21.0	A	B	✓	Ia
CLF11Dom (Domitian)	0.7 ± 0.1 <sub>p</sub>	—	—	—	–	–	–	Ia (?)
CLH11Tra (Trajan)	1.4 ± 0.1 <sub>p</sub>	26.6	23.4	—	A	B	✓	Ia
CLI11Had (Hadrian)	0.261 <sub>s</sub>	19.1	17.9	—	–	B	–	Ia
CLJ11Cri (Crimson)	0.702 <sub>s</sub>	22.2	19.7	—	–	B	–	Ia
CLK11Bur (Burgundy)	0.281 <sub>s</sub>	20.3	19.7	—	–	B	–	CC (?)
CLI11Piu (Antoninus Pius)	0.191 <sub>s</sub>	21.4	20.9	—	–	B	–	CC
CLL12Aur (Marcus Aurelius)	0.271 <sub>s</sub>	18.5	17.7	—	–	B	–	CC
CLL12Luc (Lucius Verus)	0.360 <sub>s</sub>	21.2	—	—	–	–	–	CC (?)
CLM12Com (Commodus)	0.207 <sub>s</sub>	20.9	20.6	—	–	B	–	CC
CLM12Per (Pertinax)	0.2 ± 0.03 <sub>p</sub>	22.9	21.8	—	–	B	–	Ia

Table 4.3 Full list of the high- $z$  sample.

SN name	Redshift	$N_{\text{lines}}$	Ref. / Emission-line species
Colfax	$(2.1 \pm 0.2)$	—	(SN colors)
Hendricks	(phot- $z$ )	—	—
Primo	1.550	—	Frederiksen et al. (2012)
Polk	1.090	—	(A)
Washington	(Phot- $z$ )	—	—
Wilson	1.914	1	[O III] 5007
Cleveland	1.406	4	$H\alpha$ , [O III] 5007+4959, $H\beta$
Caligula	(Phot- $z$ )	—	—
Macrinus	1.034	—	(A)
Geta	(Phot- $z$ )	0	No emission lines, only continuum
Trajan	(Phot- $z$ )	0	No emission lines, only continuum
Vespasian	1.22	—	(A)
Caracalla	(Phot- $z$ )	—	—
Obama	1.409	—	Cooper et al. (2011) & (A)
Wheeler	(phot- $z$ )	—	—
Tompkins	1.141	—	Barger et al. (2008) & (A)
Agnew	1.095	—	Vanzella et al. (2005)
Quayle	2.370	3	[O III] 5007+4959, $H\alpha$
Tiberius	1.141	—	(A)
Gore	1.020	—	(A)
Hamlin	1.220	—	Barger et al. (2008)

All hosts marked by a number in the  $N_{\text{lines}}$ -column were observed with X-shooter.

(A) marks the spectroscopic redshifts obtained from other collaborators where the spectrum has not been published yet. Most of these are obtained with the LRIS or DEIMOS instrument on the Keck telescope.

CLN12Did (Didius Julianus)	$0.852_s$	23.3	20.5	—	—	B	—	Ia
CLM12Car (Cardinal)	$0.518_s$	21.3	18.9	—	—	B	—	CC
CLO12Sep (Septimus Severus)	$0.4 \pm 0.02_p$	22.8	20.8	—	—	B	—	
CLO12Car (Caracalla)	$1.1 \pm 0.4_p$	24.8	22.1	—	(-)	B	✓	
CLP12Get (Geta)	$1.64_s$	24.8	23.7	22.5	A	B	✓	Ia
CLR12Arm (Armstrong)	$1.2 \pm 0.2_p$	28.5	26.9	26.5	A	—	—	CC
CLS12Mac (Macrinus)	$1.034_s$	24.1	23.3	22.9	A	B	✓	Ia
CLT12Ela (Elagabalus)	$0.606_s$	25.5	21.6	—	—	B	—	Ia
CLT12Ale (Alexander Severus)	$1.2 \pm 0.00_p$	—	27.0	26.3	A	—	—	
CLC12Thr (Thrax)	$0.2 \pm 0.04_p$	20.2	18.0	—	—	B	—	CC (?)
CLV12Gor (Gordian)	$0.516_s$	—	21.5	—	—	B	—	Ia

Table 4.4 Bayesian Information Criterion (BIC)

SN name	Type	$N_{\text{Bands}}$	SSP	CSF	Tau	$2 \times \text{SSP}$	Best SFH
Colfax	Ia	11	493	532	495	487	2S
Hendricks	Ia	9	15.3	15.5	17.5	13.6	2S
Primo	Ia	14	34.5	36.4	35.6	36.5	S
Polk	Ia	11	17.6	17.3	19.7	19.8	C
Washington	Ia	11	119	113	115	121	C
Wilson	Ia	10	13.5	19.0	15.9	15.8	S
Cleveland	Ia	12	82.0	81.9	84.4	83.5	C
Caligula	Ia	8	64.5	64.6	65.4	66.2	S
Vespasian	Ia	5	6.49	114	9.38	10.1	S
Trajan	Ia	5	9.44	114	10.8	75.5	S
Caracalla	Ia	15	49.5	46.5	45.0	37.6	2S
Geta	Ia	9	14.3	22.3	16.5	16.4	S
Macrinus	Ia	6	111	143	113	113	S
Obama	Ia	10	296	271	274	266	2S
Wheeler	CC	11	276	277	266	276	T
Tompkins	CC	9	493	479	495	467	2S
Agnew	CC	11	286	290	276	275	2S
Quayle	CC	13	209	283	212	212	S
Tiberius	CC	5	5.14	4.94	6.47	6.84	C
Gore	—	9	374	392	376	377	S
Hamlin	—	9	417	929	419	418	S

Table 4.5 Stellar parameters from GalMC.

SN name	SFH	$\log t_*$	$\log M_*$	$E(B - V)$	$\log \text{SFR}$	$\log t_2 / \log \tau$
Colfax	2S	$9.381^{+0.071}_{-0.636}$	$10.408^{+0.173}_{-0.373}$	$0.079^{+0.098}_{-0.053}$	$0.469^{+0.215}_{-0.108}$	$8.710^{+0.050}_{-0.055}$
Hendricks	2S	$8.093^{+0.877}_{-1.186}$	$8.038^{+0.370}_{-0.176}$	$0.210^{+0.038}_{-0.045}$	$1.178^{+0.142}_{-0.196}$	$6.370^{+0.923}_{-0.310}$
Primo	S	$6.919^{+0.019}_{-0.022}$	$8.211^{+0.027}_{-0.029}$	$0.112^{+0.007}_{-0.007}$	$0.888^{+0.011}_{-0.011}$	—
Polk	C	$8.830^{+0.207}_{-0.362}$	$10.784^{+0.182}_{-0.283}$	$0.149^{+0.154}_{-0.092}$	$1.055^{+0.217}_{-0.145}$	—
Washington	C	$9.465^{+0.170}_{-0.253}$	$8.730^{+0.159}_{-0.168}$	$0.050^{+0.034}_{-0.028}$	$-0.386^{+0.100}_{-0.097}$	—
Wilson	S	$7.239^{+0.202}_{-0.234}$	$9.106^{+0.099}_{-0.258}$	$0.284^{+0.032}_{-0.062}$	$1.129^{+0.048}_{-0.091}$	—
Cleveland	C	$8.178^{+0.054}_{-0.048}$	$9.236^{+0.016}_{-0.017}$	$0.104^{+0.015}_{-0.015}$	$1.323^{+0.023}_{-0.023}$	—
Caligula	S	$6.648^{+0.141}_{-0.053}$	$8.487^{+0.329}_{-0.187}$	$0.321^{+0.047}_{-0.037}$	$1.094^{+0.077}_{-0.073}$	—
Macrinus	S	$8.077^{+0.039}_{-0.026}$	$8.991^{+0.031}_{-0.024}$	$0.015^{+0.017}_{-0.010}$	$0.646^{+0.026}_{-0.015}$	—
Geta	S	$8.508^{+0.258}_{-0.472}$	$10.667^{+0.082}_{-0.058}$	$0.218^{+0.215}_{-0.120}$	$1.234^{+0.296}_{-0.164}$	—
Caracalla	2S	$9.302^{+0.279}_{-0.199}$	$10.497^{+0.176}_{-0.303}$	$0.258^{+0.077}_{-0.075}$	$0.958^{+0.138}_{-0.127}$	$7.602^{+0.063}_{-0.063}$
Trajan	S	$9.427^{+0.155}_{-0.156}$	$10.860^{+0.219}_{-0.187}$	$0.082^{+0.119}_{-0.056}$	$0.195^{+0.479}_{-0.230}$	—
Vespasian	S	$9.602^{+0.118}_{-0.137}$	$11.056^{+0.128}_{-0.113}$	$0.200^{+0.074}_{-0.067}$	$-0.062^{+0.239}_{-0.407}$	—
Obama	2S	$6.618^{+1.322}_{-0.390}$	$10.044^{+0.020}_{-0.018}$	$0.200^{+0.132}_{-0.012}$	$1.668^{+0.431}_{-0.038}$	$8.041^{+0.011}_{-0.007}$
Wheeler	T	$7.905^{+0.082}_{-0.625}$	$9.529^{+0.105}_{-0.384}$	$0.239^{+0.112}_{-0.051}$	$1.686^{+0.327}_{-0.128}$	$7.258^{+0.273}_{-0.305}$
Tompkins	2S	$9.111^{+0.011}_{-0.007}$	$10.419^{+0.025}_{-0.022}$	$0.202^{+0.018}_{-0.019}$	$1.025^{+0.060}_{-0.065}$	$8.423^{+0.036}_{-0.028}$
Agnew	2S	$8.023^{+0.003}_{-0.003}$	$10.113^{+0.024}_{-0.026}$	$0.193^{+0.009}_{-0.011}$	$1.275^{+0.014}_{-0.017}$	$8.393^{+0.018}_{-0.020}$
Quayle	S	$7.228^{+0.060}_{-0.142}$	$9.570^{+0.042}_{-0.118}$	$0.218^{+0.013}_{-0.023}$	$1.834^{+0.019}_{-0.034}$	—
Tiberius	C	$8.578^{+0.277}_{-0.274}$	$10.729^{+0.103}_{-0.097}$	$0.332^{+0.049}_{-0.043}$	$2.003^{+0.074}_{-0.065}$	—
Gore	S	$9.302^{+0.270}_{-0.379}$	$9.258^{+0.203}_{-0.266}$	$0.170^{+0.078}_{-0.033}$	$-0.702^{+0.263}_{-0.113}$	—
Hamlin	S	$9.645^{+0.053}_{-0.118}$	$10.931^{+0.060}_{-0.108}$	$0.150^{+0.010}_{-0.010}$	$-0.350^{+0.036}_{-0.035}$	—

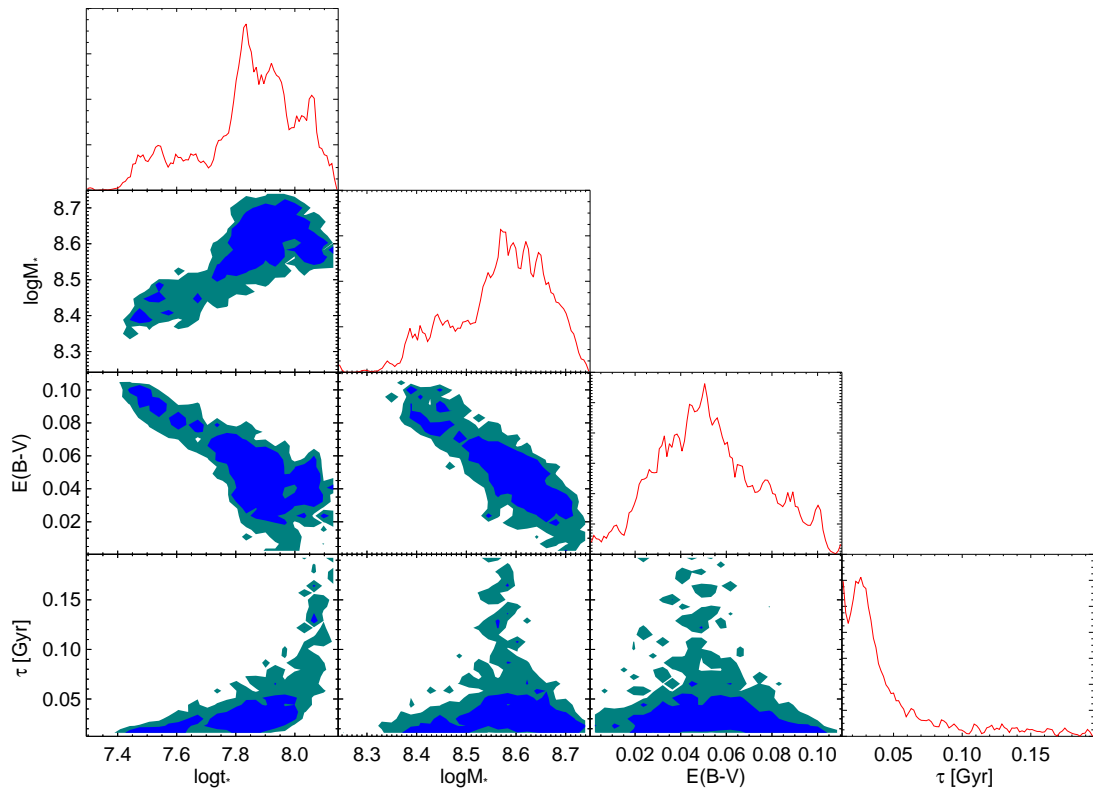


Figure 4.17 Triangular plot of the GalMC MCMC chain for Primo.

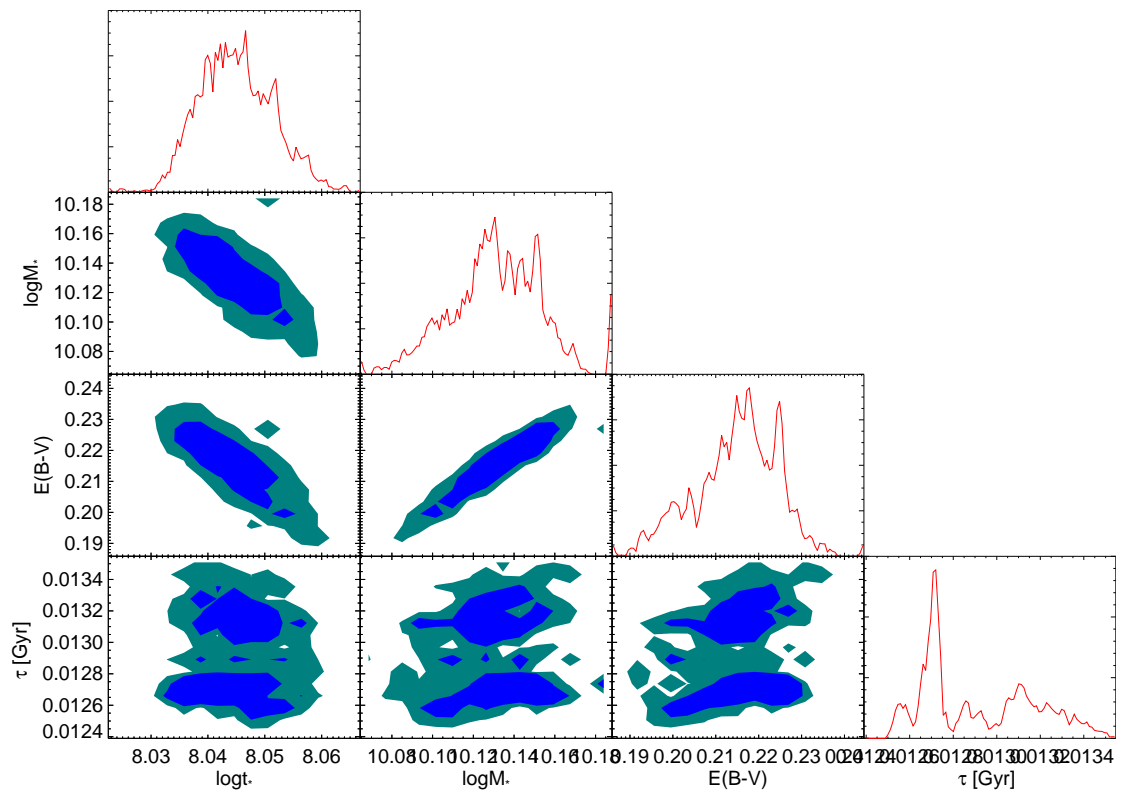


Figure 4.18 Triangular plot of the GalMC MCMC chain for Agnew.

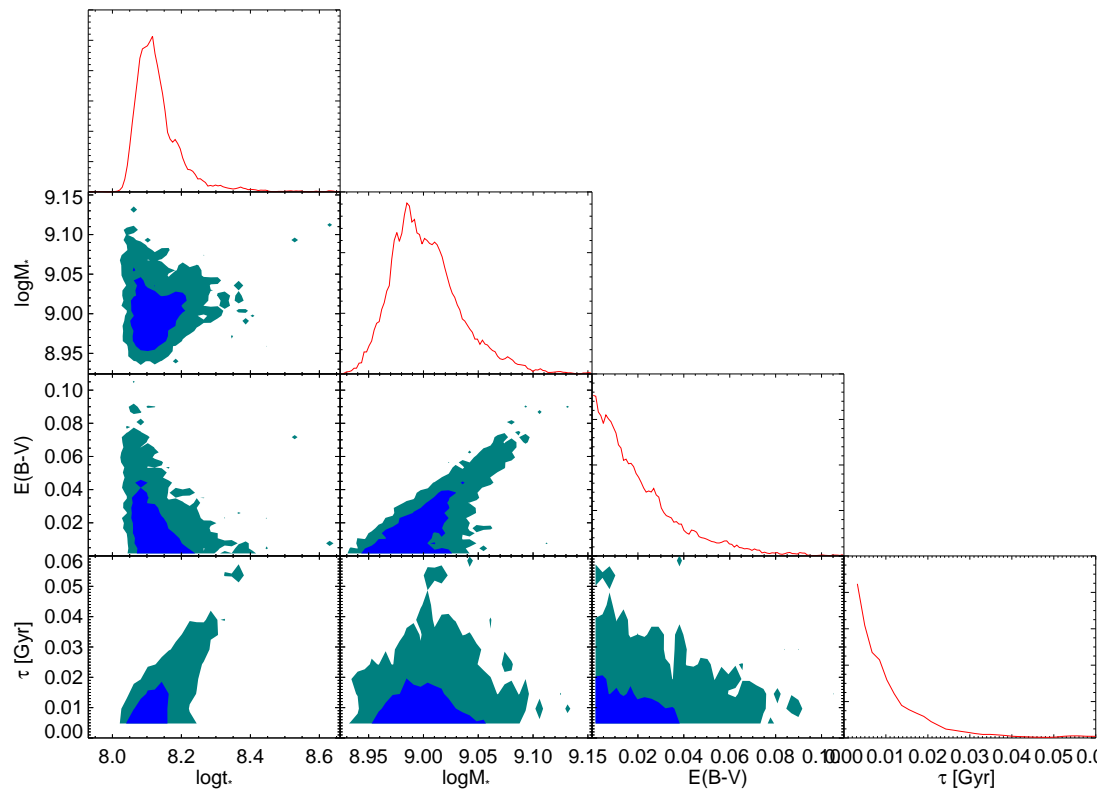


Figure 4.19 Triangular plot of the GalMC MCMC chain for Macrinus.

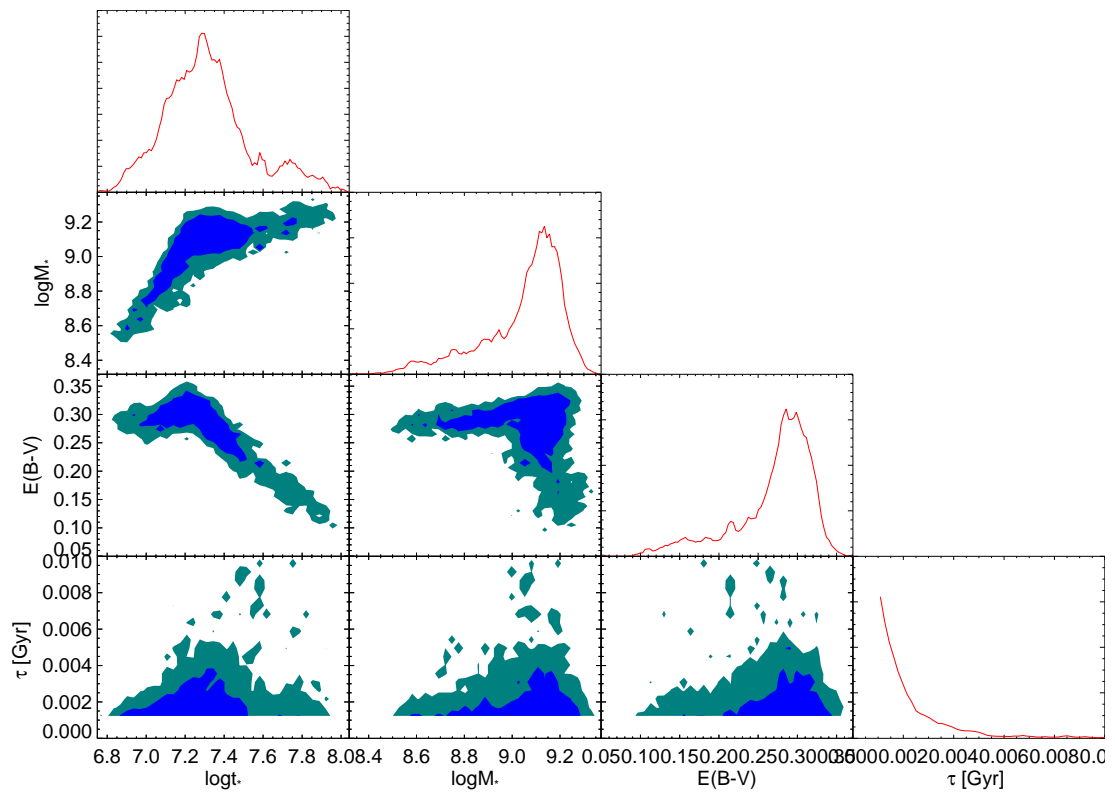


Figure 4.20 Triangular plot of the GalMC MCMC chain for Wilson.

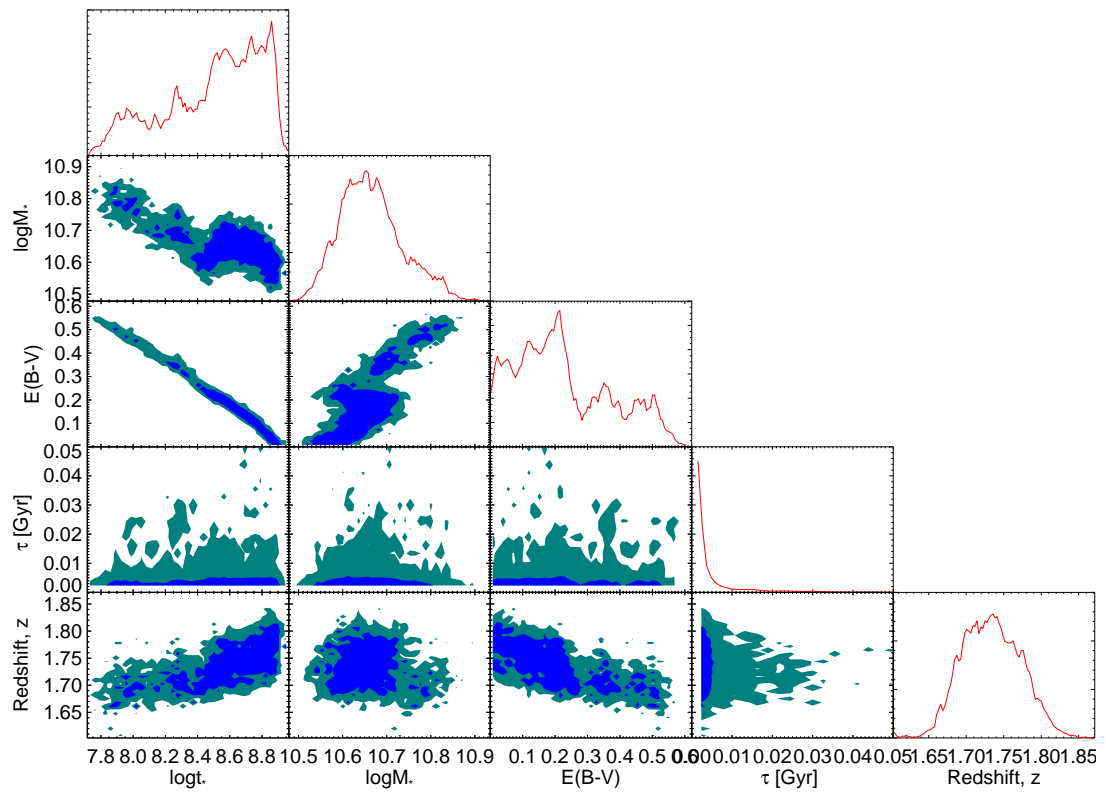


Figure 4.21 Triangular plot of the GalMC MCMC chain for Geta.

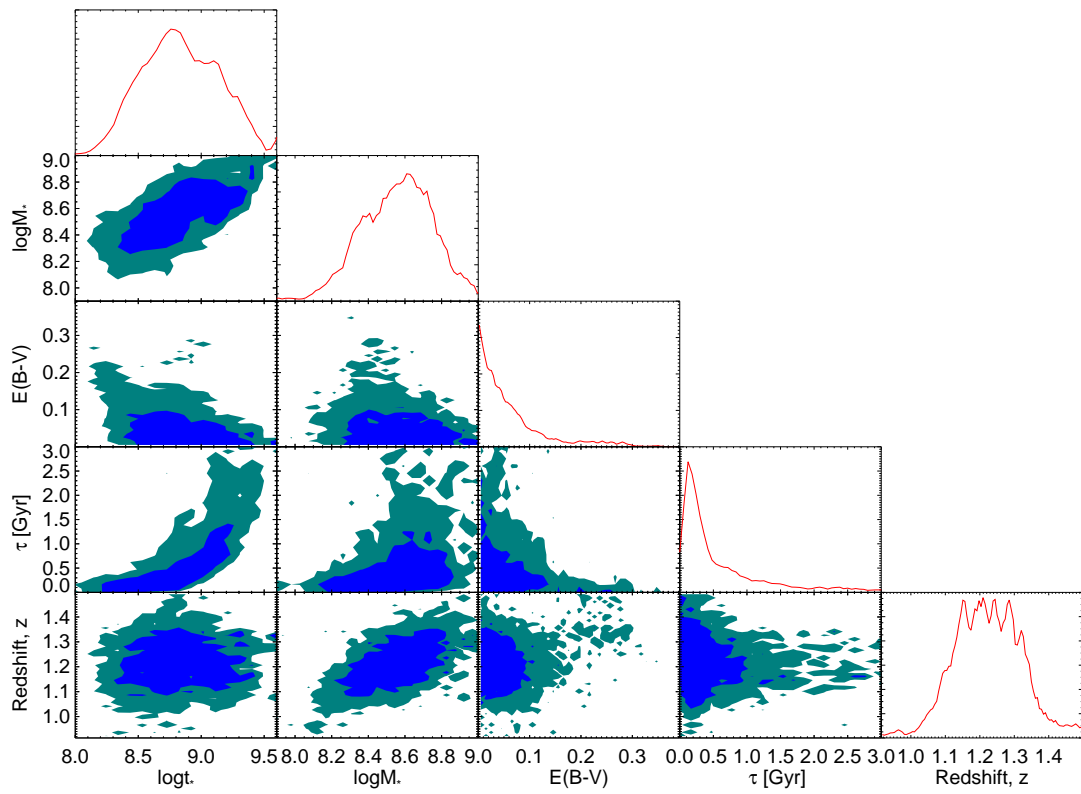


Figure 4.22 Triangular plot of the GalMC MCMC chain for Washington.

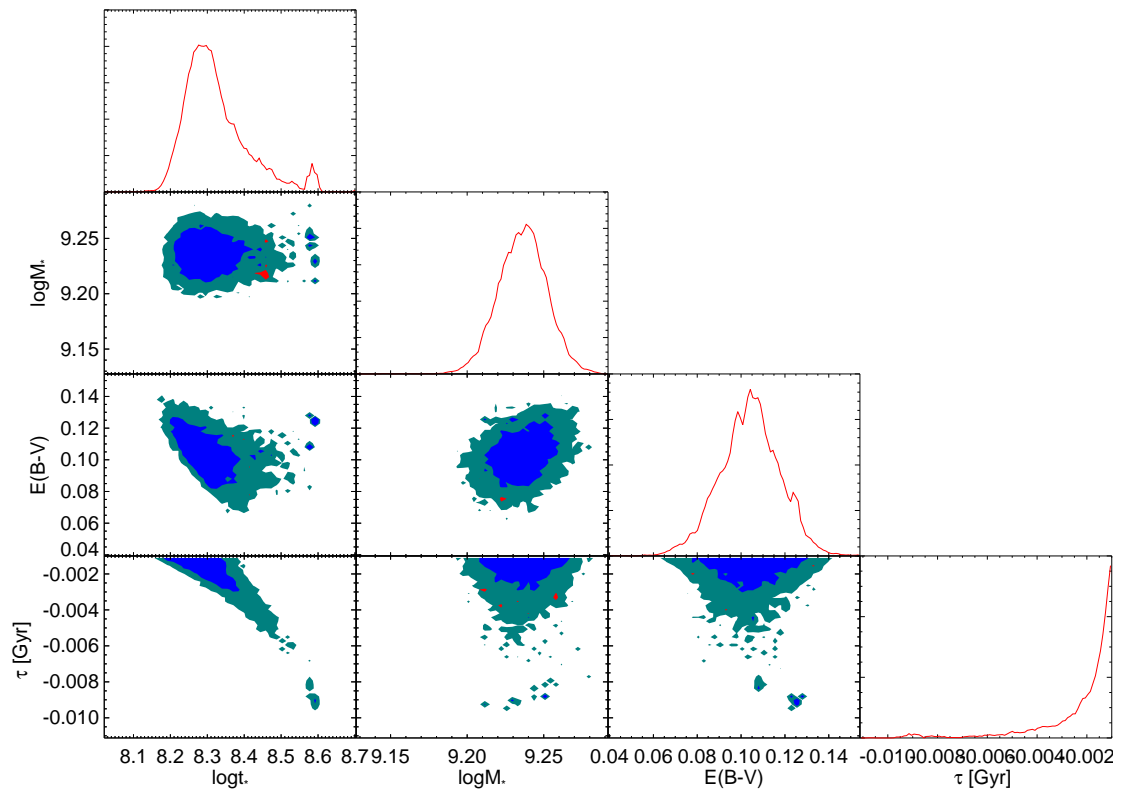


Figure 4.23 Triangular plot of the GalMC MCMC chain for Cleveland.

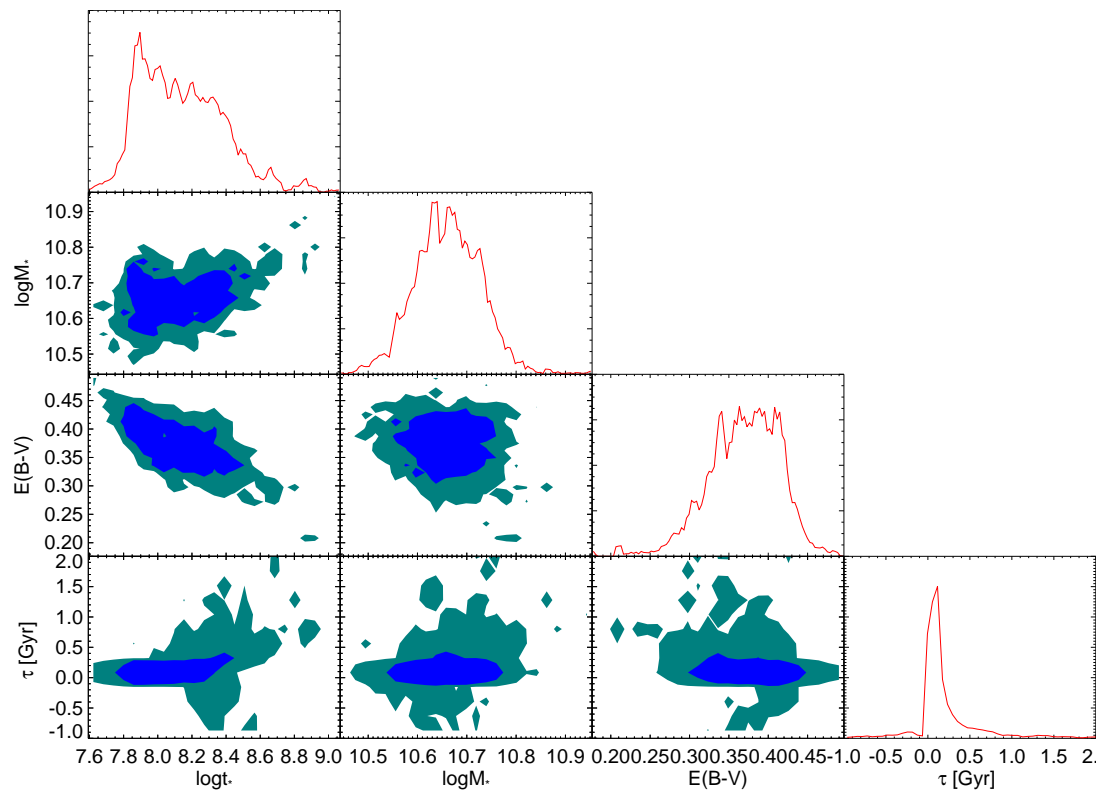


Figure 4.24 Triangular plot of the GalMC MCMC chain for Tiberius.

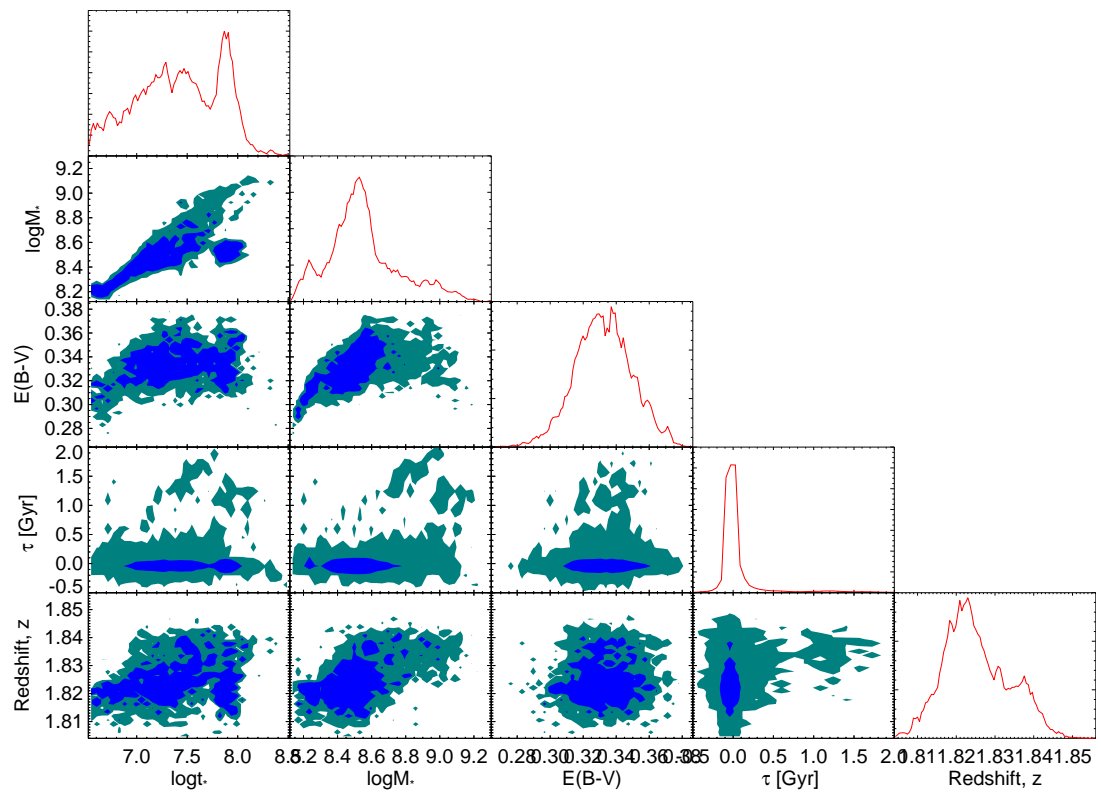


Figure 4.25 Triangular plot of the GalMC MCMC chain for Caligula.

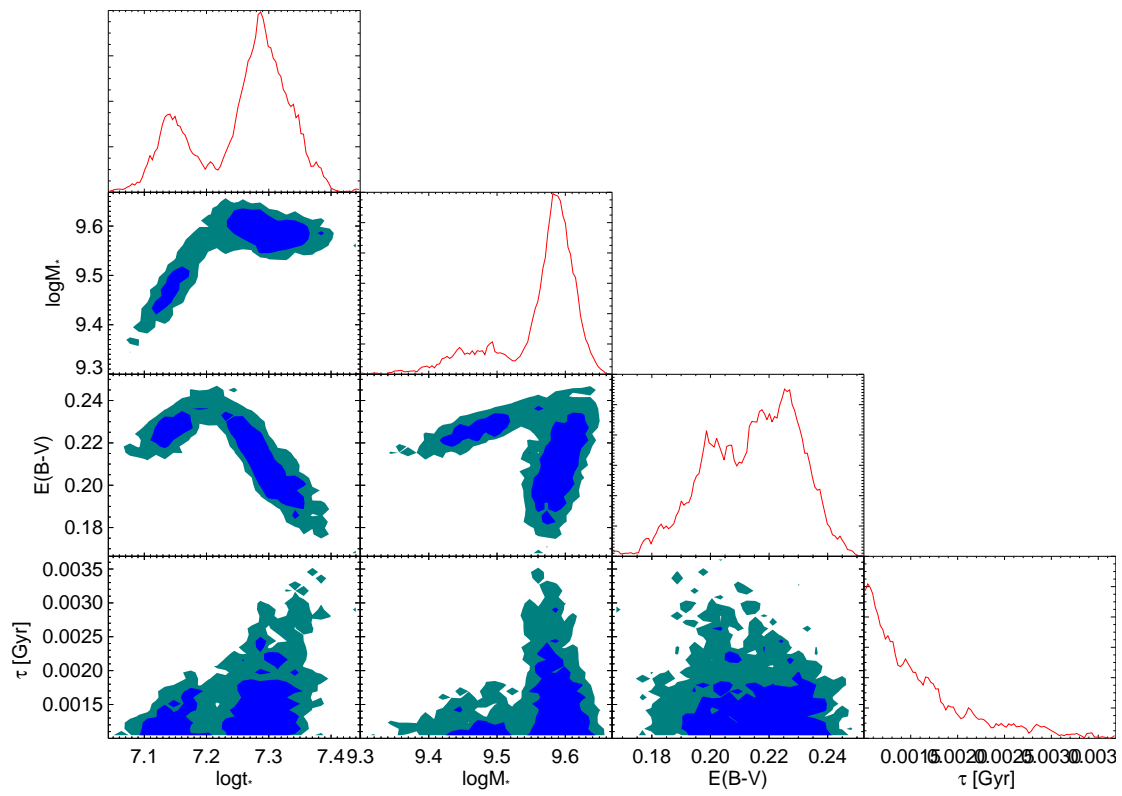


Figure 4.26 Triangular plot of the GalMC MCMC chain for Quayle.



## **Coauthor statements**



## Paper I

# The Dwarf Starburst Host Galaxy of a Type Ia SN at $z = 1.55$ from CANDELS

*Teddy F. Frederiksen, Jens Hjorth, Justyn R. Maund, Steven A. Rodney, Adam G. Riess, Tomas Dahlen,  
& Bahram Mobasher*

The Astrophysical Journal, vol. 760, p. 125, 2012

Chapter 2 is based on this paper. Teddy Frederiksen did the full data analysis and wrote the paper draft. Jens Hjorth and Justyn Maund provided extensive feedback throughout the writing and analysis process. Steven Rodney and Adam Riess (PI) are heading the CANDELS SN search where this SN was discovered. Tomas Dahlen and Bahram Mobasher provided the photometric data used in the analysis and also advised on the SED fitting analysis. All co-authors commented on the final draft that was submitted to the journal.



Teddy Frederiksen

Jens Hjorth

The rest of the co-authors have made a written accept of this statement, which are appended in the next pages.

**From:** Justyn Maund <j.maund@qub.ac.uk>  
**Subject:** Re: Co-author statement  
**Date:** 11. jun. 2013 10.07.23 CEST  
**To:** "Teddy F. Frederiksen" <teddy@dark-cosmology.dk>

---

Hi Teddy,

I have no issues with that statement

I guess you must be in the final days of pulling the thesis together (right?) - best of luck for the final push!

all the best

Justyn

On 10/06/2013 22:38, Teddy F. Frederiksen wrote:

[Dear coauthors of the Primo Host paper](#)

It is a thesis requirement at the University of Copenhagen that I provide a co-author statement for the papers that make up my thesis. I therefore ask you to read the attached statement and reply if you agree with the statement. If you have any comments or suggestions for the statement, please let me know.

Cheers,  
Teddy

Statement:

Paper I

[The Dwarf Starburst Host Galaxy of a Type Ia SN at  \$z = 1.55\$  from CANDELS](#)

Teddy F. Frederiksen, Jens Hjorth, Justyn R. Maund, Steven A. Rodney, Adam G. Riess, Tomas Dahlen, & Bahram Mobasher  
The Astrophysical Journal, vol. 760, p. 125, 2012

Chapter 2 is based on this paper. Teddy F. Frederiksen did the full data analysis and wrote the paper draft. Jens Hjorth and Justyn R. Maund provided extensive feedback throughout the writing and analysis process. Adam G. Riess and Steven A. Rodney are heading the CANDELS SN search where this SN was discovered. Tomas Dahlen and Bahram Mobasher provided the photometric data used in the analysis and also advised on the SED fitting analysis. All co-authors commented on the final draft that was submitted to the journal.

**From:** Steve Rodney <rodney@jhu.edu>  
**Subject:** Re: Co-author statement  
**Date:** 11. jun. 2013 02.07.51 CEST  
**To:** "Teddy F. Frederiksen" <teddy@dark-cosmology.dk>

---

Looks good to me.

On Monday, June 10, 2013, Teddy F. Frederiksen wrote:

Dear coauthors of the Primo Host paper

It is a thesis requirement at the University of Copenhagen that I provide a co-author statement for the papers that make up my thesis. I therefore ask you to read the attached statement and reply if you agree with the statement. If you have any comments or suggestions for the statement, please let me know.

Cheers,  
Teddy

Statement:

## **Paper I**

### **The Dwarf Starburst Host Galaxy of a Type Ia SN at $z = 1.55$ from CANDELS**

*Teddy F. Frederiksen, Jens Hjorth, Justyn R. Maund, Steven A. Rodney, Adam G. Riess, Tomas Dahlen, & Bahram Mobasher*  
The Astrophysical Journal, vol. **760**, p. 125, 2012

Chapter 2 is based on this paper. Teddy F. Frederiksen did the full data analysis and wrote the paper draft. Jens Hjorth and Justyn R. Maund provided extensive feedback throughout the writing and analysis process. Adam G. Riess and Steven A. Rodney are heading the CANDELS SN search where this SN was discovered. Tomas Dahlen and Bahram Mobasher provided the photometric data used in the analysis and also advised on the SED fitting analysis. All co-authors commented on the final draft that was submitted to the journal.

--

Sent from Gmail Mobile

**From:** Tomas Dahlen <dahlen@stsci.edu>   
**Subject:** Re: Co-author statement  
**Date:** 11. jun. 2013 00.48.20 CEST  
**To:** "Teddy Frederiksen (dark-cosmology.dk)" <teddy@dark-cosmology.dk>

1 Attachment, 6 KB

Hi Teddy,

I agree with the statement.

best,  
Tomas

On Jun 10, 2013, at 5:38 PM, Teddy F. Frederiksen wrote:

Dear coauthors of the Primo Host paper

It is a thesis requirement at the University of Copenhagen that I provide a co-author statement for the papers that make up my thesis. I therefore ask you to read the attached statement and reply if you agree with the statement. If you have any comments or suggestions for the statement, please let me know.

Cheers,  
Teddy

Statement:

Paper I

The Dwarf Starburst Host Galaxy of a Type Ia SN at  $z = 1.55$  from CANDELS

Teddy F. Frederiksen, Jens Hjorth, Justyn R. Maund, Steven A. Rodney, Adam G. Riess, Tomas Dahlen, & Bahram Mobasher  
The Astrophysical Journal, vol. 760, p. 125, 2012

Chapter 2 is based on this paper. Teddy F. Frederiksen did the full data analysis and wrote the paper draft. Jens Hjorth and Justyn R. Maund provided extensive feedback throughout the writing and analysis process. Adam G. Riess and Steven A. Rodney are heading the CANDELS SN search where this SN was discovered. Tomas Dahlen and Bahram Mobasher provided the photometric data used in the analysis and also advised on the SED fitting analysis. All co-authors commented on the final draft that was submitted to the journal.



[winmail.dat \(6 KB\)](#)

**From:** Bahram Mobasher <bahram.mobasher@ucr.edu>  
**Subject:** RE: Co-author statement  
**Date:** 10. jun. 2013 23.43.56 CEST  
**To:** "Teddy F. Frederiksen" <teddy@dark-cosmology.dk>

---

Hi Teddy

I agree with the statement. Hope all goes well with the thesis.

Best regards

Bahram

---

**From:** Teddy F. Frederiksen [teddy@dark-cosmology.dk]  
**Sent:** Monday, June 10, 2013 2:38 PM  
**To:** Steve Rodney; Adam Riess; Tomas Dahlen; Bahram Mobasher  
**Cc:** Jens Hjorth; Justyn R. Maund  
**Subject:** Co-author statement

Dear coauthors of the Primo Host paper

It is a thesis requirement at the University of Copenhagen that I provide a co-author statement for the papers that make up my thesis. I therefore ask you to read the attached statement and reply if you agree with the statement. If you have any comments or suggestions for the statement, please let me know.

Cheers,  
Teddy

Statement:

## **Paper I**

### **The Dwarf Starburst Host Galaxy of a Type Ia SN at $z = 1.55$ from CANDELS**

*Teddy F. Frederiksen, Jens Hjorth, Justyn R. Maund, Steven A. Rodney, Adam G. Riess, Tomas Dahlen, & Bahram Mobasher*  
The Astrophysical Journal, vol. **760**, p. 125, 2012

Chapter 2 is based on this paper. Teddy F. Frederiksen did the full data analysis and wrote the paper draft. Jens Hjorth and Justyn R. Maund provided extensive feedback throughout the writing and analysis process. Adam G. Riess and Steven A. Rodney are heading the CANDELS SN search where this SN was discovered. Tomas Dahlen and Bahram Mobasher provided the photometric data used in the analysis and also advised on the SED fitting analysis. All co-authors commented on the final draft that was submitted to the journal.

## Paper II

# Spectroscopic identification of a redshift 1.55 supernova host galaxy from the Subaru Deep Field Supernova Survey

*Teddy F. Frederiksen, Or Graur, Jens Hjorth, Dan Maoz, and Dovi Poznanski*  
Submitted to *Astronomy & Astrophysics, Research Notes*

Chapter 3 is based on this paper. Teddy Frederiksen did the full data analysis and wrote the majority of the paper. Or Graur wrote the introduction (except for the last paragraph) and the last paragraph of the conclusions. Figure 1 was reproduced from Graur et al. (2011a) with the new spectroscopic redshift. All co-authors provided extensive comments and discussion before submission to the Journal.



Teddy Frederiksen

Jens Hjorth

The rest of the co-authors have made a written accept of this statement, which are appended in the next pages.

**From:** Or Graur <or.graur@gmail.com>  
**Subject:** Re: Co-author statement  
**Date:** 12. jun. 2013 17.37.24 CEST  
**To:** "Teddy F. Frederiksen" <teddy@dark-cosmology.dk>  
**Reply-To:** or.graur@gmail.com

---

Hi Teddy,

Looks OK to me. Minor corrections (red - strikethrough; blue - add).

Cheers,

Or

**Chapter 3 is based on this paper. Teddy F. Frederiksen did the full data analysis and wrote the majority of the draft paper. Or Graur provided the draft for wrote the introduction (except for the last paragraph) and the last paragraph of the conclusions. Figure 1 was reproduced from Graur et al. (2011a) with the new spectroscopic redshift. All co-authors provided extensive comments and discussion before the submission to the Journal.**

On Wed, Jun 12, 2013 at 3:15 PM, Teddy F. Frederiksen <teddy@dark-cosmology.dk> wrote:

Hi Or

It is a thesis requirement at the University of Copenhagen that I provide a co-author statement for the papers that make up my thesis. I have made a draft of the co-author statement for the SDF host paper. If you can approve the statement I will sent out the statement to all co-authors for them to accept. If you have any comments, questions or suggestions to the statement please let me know.

Cheers,  
Teddy

Statement:

## **Paper II**

### **Spectroscopic identification of a redshift 1.55 supernova host galaxy from the Subaru Deep Field Supernova Survey**

*Teddy F. Frederiksen, Or Graur, Jens Hjorth, Dan Maoz, and Dovi Poznanski*

**Submitted to Astronomy & Astrophysics, Research Notes**

**Chapter 3 is based on this paper. Teddy F. Frederiksen did the full data analysis and the majority of the draft. Or Graur provided the draft of the introduction (except the last paragraph) and the last paragraph of the conclusion. Figure 1 was reproduced from Graur et al. (2011a) with the new spectroscopic redshift. All co-authors provided extensive comments and discussion before the submission to the Journal.**

--

-----  
Ad eundum quo nemo ante iit  
-----

Or Graur

American Museum of Natural History  
Astrophysics Department  
Central Park West at 79th Street

**From:** Dan Maoz <dani@wise.tau.ac.il>  
**Subject:** Re: Co-author statement  
**Date:** 16. jun. 2013 08.08.00 CEST  
**To:** "Teddy F. Frederiksen" <teddy@dark-cosmology.dk>  
**Cc:** Or Graur <or.graur@gmail.com>, Dovi Poznanski <poznanski@gmail.com>, Jens Hjorth <jens@dark-cosmology.dk>

---

Hi Teddy,  
fine with me.  
Dani

-----  
Prof. Dan Maoz, Tel-Aviv University, School of Physics and Astronomy.  
Director, Wise Observatory  
www.astro.tau.ac.il/~dani maoz@astro.tau.ac.il  
Office/Secr. +972-3-640-8538/8729/7414, Cell. +972-52-468-1489  
-----

On Sun, 16 Jun 2013, Teddy F. Frederiksen wrote:

Dear coauthors of the SDF0705 paper

It is a thesis requirement at the University of Copenhagen that I provide a co-author statement for the papers that make up my thesis. I therefore ask you to read the attached statement and reply if you agree with the statement. If you have any comments or suggestions for the statement, please let me know.

Cheers,  
Teddy

Statement:  
Paper II

Spectroscopic identification of a redshift 1.55 supernova host galaxy from the Subaru Deep Field Supernova Survey

Teddy F. Frederiksen, Or Graur, Jens Hjorth, Dan Maoz, and Dovi Poznanski

Submitted to Astronomy & Astrophysics, Research Notes

Chapter 3 is based on this paper. Teddy Frederiksen did the full data analysis and wrote the majority of the paper. Or Graur wrote the introduction (except for the last paragraph) and the last paragraph of the conclusions. Figure 1 was reproduced from Graur et al. (2011) with the new spectroscopic redshift. All co-authors provided extensive comments and discussion before submission to the Journal.

**From:** Dovi Poznanski <dovi@astro.tau.ac.il>  
**Subject:** Re: Co-author statement  
**Date:** 16. jun. 2013 08.30.59 CEST  
**To:** Dan Maoz <dani@wise.tau.ac.il>  
**Cc:** "Teddy F. Frederiksen" <teddy@dark-cosmology.dk>, Or Graur <or.graur@gmail.com>, Dovi Poznanski <poznanski@gmail.com>, Jens Hjorth <jens@dark-cosmology.dk>

---

Fine with me too.

Cheers  
Dovi

Sent from somewhere

On Jun 16, 2013, at 9:08, Dan Maoz <dani@wise.tau.ac.il> wrote:

Hi Teddy,  
fine with me.  
Dani

---

Prof. Dan Maoz, Tel-Aviv University, School of Physics and Astronomy.  
Director, Wise Observatory  
[www.astro.tau.ac.il/~dani\\_maoz@astro.tau.ac.il](http://www.astro.tau.ac.il/~dani_maoz@astro.tau.ac.il)  
Office/Secr. +972-3-640-8538/8729/7414, Cell. +972-52-468-1489

---

On Sun, 16 Jun 2013, Teddy F. Frederiksen wrote:

Dear coauthors of the SDF0705 paper

It is a thesis requirement at the University of Copenhagen that I provide a co-author statement for the papers that make up my thesis. I therefore ask you to read the attached statement and reply if you agree with the statement. If you have any comments or suggestions for the statement, please let me know.

Cheers,  
Teddy

Statement:  
Paper II

Spectroscopic identification of a redshift 1.55 supernova host galaxy from the Subaru Deep Field Supernova Survey

Teddy F. Frederiksen, Or Graur, Jens Hjorth, Dan Maoz, and Dovi Poznanski

Submitted to Astronomy & Astrophysics, Research Notes

Chapter 3 is based on this paper. Teddy Frederiksen did the full data analysis and wrote the majority of the paper. Or Graur wrote the introduction (except for the last paragraph) and the last paragraph of the conclusions. Figure 1 was reproduced from Graur et al. (2011) with the new spectroscopic redshift. All co-authors provided extensive comments and discussion before submission to the Journal.



## BIBLIOGRAPHY

---

- Acquaviva, V., Gawiser, E., & Guaita, L. 2011, *ApJ*, 737, 47
- Asplund, M., Grevesse, N., Sauval, A. J., & Scott, P. 2009, *ARA&A*, 47, 481
- Atek, H., Kunth, D., Schaerer, D., Hayes, M., Deharveng, J. M., Östlin, G., & Mas-Hesse, J. M. 2009, *A&A*, 506, L1
- Baldwin, J. A., Phillips, M. M., & Terlevich, R. 1981, *PASP*, 93, 5
- Barger, A. J., Cowie, L. L., & Wang, W.-H. 2008, *ApJ*, 689, 687
- Benítez, N. 2000, *ApJ*, 536, 571
- Bloom, J. S., et al. 2012, *ApJ*, 744, L17
- Brandt, T. D., Tojeiro, R., Aubourg, É., Heavens, A., Jimenez, R., & Strauss, M. A. 2010, *AJ*, 140, 804
- Brinchmann, J., Charlot, S., White, S. D. M., Tremonti, C., Kauffmann, G., Heckman, T., & Brinkmann, J. 2004, *MNRAS*, 351, 1151
- Brocklehurst, M. 1971, *MNRAS*, 153, 471
- Bruzual, G., & Charlot, S. 2003, *MNRAS*, 344, 1000
- Calzetti, D. 2001, *PASP*, 113, 1449
- Calzetti, D., Armus, L., Bohlin, R. C., Kinney, A. L., Koornneef, J., & Storchi-Bergmann, T. 2000, *ApJ*, 533, 682
- Cardelli, J. A., Clayton, G. C., & Mathis, J. S. 1989, *ApJ*, 345, 245
- Chabrier, G. 2003, *PASP*, 115, 763
- Childress, M. J., et al. 2013a, *ArXiv e-prints*
- . 2013b, *ArXiv e-prints*
- Christensen, L., et al. 2012, *MNRAS*, 427, 1953
- Conley, A., et al. 2011, *ApJS*, 192, 1
- Cooper, M. C., et al. 2011, *ApJS*, 193, 14
- Daddi, E., et al. 2007, *ApJ*, 670, 156
- Dahlen, T., Strolger, L., & Riess, A. G. 2008a, *ApJ*, 681, 462
- Dahlen, T., Strolger, L.-G., & Riess, A. G. 2008b, *ApJ*, 681, 462

Dahlen, T., et al. 2010, *ApJ*, 724, 425

Dayal, P., Ferrara, A., & Dunlop, J. S. 2013, *MNRAS*, 430, 2891

Dilday, B., et al. 2008, *ApJ*, 682, 262

D’Odorico, S., et al. 2006, in *Society of Photo-Optical Instrumentation Engineers (SPIE) Conference Series*, Vol. 6269

Elbaz, D., et al. 2007, *A&A*, 468, 33

—. 2011, *A&A*, 533, A119

Feldmann, R., et al. 2006, *MNRAS*, 372, 565

Fitzpatrick, E. L. 1999, *PASP*, 111, 63

Frederiksen, T. F., Hjorth, J., Maund, J. R., Rodney, S. A., Riess, A. G., Dahlen, T., & Mobasher, B. 2012, *ApJ*, 760, 125

Gallagher, J. S., Garnavich, P. M., Berlind, P., Challis, P., Jha, S., & Kirshner, R. P. 2005, *ApJ*, 634, 210

Gao, Y., & Pritchett, C. 2013, *AJ*, 145, 83

Graur, O., et al. 2011a, *MNRAS*, 417, 916

—. 2011b, *MNRAS*, 417, 916

—. 2013, *ArXiv e-prints*

Grogin, N. A., et al. 2011, *ApJS*, 197, 35

Hamuy, M., Trager, S. C., Pinto, P. A., Phillips, M. M., Schommer, R. A., Ivanov, V., & Suntzeff, N. B. 2000, *AJ*, 120, 1479

Hayden, B. T., Gupta, R. R., Garnavich, P. M., Mannucci, F., Nichol, R. C., & Sako, M. 2013, *ApJ*, 764, 191

Hayes, M., Schaerer, D., Östlin, G., Mas-Hesse, J. M., Atek, H., & Kunth, D. 2011, *ApJ*, 730, 8

Hillebrandt, W., & Niemeyer, J. C. 2000, *ARA&A*, 38, 191

Hinshaw, G., et al. 2012, *ArXiv e-prints*

Howell, D. A. 2011, *Nature Communications*, 2

Iben, Jr., I., & Tutukov, A. V. 1984, *ApJS*, 54, 335

Jones, D. O., et al. 2013, *ApJ*, 768, 166

Kelly, P. L., Hicken, M., Burke, D. L., Mandel, K. S., & Kirshner, R. P. 2010, *ApJ*, 715, 743

Kennicutt, Jr., R. C. 1998, *ARA&A*, 36, 189

Kewley, L. J., & Dopita, M. A. 2002, *ApJS*, 142, 35

Kewley, L. J., & Ellison, S. L. 2008, *ApJ*, 681, 1183

Kirshner, R. P. 2010, *Foundations of supernova cosmology*, ed. P. Ruiz-Lapuente, 151

Kobulnicky, H. A., & Kewley, L. J. 2004, *ApJ*, 617, 240

Koekemoer, A. M., et al. 2011, *ApJS*, 197, 36

Komatsu, E., et al. 2011, *ApJS*, 192, 18

Kowal, C. T. 1968, *AJ*, 73, 1021

Kriek, M., van Dokkum, P. G., Labbé, I., Franx, M., Illingworth, G. D., Marchesini, D., & Quadri, R. F. 2009, *ApJ*, 700, 221

Laidler, V. G., et al. 2007, *PASP*, 119, 1325

Lampeitl, H., et al. 2010, *ApJ*, 722, 566

Lara-López, M. A., López-Sánchez, Á. R., & Hopkins, A. M. 2013, *ApJ*, 764, 178

Lara-López, M. A., et al. 2010, *A&A*, 521, L53+

Lee, S.-K., Idzi, R., Ferguson, H. C., Somerville, R. S., Wiklind, T., & Giavalisco, M. 2009, *ApJS*, 184, 100

Leibundgut, B. 2000, *A&A Rev.*, 10, 179

Maiolino, R., et al. 2008, *A&A*, 488, 463

Mannucci, F., Cresci, G., Maiolino, R., Marconi, A., & Gnerucci, A. 2010, *MNRAS*, 408, 2115

Mannucci, F., Della Valle, M., Panagia, N., Cappellaro, E., Cresci, G., Maiolino, R., Petrosian, A., & Turatto, M. 2005, *A&A*, 433, 807

Mannucci, F., Salvaterra, R., & Campisi, M. A. 2011, *MNRAS*, 414, 1263

Maoz, D., & Mannucci, F. 2012, *PASA*, 29, 447

Maoz, D., Mannucci, F., & Brandt, T. D. 2012, *MNRAS*, 426, 3282

Maoz, D., Mannucci, F., Li, W., Filippenko, A. V., Della Valle, M., & Panagia, N. 2011, *MNRAS*, 412, 1508

Maoz, D., Mannucci, F., & Nelemans, G. 2013, *ArXiv e-prints*

March, M. C., Trotta, R., Berkes, P., Starkman, G. D., & Vaudrevange, P. M. 2011, *MNRAS*, 418, 2308

McGaugh, S. S. 1991, *ApJ*, 380, 140

Meyers, J., et al. 2012, *ApJ*, 750, 1

Nomoto, K. 1982, *ApJ*, 253, 798

Nugent, P. E., et al. 2011, *Nature*, 480, 344

Oesch, P. A., et al. 2010, *ApJ*, 709, L16

Osterbrock, D. E., & Ferland, G. J. 2006, *Astrophysics of gaseous nebulae and active galactic nuclei* (University Science Books)

Perlmutter, S., et al. 1999, *ApJ*, 517, 565

Pettini, M., & Pagel, B. E. J. 2004, *MNRAS*, 348, L59

Phillips, M. M. 1993, *ApJ*, 413, L105

—. 2012, *PASA*, 29, 434

Phillips, M. M., Lira, P., Suntzeff, N. B., Schommer, R. A., Hamuy, M., & Maza, J. 1999, *AJ*, 118, 1766

Postman, M., et al. 2012, *ApJS*, 199, 25

Prieto, J. L., Stanek, K. Z., & Beacom, J. F. 2008, *ApJ*, 673, 999

Richard, J., Jones, T., Ellis, R., Stark, D. P., Livermore, R., & Swinbank, M. 2011, *MNRAS*, 413, 643

Riess, A. G., & Livio, M. 2006, *ApJ*, 648, 884

Riess, A. G., Press, W. H., & Kirshner, R. P. 1996, *ApJ*, 473, 88

Riess, A. G., et al. 1998, *AJ*, 116, 1009

Rodney, S. A., et al. 2012, *ApJ*, 746, 5

Scannapieco, E., & Bildsten, L. 2005, *ApJ*, 629, L85

Schlafly, E. F., & Finkbeiner, D. P. 2011, *ApJ*, 737, 103

Schlegel, D. J., Finkbeiner, D. P., & Davis, M. 1998, *ApJ*, 500, 525

Smith, M., et al. 2012, *ApJ*, 755, 61

Strolger, L.-G., Dahlen, T., & Riess, A. G. 2010, *ApJ*, 713, 32

Sullivan, M., et al. 2006, *ApJ*, 648, 868

—. 2010, *MNRAS*, 406, 782

—. 2011, *ApJ*, 737, 102

Suzuki, N., et al. 2012, *ApJ*, 746, 85

Thielemann, F.-K., Brachwitz, F., Höflich, P., Martinez-Pinedo, G., & Nomoto, K. 2004, *NewAR*, 48, 605

Thomson, M. G., & Chary, R. R. 2011, *ApJ*, 731, 72

Tremonti, C. A., et al. 2004, *ApJ*, 613, 898

Vanzella, E., et al. 2005, *A&A*, 434, 53

Vernet, J., et al. 2011, *A&A*, 536, A105

Wang, B., & Han, Z. 2012, *NewAR*, 56, 122

Webbink, R. F. 1984, *ApJ*, 277, 355

Whelan, J., & Iben, Jr., I. 1973, *ApJ*, 186, 1007

Whitaker, K. E., van Dokkum, P. G., Brammer, G., & Franx, M. 2012, *ApJ*, 754, L29

Whitaker, K. E., et al. 2011, *ApJ*, 735, 86

Wilson, O. C. 1939, *ApJ*, 90, 634

Wuyts, S., et al. 2011, *ApJ*, 742, 96

York, D. G., et al. 2000, *AJ*, 120, 1579

Zwicky, F. 1938, *Physical Review*, 53, 1019